Norwegian University
of Life Sciences

Master's Thesis 2024 30 ECTS
Faculty of Biosciences - BIOVIT

Utilizing Multi-Spectral Time-Series Data for GWAS in Spring Wheat: A Comparison of Conventional and Machine-Learning Approaches

Awo Arab
Master of Science in Data Science

Abstract

Plant breeding is the practice of breeding plants with desirable traits, for example, resistance to local pathogens, adaptation to environmental stressors, and increased yield. With the recent development of high-throughput phenotyping using remote sensing technologies and multispectral sensors, researchers can derive metrics (i.e., bands and vegetation indices) that correlate with important agronomic traits like yield and maturity time to study these traits in a high-throughput manner. There lies great potential in multispectral data for dissecting the genetic architecture of spring wheat (*Triticum aestivum*), and previous studies in a variety of crops (wheat, maize, and rice) have identified both known and novel genetic regions influencing agronomic traits.

This thesis explored the integration of multispectral time-series with Genome-Wide Association Studies (GWAS) in spring wheat. Given that spectral time-series are not typically used in association studies, we also implemented a machine learning (ML) alternative based on genetic algorithms and support vector regression (GA-SVR) for comparison with conventional GWAS using mixed linear models (MLM). Both GWAS approaches were employed on agronomic traits data and spectral phenotypes derived from the multispectral time-series.

Our results demonstrated that spectral phenotypes had moderate to large heritability, and correlated well with certain traits such as grain yield. We identified several spectral Quantitative Trait Loci (QTL) containing or near genes, like *Rht-B1* and *Vrn-A1*, that overlapped with agronomic QTL related to the function of these genes. We also identified temporal genetic patterns, where certain spectral regions were significant only in specific time-periods (e.g., grain filling). In addition, the MLM detected few QTL associated with yield and protein content that overlap with spectral QTL. This suggests that the data or model may not be adequate for identifying spectral QTL related to complex physiological traits. On the other hand, the GA-SVR method produced a greater number of significant markers and QTL compared to MLM. It also found more spectral QTL overlapping with regions identified for yield and protein content, indicating GA-SVR may be suitable for capturing and dissecting more complex traits. However, results should be interpreted with care, as confounding variables were not accounted for in the GA-SVR pipeline.

In conclusion, this thesis demonstrates the potential usefulness of multispectral time-series for GWAS, because we identified temporal differences in significant spectral QTL, as well as basic genes related to height and maturity time. The GA-SVR method provided an alternative to MLM, and it is interesting to see that it returns different genomic regions, indicating that it might be capturing different information compared to MLM, and thus potentially overcoming some of the weaknesses of MLM. However, the effects of confounding variables in the GA-SVR pipeline remains unknown and requires further investigation.

Acknowledgements

I would first like to extend my heartfelt gratitude to my advisory team, which consisted of my main supervisor Sahameh Shafiee and co-supervisors Tomasz Mroz, and Morten Lillemo. They have all contributed tremendously to both my thesis and my motivation for using data to understand biological problems.

The expertise and knowledge in remote sensing and high-throughput phenotyping provided by Sahameh has helped me greatly in understanding and appreciating precision agriculture. Sahameh's guidance during pipeline development, finding relevant literature, discussion of results, and detailed revisions helped me greatly with my thesis writing. I therefore want to express my deepest appreciation for my main supervisor's help and guidance.

The continuous help during code development, interpretation of results and discussion of their significance provided by Tomasz has been essential to developing my research objectives and writing my thesis. The advice received on both code related issues and implications of results has been priceless.

I would also like to acknowledge Morten's detailed and constructive comments, and appreciate the time spent discussing the implications of my results. These contributions have improved the quality of my work.

Next, I would like to acknowledge the insightful and constructive feedback provided by Harkingto Harkingto. I appreciate the time spent reading my thesis and helping me further improve my work.

Lastly, I would like to thank my parents and close friends for their support and encouragement during my thesis writing.

Contents

List of Tables

List of Figures

Abbreviations

AUC Area Under Curve

BH Benjamini–Hochberg

BH Broad Sense Heritability

BLUP Best Linear Unbiased Predictor

BLUE Best Linear Unbiased Estimator

CNN Convolutional Neural Networks

DH Days to Heading

DFH Days From Heading

DM Days to Maturity

FDR False Discovery Rate

GA Genetic Algorithm

GFD Grain Filling Duration

GF Grain Filling Stage

GPC Grain Protein Content

GNDVI Green Normalized Difference Vegetation Index

GWAS Genome Wide Assocation Studies

GY Grain Yield

HEAD Heading Stage

HTP High Throughput Phenotyping

LD Linkage Disequilibrium

LOCF Last Observation Carried Forward

MAF Minor Allele Frequency

ML Machine Learning

MLM Mixed Linear Models

NDVI Normalized Difference Vegetation Index

NIR Near Infrared

PCA Principal Component Analysis

PC Principal Components

PH Plant Height

PUK Pearson's Universal Kernel VII

QTL Quantitative Trait Loci

RBF Radial Basis Function

REML Restricted Likelihood Estimation

SR Simple Ratio

SNP single nucleotide polymorphism

SVM Support Vector Machines

SVR Support Vector Regression

UAV Unmanned Aerial Vehicles

VEG Vegetative Stage

VI Vegetation Indices

1 Introduction

1.1 Background

Precision agriculture has emerged as a research area with the objective of employing technology and data-driven solutions in farming practices to increase productivity, and improve efficiency (Nowak 2021). Often PA-research is often facilitated by technological platforms that produce fast, accurate and large volumes of informative data for various purposes, one of them being plant breeding. Plant breeding is the practice of breeding plants with desirable traits like for example resistance to local pathogens, adaptation to environmental stressors and increased yield (Jangra et al. 2021). To successfully breed crop with such desirable traits both genetic and phenotypic variation have to be studied and quantified (Jang et al. 2020). Large-scale analysis of phenotypic variation can be achieved through the use of remote imaging and sensor technologies, also referred to as high throughput phenotyping (HTP). On the other hand, genetic variation can be studied using Genome Wide Assocation Studies (GWAS). For this thesis, both HTP and GWAS play a central role, as we will integrate HTP-derived data in GWA-study of spring wheat varieties (*Triticum aestivum*).

HTP-platforms that have been employed for plant breeding are satellite and unmanned aerial vehicles (UAVs) imaging, soil sensors, and deployment of field robots (Han et al. 2020, Hassan et al. 2021, Burud et al. 2017). HTP is particularly useful because it allows researchers to objectively quantify observable features like biomass, grain quality and canopy cover with greater precision compared to human observers (Jangra et al. 2021). Also, HTP can be used to quantify physiological traits like chlorophyll and water content, soil nitrogen levels, and root physiology (van Dijk et al. 2021, Sarić et al. 2022). A further benefit of HTP is that it is non-destructive, which allows for repeated measurements of the same samples over time (Sarić et al. 2022). This enables researchers to study temporal patterns in phenotypic variation in detail as done by Wang et al. (2021). In their study, a large maize population was monitored using time series of Normalized Difference Vegetation Index (NDVI) collected using UAV-based multispectral imagery. Their results demonstrated the usefulness of multispectral data for genetic dissection of NDVI. Overall they uncovered temporal changes in genetic effects, as well as interactions between genes and environments that control NDVI. Overall, their study also demonstrates how HTP can monitor and quantify traits that are challenging to measure.

Among the popular HTP-platforms is UAV-imagery, because they are cost-effective and easy to use to collect large volumes of spectral imaging data (Burud et al. 2017, Ang & Seng 2021). For example, UAVs have been used to monitor important developmental stages like senescence in bread wheat as done by Hassan et al. (2021). In their research, multispectral imaging data derived from UAVs were used to quantify senescence, as well as identify genetic regions associated with different developmental stages (including senescence). Furthermore, the research of Rodrigues et al. (2018) exemplifies how UAV-imaging allows researchers to predict and quantify more complex traits like grain yield and grain protein content by using spectral data that correlate with underlying traits. In their research they used vegetation indices that correlate with nitrogen utilization to predict grain yield and grain protein content. In general, HTP enables researchers to measure secondary traits that are closely related to the main trait of interest. Overall, HTP can be used to quantify and monitor challenging-to-measure traits through spectral data analysis.

Moreover, researchers can integrate and combine various HTP-platforms, resulting in diverse, multi-modal data (Han et al. 2020, Chlingaryan et al. 2018). This approach could be more informative than relying on only one HTP-technology as it may reveal additional patterns in phenotypic variation. As demonstrated by Han et al. (2020) multi-modal data may enhance model predictions, leading to improved accuracy. In their research they used soil sensors, weather data and spectral imaging to predict end-of-season grain yield

in winter wheat.

Although data derived from HTP-platforms is useful, the high dimensionality and heterogeneity (in terms of modes and spatial variation) provides a challenge for researchers (Ang & Seng 2021). In such data, there may also be non-linear relations and complex interactions that are difficult to model using conventional statistical methods (van Dijk et al. 2021). To solve this issue, machine-learning methods can be used, since such methods have proven themselves to perform well with heterogeneous, noisy and large data (Ang & Seng 2021, van Dijk et al. 2021). Machine Learning (ML) methods describe a broad range of algorithms, both parametric and non-parametric, that learn from data and try to optimize a given objective function or task (van Dijk et al. 2021). For the purposes of analyzing HTP-data, multiple ML-models have been employed for purposes such as predicting yield potential, identifying superior lines resistant to disease, and finding genomic regions associated with important agronomic traits (Mu et al. 2019, Fei et al. 2022, González-Camacho et al. 2018, Yoosefzadeh-Najafabadi et al. 2022). In the research by Mu et al. (2019), they developed Convolutional Neural Networks (CNN), a variant of deep learning algorithms, to predict winter wheat yield. The input to the network was 19 different spectral indices captured using satellite imagery collected over multiple seasons in different geographical regions. They concluded that the CNN effectively extracted features related to yield, and their model performance was satisfactory for most regions. Likewise, Fei et al. (2022) applied multi-layer neural networks on hyperspectral images collected using spectrometers to predict grain yield in bread wheat using data recorded at various growth stages.

Keep in mind that spatial hyperspectral images are high-dimensional, since such data form a hyperspectral cube (2 spatial dimensions in addition to a spectral dimension). Deep learning networks are well suited for extracting features from such high-dimensional data, and the work of Fei et al. (2022) demonstrated that the network performed well for yield prediction. In addition to feature extraction and trait prediction, ML-methods can be used for plant breeding purposes by uncovering the genetic architecture of complex traits as seen in the research of González-Camacho et al. (2018) and Yoosefzadeh-Najafabadi et al. (2022). González-Camacho et al. (2018) demonstrated that random forest and support vector regression can be used for genomic selection in wheat to breed rust-resistant lines. The work of Yoosefzadeh-Najafabadi et al. (2022) showcased the use of ML-methods to uncover genetic variants associated with yield related traits in soybean. In their work, they compared ML-methods and conventional statistical models to identify such variants. Interestingly, they found that the ML-methods yielded more significant hits, and that the identified markers overlap with previously reported Quantitative Trait Loci (QTL). QTL are genomic regions that correlate with phenotypic variation of a quantitative trait (Myles & Wayne 2008). Identifying such regions for a given trait is of great interest in plant breeding, since QTL can be used in plant breeding to select superior lines that contribute to the improvement of crop (Asíns 2002).

Although traits studied so far have mostly been traditional agronomic traits (like yield and height), also spectral phenotypes, which are derived from multispectral or hyperspectral data, can serve as quantitative traits. In fact relating genomic regions to spectral phenotypes has improved researchers' understanding of the genetic basis for plant growth (Xiao et al. 2022). This may be done by conducting GWAS. GWAS is used in plant breeding to identify genetic variants associated with important traits, like yield or disease resistance. With GWAS, one can locate genetic markers linked to these traits by examining the genomes of different crop varieties. Plant breeders use GWAS identify markers that correlate well with traits of interest, which can then be used to breed new plant varieties with improved characteristics (Asíns 2002). Traditionally, associations studies have been conducted using traits that are measured once during the season (like heading date) or using end-of-season traits (like grain yield) as seen in the studies by Mroz et al. (2023), Shariatipour et al. (2021), Li et al. (2019), and Pang et al. (2020) which all studied wheat varieties. As discussed earlier, with the emergence of HTP-technology, some researchers have employed features derived from imaging and sensor technology as traits to perform association analysis (Xiao et al.

2022). However, the use of HTP for GWAS is still limited in various crops including wheat, as reviewed by Xiao et al. (2022).

Unlike traditional end-of-season phenotyping, spectral phenotyping enables researchers to identify temporal patterns in phenotypic variations which can be used to uncover temporal controls in genetic effects (Wang et al. 2021, Guo et al. 2018). This can be extremely useful for complex traits such as growth and yield related traits, since we assume such traits are affected by many different small-effect loci over a longer of period of time (Gao et al. 2023). For example, in the research by Hassan et al. (2021), they identified novel genes that control senescence-timing in bread wheat using multispectral data. Similarly, Gao et al. (2023) used features derived from hyperspectral imaging (i-traits) for GWAS in bread wheat. Their study identified temporal patterns in significant associations, where some associations were only significant at certain developmental stages. They also found some pleiotropic regions (related to multiple i-traits) which identified a previously reported region which affect flowering date. Another study by Feng et al. (2017) showed similar use of i-traits derived from hyperspectral imaging and identified a gene controlling chlorophyll content in rice. Both studies by Feng et al. (2017) and Gao et al. (2023) used spectral data collected at specific time-points without any attempt at summarizing the data in any manner. Such summary statistics of spectral dynamics over the season may be useful, as shown the research of Wang et al. (2021) and Guo et al. (2018). In Wang et al. (2021) they fitted p-splines to the spectral time-series and derived summary statistics like maximum growth rate and point of inflection. They found more genomic associations using these features compared to using spectral data collected at specific time-points. Likewise, in Guo et al. (2018), they used both i-traits measured at specific time points as well as deriving summary statistics like derivatives and amplitudes of different spectral bands. The resulting analysis identified multiple genomic regions associated with important traits in rice, the most interesting one being a previously reported gene which controls chlorophyll content.

In light of the research reviewed so far, spectral time-series hold significant potential for identifying genetic regions linked to important traits or developmental stages in wheat. Therefore this thesis will integrate multispectral time-series with GWAS in spring wheat. Furthermore, given that spectral phenotypes have not typically been employed in association studies, exploring alternative ML-algorithms also presents an interesting opportunity to compare ML and classic GWAS. Hence, an alternative ML-pipeline will also be explored in this thesis.

1.2 Problem Statement & Objectives

The spectral data used in this study is a time series, which provides an interesting opportunity to explore different growth stages in spring wheat, like heading and grain filling stages. Spectral data captured at different developmental stages may provide valuable insight into genes crucial to those specific stages. **Therefore, we sample spectral data from comparable growth stages within each season to perform GWAS**.

Moreover, accumulated metrics such as Area Under the Curve (AUC) can be used to characterize crop development across the entire season. Performing GWAS on AUC may reveal the same or different genetic regions as reflectance data captured at specific time-points. GWAS using accumulated metrics may also reveal genetic associations related to complex trait such as grain yield and protein content, since they capture spectral information from the entire season. **Therefore, we will also include the AUC-values of vegetation indices for a GWA-study**.

Finally, given that we have data on agronomic traits as well, we will also conduct GWAS on these traits. By performing GWAS on agronomic traits, we may be able to identify agronomic QTL that overlap

with identified spectral QTL. Identifying overlapping QTL may enhance our understanding of identified spectral QTL, especially if the genomic regions have not been previously described. **We will therefore be performing GWAS on the agronomic traits, as it may reveal shared QTL between agronomic traits and spectral phenotypes.**

Finally, two different approaches will be used to identify significant markers. The first method is conventional GWAS using mixed-linear models (MLM), and this will be carried out according to the methodology described in Mroz et al. (2023). Their study also performed GWAS on the same wheat panel used in this study. The second method is a single nucleotide polymorphism (SNP) selection pipeline using support vector regression (SVR) and genetic algorithms (GA). This ML approach has been previously been described by de Oliveira et al. (2014). We implement the two different pipelines because multispectral data are not typically used for GWAS, and the literature on this topic is limited. Therefore it is worth exploring an ML-alternative, since ML is well suited for HTP-data. In addition to implementing both approaches, we will also be **comparing the resulting assocaitions to see if we identify the same genomic regions using ML and MLM**.

To summarize, the objectives of this thesis is:

1. *Perform conventional GWAS using MLM on both spectral phenotypes and agronomic traits, and compare identified QTL. Look into literature to see if the identified agronomic QTL have previously been described and can thus explain identified spectral QTL.*

2. *Implement an ML-alternative for SNP-selection for spectral phenotypes and agronomic traits, and compare identified QTL to those identified using conventional GWAS.*

In conclusion, it is important to highlight that while some research has been conducted using spectral imaging features for GWAS, an even smaller number have explored the use of spectral time series. Additionally, there are few ML pipelines developed specifically for association studies. Therefore, this thesis is novel in that it integrates multispectral time-series with association studies. Also, we develop and test the feasibility of an alternative ML pipeline.

2 Theory

2.1 Remote Sensing for High Throughput Phenotyping

HTP and UAV-based Systems

High-throughoutput phenotyping (HTP) are a collection methods that utilize imaging or sensor technologies for rapid and accurate phenotyping. Unlike traditional phenotyping, which can be labor-intensive and slow, such platforms can be automated and yield large volumes of data (Xiao et al. 2022, Jangra et al. 2021). Furthermore, HTP can be non-invasive, meaning that traits can be monitored through time without needing to destroy crop for sampling (Xiao et al. 2022, Gao et al. 2023). Essentially, HTP allows us to monitor traits at various stages of crop development and may thus reveal temporal patterns phenotypic and genetic variation (Gao et al. 2023, Wang et al. 2021).

HTP-platforms can be used in controlled conditions, such as greenhouses, or in the field. Typically, unmanned aerial vehicles (UAVs) are used for phenotyping crop under field conditions, and for this report UAVs have been used to do exactly this. Moreover, the UAVs are generally equipped with spectral sensors that detect the reflectance of visible light and beyond visible light from the crop canopy (Burud et al. 2017, Sarić et al. 2022).

While phenotyping in field conditions provide a more realistic estimate of crop performance, it may be challenging for a variety of reasons (Jangra et al. 2021). For instance, rain, cloud, and lodging cover can reduce the quality of spectral reflectance collected by UAVs (Sarić et al. 2022). In addition, changing solar illumination, which can occur throughout the day, may also significantly affect the spectral data captured (Shafiee et al. 2023). For this study, weather data was cross-referenced in order to explain and exclude flight missions were weather had an impact on the spectral reflectance data (see section 3.2)

Multispectral Data: Bands & VIs

Multispectral sensors capture discrete bands of light reflected from the crop canopy. The reflected light provides optical information detailing things like condition of the crop's tissue, biochemical components such as water and chlorophyll-content, and photochemical activity (Sarić et al. 2022, Jangra et al. 2021). Specific spectral bands contain different types of information. For example, near infrared (NIR) can be used to measure water content in soil and crop tissue (Sarić et al. 2022). Also, visible light can be used to evaluate morphological traits, such as greenness, height, structure, or discolouration due to disease (Azim et al. 2021, Xiao et al. 2022, Sarić et al. 2022).

Although spectral bands may be useful, they can also be noisy because they are easily affected by background reflectance and changing solar illumination (Shafiee et al. 2023, Sarić et al. 2022). Therefore, in addition to including spectral bands in our analysis, we will also derive vegetation indices (VIs). VIs are less noisy compared to spectral bands, and are derived using one or more combinations of spectral bands (Sarić et al. 2022, Verrelst et al. 2015, Hatfield et al. 2008). VIs are also useful because they tend to enhance the spectral information contained in the separate bands they are computed from (Verrelst et al. 2015). Selected VIs for this report are normalized difference vegetation index (NDVI), green normalized difference vegetation index (GNDVI), and simple ratio index (SR). NDVI was first described by Deering (1978), and it is derived using the NIR and red bands. These bands are indicators of vegetation health and vigour, as healthy crop emit light in the red to NIR region (Chang-Brahim et al. 2024). For these reasons, NDVI is widely used, since it is an indicator of greenness, vegetation density, and plant health

(Hatfield et al. 2008). NDVI, however, saturates easily for red band when vegetation is dense due high chlorophyll content. In other words, NDVI is not as sensitive for regions with high vegetation density. Using the green or red-edge bands instead solves this issue of saturation for highly dense vegetation as they are sensitive to higher chlorophyll content (Hatfield et al. 2008, Rahman & Robson 2016). Therefore, GNDVI is a useful VI, as it does not suffer from the same issues of saturation as NDVI does. GNDVI, uses the green band instead of red, which solves the issue of saturation. It therefore specifically targets green vegetation, and can be used for vegetation monitoring (Gillani et al. 2023). It is also better suited for evaluating chlorophyll content, and it is correlated with water and nitrogen content (Gillani et al. 2023, Yang et al. 2020). Another interesting VI is SR, which was first described by Birth & McVey (1968). SR is the simplest of the three indices, and it is a ratio between the NIR and red bands. The red band is sensitive to chlorophyll content, since red light is absorbed by chlorophyll, while NIR is sensitive to differences in leaf structure (Silleos et al. 2006). Therefore, this index is suitable for studying vegetation biomass, while being robust to differences in landscape causing variable illumination.

All three VIs (NDVI, GNDVI and SR) capture important crop properties such as vegetation density, health, and moisture content, while complementing each others weaknesses, such as sensitivity to topographic variations and saturation. Therefore, we have chosen to use these three VIs, as they may provide a complete picture that can help us better understand crop status and the agronomic traits under study. In addition to VIs, we will also be using spectral bands, as they provide insight into important physiological traits such a photo-chemical activity and chlorophyll content.

2.2 Experimental Design and MLM

There are two main sources of effects that contribute to the observed phenotypes, namely environmental and genetic effects. To account for and separate the two sources of variance, mixed linear models (MLMs) are used, because such models contain both random and fixed effects. Often, random effects are nuisance-factors whose variance we want to eliminate or account for while modelling fixed effects (Mathews & Crossa 2022). In plant breeding, field trial data often contains noise that can be attributed to environmental factors (like water or fertility gradients) or statistical design (like blocking effects) Mathews & Crossa (2022). MLMs is therefore useful, since it allows us to account for and separate these effects from genetic effects.

In its most basic form, MLM can be described as:

$$\mathbf{y} = X\mathbf{b} + Z\mathbf{u} + \mathbf{e}$$
$$\begin{bmatrix}\mathbf{u}\\ \mathbf{e}\end{bmatrix} \sim N\left(\begin{bmatrix}G & 0\\ 0 & R\end{bmatrix}\right)$$

The term $\mathbf{b}$ are fixed effects to be estimated, and their estimates are referred to as best linear unbiased estimators (BLUEs). On the other hand, $\mathbf{y}$ and $\mathbf{u}$ are random effects to be predicted, and their solutions are called best linear unbiased predictors (BLUPs). The matrices X and Z are design matrices for the fixed and random effects respectively. Normally, we assume the random effects follow a multivariate normal distribution with mean 0, and that they have a specific variance-covariance structure (denoted by G and R).

In addition to MLM, experimental designs with blocking is used in field trials to group plots in close proximity, since we anticipate that they will be more similar to each other (Mathews & Crossa 2022). Alpha-lattice designs are among the most widely used blocking-designs (Piepho et al. 2006, Kumar et al. 2020), and it is used for the field trials described in our study. Its purpose is to allow for many treatments

while having block sizes that are small enough to account for the heterogeneity within each block (Piepho et al. 2006, Kumar et al. 2020).

Furthermore, for this study there are spatial effects (such column position of a plot), temporal effects (time of the flight missions), and environmental effects (season) that we need to consider when modelling the multispectral time-series. Therefore, MLMs are used to estimate the variance and separate these sources of variance from the computed BLUEs for genotypic effects.

Prior to setting genotype as a fixed effect for BLUEs computation, we model it as a random effect to compute broad sense heritability (H^2). It is simply a measure of the experiment's repeatability, and provides a measure of the proportion of total phenotypic variance that can be attributed to genetic effects (Schmidt et al. 2019). It can also be described as a measure of repeatability, which is a useful metric when evaluating the quality of field trials (Schmidt et al. 2019).

2.3 Genome-Wide Association Studies

Association Studies

GWAS is a tool which facilitates the discovery of causal variants by identifying the approximate regions casual variants are located in. It does so by using markers (like single nucleotide polymorphisms, or SNPs) to identify genomics regions that are significantly associated with a trait(Xiao et al. 2022). The identified markers do not need to be casual variants themselves, however, they may be in linkage with casual variants. GWAS is therefore an exploratory analysis, and the identified regions need to be further annotated and functionally validated before making any conclusions about causality. Furthermore, GWA-studies are successful only if the population size under study is large enough, has high genetic diversity, and if the trait under study has high heritability (Sukumaran et al. 2022, Xiao et al. 2022).

The underlying mechanism which GWAS takes advantage of is linkage disequilibrium (LD). LD describes how different loci are associated due to proximity on the chromosome and limited recombination occurring in these regions (linkage) (Hedrick 2011, Sukumaran et al. 2022). In other words, we anticipate that certain genomic regions will more often be inherited in unison (coupling), or alternatively, always segregate (repulsion) from one generation to the next due to LD. In other words, we will observe non-random associations between different genomic regions due to LD.

Despite its usefulness, GWA-studies have to correct for multiple factors like multiple-testing, relatedness and population structure. Multiple hypothesis-testing have to be corrected for because of the high number of markers tested will inevitably lead to false-positive associations (Saini et al. 2021). The main correction methods used for GWAS on wheat populations are Bonferroni correction and Benjamini–Hochberg method (BH) (Saini et al. 2021). Bonferroni correction of p-values ensures that the family-wise error rate for a collection of n-tests is below or at a given significance level α, while BH-procedure controls the false discovery rate (FDR) and ensures that it is below a certain level α (Chen et al. 2021). There is no consistent correction-scheme when reviewing literature on GWAS in wheat population, and some studies employ p-value thresholds instead (like $p < 0.001$) as described by Saini et al. (2021). Although Bonferroni correction is stringent, resulting associations are unlikely to be false-positive, and therefore worth further study (Saini et al. 2021). However, it may yield many false negatives, making FDR correction a preferred balance between false positives and missed associations. As there is no consensus, this study compares GWAS results using Bonferroni-correction and an alternative p-value threshold ($p < 0.001$) (see 3.4).

Accounting for Population and Kinskip Structures via MLM

MLM is the most widely used GWAS model (Saini et al. 2021, Lozano et al. 2023). As discussed earlier, MLM can be used to account for factors influencing the target variable (confounding variables). We need to consider two confounding variables: 1) population structure, 2) familial relatedness (kinship) (Yu et al. 2006, Zhang et al. 2010). Failing to account for these variables will result in spurious associations (Zhang et al. 2010, Lozano et al. 2023). To account for these factors using MLM, we first add population structure as a fixed effect to the model. Next, kinship (computed using pedigrees or markers) is accounted for by modelling it in the covariance-structure of the random effect of individuals (Zhang et al. 2010).

Population structure may be modelled using principal component analysis (PCA) or admixture-models (Engelhardt & Stephens 2010). PCA is a procedure which takes a set of observations (individuals), and projects them onto a lower-dimensional subspace using linear combinations of the original features (Engelhardt & Stephens 2010). These linear combinations (principal components, PCs) are created so that they capture the most variance in the observations, while being orthogonal (i.e. uncorrelated). PCA is done using the genotype matrix (G), hence the original features used to create PCs in this case is the genetic markers of individuals. By performing PCA on G, the resulting PCs capture genetic variation between individuals (Engelhardt & Stephens 2010). For example, observations that are close in the subspace spanned by PCs are assumed to be more genetically similar compared to those further apart. These PCs may be added as covariates in an MLM to remove the effect of population structure on GWAS. By using PCs in this manner, we are assuming that the genetic variation they capture is variation which arises as a result of population structure, which may not always be the case (Xu 2022).

An alternative method is deriving a Q matrix from admixture analysis (Engelhardt & Stephens 2010). Admixture models attempt to determine the proportion of an individual's ancestry that can be attributed to a specific population (Engelhardt & Stephens 2010, Xu 2022). These estimated proportions are summarized in a matrix Q, where each entry signifies the probability of a sample belonging to a given ancestral population (or sub-population). Similarly to PCs, columns in Q may be added as fixed effects in the MLM to control for population structure. In choosing between the two methods, the work by Zhao et al. (2007) shows that the MLM with Q-matrix (with kinship matrix, K) performed similarly to MLM with PCs (with K-matrix).

Although MLM can account for population structure and kinship, the model does have some drawbacks. First, MLM is a single-locus model which may not capture complex traits affected by multiple loci well (Saini et al. 2021). MLM evaluates each SNP independently, however, complex traits are known to be controlled by many small-effect loci which may not be revealed with small populations using MLM (Zhang et al. 2010). Alternative multi-locus models exist, like the multi-locus mixed-model (MLMM) (Segura et al. 2012). Unlike MLM, MLMM is capable of accounting for causative alleles that are spread across multiple loci using a forward-backward stepwise linear mixed-model regression (Segura et al. 2012). Additionally, these models can be further extended to multi-trait variants that consider the co-variance between traits and between environments under study Lozano et al. (2023).

For this report, we are studying a natural population of wheat varieties originating from multiple countries. For this reason, we expect there to be strong population structure present in the wheat panel, as shown in the work by Nannuru et al. (2022) and Mroz et al. (2023). We will therefore be including population structure as a co-variate in our analysis using the Q-matrix derived in the work by Nannuru et al. (2022). Also, it becomes natural to derive kinship from the markers themselves, as there is no pedigree information available. Hence the model to be used in this report is a $Q + K$ MLM.

2.4 Machine Learning & Genetic Algorithm for GWAS

Support Vector Regression

Support vector regression (SVR) is an extension of support vector machines (SVM), where the response variable is continuous. SVM is a binary classification algorithm whose objective is to maximize the margin, which refers to the distance between a separating hyperplane and samples closest to this hyperplane in the feature space (Raschka & Mirjalili 2019*a*). The purpose of the separating hyperplane is to ensure that samples belonging to different classes are positioned on opposite sides of the plane. To achieve this, the hyperplane should have the two following properties:

$$\begin{gathered}\text{For all samples } i \in [1, n] \\ w_0 + w_1 x_{i1} + w_2 x_{i2} + \cdots + w_n x_{in} = -1 \quad \text{if } y_i = -1 \\ w_0 + w_1 x_{i1} + w_2 x_{i2} + \cdots + w_n x_{in} = 1 \quad \text{if } y_i = 1\end{gathered}$$

Note that x_{ij} refers to a feature belonging to sample i, and y_i the class of sample i. The weights w are associated with each feature, and need to be determined via an optimization algorithm. To determine the weights a loss function is needed, which is what we will define in the equations below by combining the two constraints on the hyperplane (Raschka & Mirjalili 2019*a*):

$$\begin{gathered}\frac{\mathbf{w}^T(\mathbf{x}_p - \mathbf{x}_n)}{||\mathbf{w}||} = \frac{2}{||\mathbf{w}||} \\ \Rightarrow M = \frac{2}{||\mathbf{w}||}\end{gathered}$$

The term M refers to the margin which we want to maximize in SVM. Although the overall goal is to maximize the margin, most optimization algorithms in ML are defined to solve minimization problems. Hence we inverse the expression for M to derive a loss function to be minimized. Furthermore, the definition of the margin above requires that all samples are classified correctly. This is called hard-margin classification (James et al. 2013, Raschka & Mirjalili 2019*a*). It is difficult, and at times impossible, to find such a hyperplane, hence we introduce slack variables ξ to allow for some misclassification to occur (James et al. 2013, Raschka & Mirjalili 2019*a*). This version is called soft-margin classification and the loss for this is (Raschka & Mirjalili 2019*a*):

$$J(\mathbf{w}) = \frac{1}{2}||\mathbf{w}|| + C\left(\sum_{i=1}^{n} \xi_i\right)$$

C is a regularization term which determines how much the model should be penalized for misclassifications.

The concepts SVM is built on can be extended to solve continuous or regression problems as well, which is what SVR does. For SVR, the optimization problem is not finding a separating hyperplane, but rather minimize the regression error. This may be expressed as the following regression problem (for the linear case) (González-Camacho et al. 2018):

$$f(\mathbf{x}) = \mathbf{w}^T\mathbf{x} + w_0$$

To find the most appropriate solution, we use the same loss function as earlier, however the slack variables is replaced with the regression error which is defined as $|f(x) - y|$ (González-Camacho et al. 2018).

Moving on, one should note that there is no obvious way to account for confounding variables when using SVR for SNP identification. Accounting for kinship becomes difficult, since there is no specific variance structure we can incorporate relatedness into when using SVR. On the other hand, population structure may be accounted for by including principal components (PCs) or Q-matrix in the feature set. When the PCs (or Q-matrix columns) are included in the feature set, we are including information we have about population structure in the SVR-model. The *phenoRegressor.SVR* in the R package GROAN uses such an approach, where PCs can be included as co-varieties in the feature set for the SVR-function (Nazzicari & Biscarini 2022).

Kernel Methods and Pearson's Universal Kernel

The SVR algorithm described so far can only solve linearly separable problems. However, with the use of kernel-methods, SVR can solve non-linear problems as well (Raschka & Mirjalili 2019*b*). Kernel methods are an efficient way of computing projections of samples onto a higher dimensional space where classes are more easily separable by a linear hyperplane (James et al. 2013, Raschka & Mirjalili 2019*b*). For SVR, the regression problem changes into the following when using a kernel function K (González-Camacho et al. 2018):

$$f(\mathbf{x}) = w_0 + \sum_{i=1}^{n} \alpha_i K(\mathbf{x_i}, \mathbf{x_j})$$

Various kernels exist, each appropriate to its set of classification or regression problems (Üstün, Melssen & Buydens 2006). A special property of kernels is that they measure similarity between samples in different manners (James et al. 2013, González-Camacho et al. 2018). Among these kernels is Pearson's Universal Kernel VII (PUK), which was first described by Üstün, Melssen & Buydens (2006):

$$K(x_i, x_j) = \frac{1}{\left[1 + \left(\frac{2\sqrt{\|x_i - x_j\|^2}\sqrt{2^{(1/\omega)}-1}}{\sigma}\right)^2\right]^{\omega}}$$

Compared to polynomial or radial basis function (RBF) kernels, PUK generalizes better to a wide range of regression problems (Üstün, Melssen & Buydens 2006). This is because it has two hyperparameters σ and ω, which enables it to from various peak-shapes like Gaussian or Lorentzian shapes (Üstün, Melssen & Buydens 2006, Qifu et al. 2009). The idea of using the PUK function for SVR is that the user avoids having to switch between multiple kernels and having to tune their hyper-parameters, which can be time-consuming and computationally expensive. Instead, the user may use this universal kernel and tune it to achieve similar results.

Genetic Algorithms for Feature Selection

Genetic algorithms (GAs) are optimization algorithms inspired by evolutionary biology, meaning that concepts like mutation, selection, crossover and fitness are used to find optimal solutions (Scrucca 2013). GA is a flexible optimization algorithm because it can solve a wide range of optimization problems, including problems that are non-differentiable, combinatorial problems and problems that require integer solutions (Scrucca 2013, Lambora et al. 2019). This makes GA suitable for solving problems involving feature selection, since selected features can be assigned integer values 0 and 1, while still allowing us to define a

real-valued performance function. When GA is used for feature selection, then a set of features make up a chromosome (i.e. a solution), while a single feature represents a gene (which has value 0 or 1).

As mentioned, GA works by maximizing a function f (fitness), which for feature selection can be described as the following:

$$\text{Select } \{x_j\} \text{ so that:} \quad f = \max_{x_i \in X} f(x_1, x_2, \ldots, x_k), \quad X \in \{0, 1\}$$

Before outlining the workflow of GA, we will first discuss genetic operators used to mimic evolutionary processes. The first is selection, which determines solutions which solutions will be part of the reproducing population (Scrucca 2013). Typically, linear rank selection is used, which entails that the solutions are first sorted and then assigned rank based on their fitness values. Probabilities p is assigned to each solution based on this ranking, where p denotes the the probability of reproducing. A reproducing population is made by sampling from the original population using p as weights. The selection strategy is normally combined with elitism, in which the k fittest individuals are passed on to the next generation regardless of their assigned p-value (Lambora et al. 2019).

The two other operations, mutation and crossover, define how new solutions (offspring) should be generated (Scrucca 2013, Lambora et al. 2019).

From the reproducing population, the mutation operator generates new solutions by randomly modifying the genes of a given solution (Lambora et al. 2019). Various mutation methods exist, such as adding Gaussian noise to the vector of solutions, or altering values at random vector positions with equal probability (uniform random mutations, see Figure 1) (Scrucca 2013).

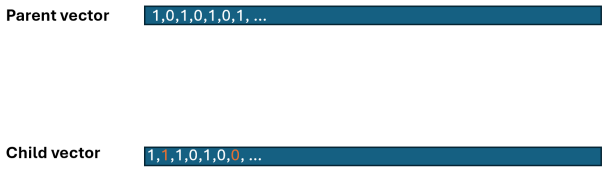

Figure 1: Illustration of mutation of genes (features included or not). The blue lines signify chromosomes (solutions), while the change in genes is highlighted in orange.

The crossover operator produces new solutions by randomly combining the genes of two other solutions (Lambora et al. 2019). Similar to the actual cross-over of chromosomes, one or more points of cross-over is randomly assigned to the two parent solutions, and combined solutions are generated (see Figure 2 for one-point cross-over).

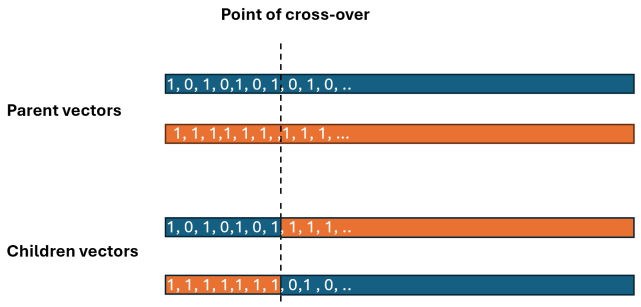

Figure 2: Illustration of one-point cross-over. The numbers refer to genes (features included or not), and the orange/blue lines are chromosomes (solutions)

We may now describe the workflow of GAs: (Lambora et al. 2019):

1. Initialize a random population of solutions $\theta_i^{(0)}$ of size n, and let k denote the current generation (which is 0 for the initial population):
$$\{\theta_1^{(0)}, \theta_2^{(0)}, \ldots, \theta_n^{(0)}\}$$
2. Define a fitness function $f(\theta_i^{(k)})$ which evaluates the performance of an individual solution with respect to the defined problem.
3. Assign each individual solution a value $p_i^{(k)}$ which denotes its probability of being part of the reproducing population. Usually, scaled fitness values that lie between $[0, 1]$ are used to compute $p_i^{(k)}$.
4. Sample from the current population using the generated probabilities $\{p_1^{(0)}, p_2^{(0)}, \ldots, p_3^{(0)}\}$ as weights to create a reproducing population.
5. Let cross-over, mutation and elitism generate new solutions from the reproducing population which form the next generation $k + 1$:
$$\{\theta_1^{(1)}, \theta_2^{(1)}, \ldots, \theta_n^{(1)}\}$$
6. Repeat steps 3-5 until a convergence criteria or maximum iteration criteria is met.

For this report, GA will be used as a wrapper to select features (SNPs) for the SVR-model. GA are suitable for identifying not only SNPs that are important to predict the spectral phenotype, but may also capture interactions between SNPs as shown in the work by (Mooney et al. 2012). GA-wrappers have been used in combinations for SVR for SNP selection in both animal (de Oliveira et al. 2014), and for human studies (Mooney et al. 2012, Díez Díaz et al. 2021).

3 Methodology

3.1 Data Collection: Spectral, Agronomic and Genotypic

Trial Design and Lines

As described by Mroz et al. (2023), a spring wheat panel (MASBASIS) from the Norwegian University of Life Sciences (NMBU) was studied for this report. The panel consisted of both Norwegian and Scandinavian wheat lines, and non-Scandinavian lines provided by International Maize and Wheat Improvement Cente (CIMMYT) originating from countries such as Brazil, France and UK. This report limits itself to data collected at one research field near NMBU (Vollebekk), and considers only 4 seasons (2019-2022). Within each season, field trials with an alpha lattice design was conducted with 46 blocks in 2019, and 48 blocks in the remaining seasons. One block contained 6 plots, and wheat lines were assigned to plots at random and replicated twice (randomized trial). Prior to analysis, border plots and plots showing lodging were removed to avoid border effects and effects lodging has on spectral imaging data. Number of unique lines within each season can be found in Table 1.

Multispectral Data Collection

Multispectral data was collected using UAVs, as described in Mróz et al. (2024) and Shafiee et al. (2024). UAVs were equipped with multispectral sensors, and two different sensors were used to collect spectral data. Micasense RedEdge-M Camera was used in seasons 2019-2020, and DJI Phantom 4 Multispectral (DJI-P4M) was used in seasons 2021-2022. For each plot in the field, the median spectral reflectance value was computed for bands blue, green, red, red-edge and NIR. Details of this process is described in Shafiee et al. (2024). These median band-values per plot are among the spectral phenotypes used for GWAS. The frequency of flight missions differs between seasons (see Table 1). Despite this, the dates of flight missions encompass a short period before heading, the entirety of the heading-stage, and the beginning to middle of maturity-stage.

Table 1: Number of unique lines from the MASBASIS-panel, number of flight missions within each season, and cameras used within each season.

Season	Number of Lines	# Flight missions	Sensor used
2019	220	7	RedEdge-M
2020	268	12	RedEdge-M
2021	293	22	DJI-P4M
2022	296	23	DJI-P4M

Agronomic Traits Collection

Agronomic traits recorded in the field were grain yield (GY, g/m2), days to heading (DH, dss), days to maturity (DM, dss), plant height (PH, cm), grain protein content (GPC, %). The collection of these traits are described in Mroz et al. (2023) and Mróz et al. (2024). GY, PH and GPC were measured at the end of each season. DH and DM were recorded when at least 50 % of plants within a plot had reached the respective states (heading or maturity). Correlations between agronomic traits and spectral phenotypes

were computed prior to GWAS. Also, mean DH and DM were computed and used to identify different development stages, and to adjust the frequency within each season.

Genotypic Data Collection

Lines were genotyped using TraitGenetics 25 K SNP Chip, and the methodology is further described in (Nannuru et al. 2022). The markers were filtered such that only markers with minor allele frequency (MAF) greater than 0.05 and missing values less than 10 % were kept, making the genotypic dataset identical to the one used by (Mroz et al. 2023). Heterozygous individuals were input as 1 prior to analysis with GAPIT, and as missing values for analysis with GA-SVR.

3.2 Preprocessing of Spectral Data

Computation of VIs

VIs were derived from median spectral reflectance bands for each plot, and used as spectral phenotypes as well. NDVI, GNDVI and SR were computed according to Table 2.

Table 2: Computation of vegetation indices using median spectral reflectance

Vegetation Index	**Formula**	**Reference**
NDVI	$\frac{NIR-R}{NIR+R}$	Deering (1978)
GNDVI	$\frac{NIR-G}{NIR+G}$	Buschmann & Nagel (1993) Gitelson & Merzlyak (1994) Gitelson & Merzlyak (1996)
SR	$\frac{NIR}{R}$	Birth & McVey (1968)

Missing Value Imputation

Missing values for agronomic traits and spectral reflectance values were treated differently. For agronomic data, plot numbers with missing values for agronomic traits were removed.

Spectral reflectance values were measured multiple times during the season (time-series). Therefore, missing values for spectral reflectance bands were imputed using the last observation prior to the date with the missing value (last observation carried forward method, LOCF). This was done since the number of flight mission within each season differed (see Table 1). Hence, to ensure that we had flight mission from comparable growth stages, we had to sample spectral data for dates with missing values using the LOCF-method.

Outlier Detection for Spectral Data

Outlier detection was performed only for the spectral reflectance data using hierarchical clustering along the time-axis with the R package TSclust (v.1.3.1). The purpose of clustering was finding a group of time-points whose spectral reflectance values deviate greatly from the remaining time-points. After each

clustering, a dendrogram was made and 5 groups were made (using base R-function cutree). Potential outliers were identified by finding the group that contained the fewest time-points. Weather data was cross-referenced to explain these outliers, and outliers that could be explained by this data (such as recent rainfall) were excluded from further analysis.

Adjusting Frequency of Time-Series and Binning

Time series of spectral data was sampled so that time-points across seasons were from comparable developmental stages. The stages are defined according to the work of Krause et al. (2019) (see Table 3). As described in Shafiee et al. (2024), the sowing dates as well as mean DH within each season were used to find a reference to the following days from heading (DFH): -2, 5, 17, 24, 31, 40. These specific values for DFH were selected because most seasons contain flight missions corresponding to or close to these time-points. The reference point for DFH (DFH = 0) was computed by averaging the DH values for all the plots in the field for each season. This mean value was set as DFH = 0.

Figures displaying the six selected time-points with growth-stages and distribution of DH/DM is given in the appendix (A1). Also in the appendix are plots of the adjusted frequency for average spectral reflectance values and VIs (A2).

In addition to having 6 time-points, we created time-bins HEAD and GF (see Table 3), where the HEAD-bin contained T1-T2, while GF-bin contained T3-T6. The use of these bins are elaborated on in section 3.4

Table 3: Developmental stages and their definitions with respect to DH and DM

Stage	Definition according to Krause et al. (2019)
Vegetative stage (VEG)	"Period between germination and 50% of plots at heading"
Heading stage (HEAD)	"Period between 50% of plots at heading and 100% of plots at heading"
Grain Filling (GF)	"Period between 100% of plots at heading and 100% of plots at maturity"

Computations of AUC-values for VIs

Area under the curve (AUC-value) was computed for the VIs of respective plots. The computation was done using the R-package DescTools (v. 0.99.53). AUC-values were computed by using a trapezoid-method. The computed AUC-values for VIs per plot were among the spectral phenotypes for GWAS. Distribution of computed plot AUC-values within each season are given in the appendix (Figure A3).

Correlation Between Agronomic Traits and Adjusted Spectral Data/AUC-values

After frequency adjustment, Pearson's correlation coefficient was computed between agronomic traits and the following: spectral bands and VIs at each time-point (see Figure 7), and AUC-values of VIs (see Figure 8). Purpose of correlation computations was to investigate if there were linear relationships between agronomic traits of interest (GY, DM, DH, PH and GPC) and the spectral reflectance data at given time-points or accumulated VIs.

3.3 Statistical Models (BLUEs)

For all traits (spectral bands, VIs, AUC-values and agronomic traits) BLUE was computed for the genotypic effect. This was done to account for and remove the effects of spatial variation, environmental effects, and statistical design in the estimated BLUEs for genotype. Since the spectral bands and VIs are time-series, while the AUC-values and agronomic traits are not, we have defined the BLUEs for the latter group differently. Note that BLUEs definitions are similar to those defined in the research by Mroz et al. (2023). Also, in the model definitions upper-case letters (excluding the random error term) refer to random effects (BLUPs), while the lower-case letters refer to fixed effects (BLUEs).

Note that prior to fitting the models specified below, the genotypic effect was modelled as a random effect This was to estimate the the amount of variance attributed to genotype (σ_g^2) compared to the random error term (σ_e^2).

Spectral Bands and VIs

The first model is the **flight trial means**, which are the **mean phenotypic value of spectral bands/VIs at a given time-point for one year and one location** (e.g. T1 for Vollebekk in 2019):

$$P_{ijkl} = \mu + g_i + R_j + R : B_{jk} + C_l + e_{ijkl} \tag{1}$$

The symbols signify the following:

- P_{ijk} is the mean phenotypic value of line (genotype) i, for replicate j, under block k and given location column l.
- μ is the overall mean phenotypic effect
- g_i is the effect of line (genotype) i
- R_j is the effect of replicate j
- $R : B_{jk}$is the effect of block k nested under replicate j
- C_l is the effect of column l
- e_{ijkl} is the random error term

The second model is the **trial means**, which describe **the mean phenotypic value of spectral bands/VIs across time-points for one year and location** (e.g. Vollebekk in 2019):

$$P_{ijklm} = \mu + g_i + T_m + T : R_{jm} + T : R : B_{jkm} + T : C_{lm} + e_{ijklm} \tag{2}$$

T_m is the random effect of time-point m, and all variables except the genotypic effect is nested under this. With nesting we are able to account for variability occurring due to repeated measurements over time, and eliminate this in our estimated BLUEs for trial means. The paper by Krause et al. (2019) had a similar when computing BLUES across all time-points within a season.

The third model is the **global means**, which are **the mean phenotypic value of spectral bands/VIs across seasons and across time-points**(e.g. Vollebekk across 2019-2022):

$$\begin{aligned} P_{ijklm} = \mu + g_i + Y_n + Y:T_{mn} + Y:T:R_{jmn} \\ + Y:T:R:B_{jkmn} + Y:T:C_{lmn} + e_{ijklnm} \end{aligned} \tag{3}$$

Y_n is the random effect of season/year n, and all terms except the genotypic effect are nested under this in the global means. Similar BLUEs were estimated in the papers by Mroz et al. (2023) and Mróz et al. (2024), however, they were referred to as cross-season means. For this thesis, there is only one location, thus we refer to cross-season means as global means.

Agronomic traits and AUC-values of VIs

Note that both agronomic traits and AUC-values are traits measured once per season. Hence we define the exact same BLUEs for these phenotypes.

The first model is **the seasonal trial means**, which defines **the mean phenotypic value of a phenotype P for a given year and location**:

$$P_{ijkl} = \mu + g_i + R_j + R:B_{jk} + C_l + e_{ijkl} \tag{4}$$

P_{ijkl} refers to either the mean AUC-value for a VI or the mean value for a agronomic trait. The remaining terms are defined in the same manner as earlier.

The next model is **the global means for AUC-values of VIs**, which defines**mean phenotypic of a phenotype P across years and for a given location**:

$$P_{ijklm} = \mu + g_i + Y_m + Y:R_{jm} + Y:R:B_{jkm} + Y:C_{lm} + e_{ijklm} \tag{5}$$

Broad-Sense Heritability

Broad-sense heritability (H^2) was computed only for flight trial means seasonal trial means (for both AUC-values and agronomic traits). H^2 was computed by modelling the genotypic effect in equations 2 and 4 as a random effect on the slope so that it is: $g_i \sim N(0, \sigma_g)$. Using this, H^2 is defined as:

$$H^2 = \frac{\sigma_g^2}{\sigma_g^2 + \sigma_e^2} \tag{6}$$

Model Fitting and Solving Convergence Issues

All models were fitted using the R-package lmerTest (v. 3.1.3) and with restricted likelihood estimation (REML). During the fitting of some models, we received error or warning messages related to convergence.

Therefore, prior to fitting, the spectral bands values, VIs and AUC-values of VIs were scaled (using base scale-function in R). This was done to aid the optimization process. Despite this, some models still had convergence failure warnings. To solve this the following procedure was implemented to rule out the possibility of false convergence (inspired by the notebook (*lme4 Convergence Warnings: Troubleshooting* 2024))

1. Check for singularity.
2. Restarting the fitting using more iterations. If warning does not disappear, then do 3.
3. Restarting the fitting using a new solver and add more iterations.

Re-estimated models and those estimated initially were compared using model performance metrics such as Akaike's information criterion (AIC), Bayesian information criterion (BIC), and log-likelihood. All re-fitted models using the procedure above either resulted in the same performance (indicating false convergence-failure warning), or better (indicating that the initial model had not converged towards to an optimal solution). All models with convergence warnings were replaced with the ones refitted using the procedure described above.

3.4 Conventional GWAS-Implementation Using MLM

Mixed Linear Modelling with GAPIT

GWAS was performed using GAPIT 3.4 (v. 2023.9.5). Input data provided were genetic markers (SNPs), genetic map, and a population structure file containing a Q-matrix. Phenotypic input data were the estimated BLUEs described in section 3.3. Peak detection algorithm selected was the single locus, **mixed-linear model (MLM)**. Other agruments in the GAPIT-function was the minor allele frequency (MAF), which was set to MAF > 0.05

Criteria for Significant Associations

We used the following criteria for significant associations to identify consistent peaks in GAPIT-results, which are associations that were replicated across multiple environments (e.g., flight trials or trial means).

1. Passed Bonferroni correction for the global means, and for two different environments (flight trials or trial means). Otherwise, we have
2. Passed a lowered p-value threshold of $p < 0.001$ for global means, and for at least two different environments.

Due to few significant hits with Bonferroni correction, the second criteria was used for all GWAS-runs for further comparative analysis.

Time-points of flight trials were binned prior to determining if the associations were replicated across seasons. Time-points were binned according to definitions in Table 3, so that T1-T2 correspond to the heading stage (HEAD), and T3-T6 correspond to grain filling stage (GF). This was done to down-sample the resolution of time-points, making it easier to compare if associations had been replicated across seasons.

Expanding Regions around Peaks

To identify QTL we expanded the regions around consistent peaks. A window of 40 Mbp, as done in Mroz et al. (2023), was used to search for significant SNPs ($p < 0.001$) that were replicated in at least 2 environments and significant for global means as well.

3.5 SNP-Identification Using Genetic Algorithms and Support Vector Regression

The analysis was adopted from the article by de Oliveira et al. (2014). The alternative ML-pipeline was only implemented for AUC-values and agronomic traits. This is because fitting SVR is computationally expensive, and time-consuming. It was impractical to fit SVR-models for all spectral phenotypes due to limited computational resources and time.

The pipeline for GA-SVR consists of 3 main steps:

1. Group SNPs based on the significance of their correlation (Spearman's) with a given phenotype.
2. Fit SVR with PUK-kernel to each group where SNP are the predictors, and a given phenotype are the target variable (AUC-value or agronomic trait). Also, perform k-fold cross-validation to identify optimal kernel parameters for each group.
3. Select the best performing group and do feature selection by combining the identified SVR-model and a custom GA-wrapper.

Grouping SNPs Using Spearman's Correlation

Spearman's rank correlation coefficient was computed between individuals SNPs and BLUEs of a given phenotype. The resulting p-value was used to group the SNPs into 5 groups. Table 4 shows p-value thresholds used to group SNPs.

Table 4: SNP-grouping, which is similar the method outlined in de Oliveira et al. (2014). P-value refers to Spearman's correlation test computed for phenotype and individual SNPs.

Group no.	p**-value**
1.	$< 10^{-5}$
2.	$< 10^{-6}$
3.	$< 10^{-7}$
4.	$< 10^{-8}$
5.	$< 10^{-9}$

Model Performance Evaluation

For the remaining parts of the pipeline, model performance was evaluated using Pearson's correlation coefficient (r). It was used to evaluate the performance of each fold during the cross-validation step, and it was used to select the best performing group (as described in the next sections). Furthermore, it was

used in the fitness-function developed for the GA-wrapper. r was computed using the formula specified in Equation 7. The metric was computed using the SciPy-package (v. 1.11.2) (Virtanen et al. 2020).

$$r = \frac{\sum(x - \bar{x})(y - \bar{y})}{\sqrt{\sum(x - \bar{x})^2 \sum(y - \bar{y})^2}} \tag{7}$$

Cross-Validation with SVR & Model Performance Metric

SVR-models with Pearson Universal Kernel VII (PUK) were fitted to each group. The kernel is currently only implemented in Weka, hence a custom Python implementation as used (Phillips 2017). In addition, 10-fold cross-validation was performed on the individual groups. This was done to identify optimal hyper-parameters for the kernel terms ω and ϵ. Model performance within each fold was evaluated by r between predicted phenotype and real phenotype.

The group which produced the highest average r was selected for further analysis. All cross-validation and SVR-fitting was performed in Python using Sci-Kit Learn (v. 1.4.0) (Pedregosa et al. 2011).

GA-Wrapper with SVR

A GA-wrapper for feature selection was implemented using the R-package GA (v.3.2.4). The algorithm implemented was a binary algorithm, which encodes features (i.e. SNPs) as 0 or 1, where 1 means the feature was included in the predictor-set for SVR, and 0 means it was not included. A custom fitness function was made so that the GA was tasked to select the best subset of features producing r between the SVR predicted phenotype and the true phenotype. Selected parameters for the GA-wrapper is given in Table 5. Genetic operators were set to default-modes, meaning that linear rank selection, single-point cross-over and uniform random mutation were used.

Table 5: Parameter settings for GA

Parameter Name	**Value/Setting**
P(crossover)	0.8
P(mutation)	0.1
Generations	20
Population size	50
Elitism	1

Final Evaluation of Selected SNPs

The GA-SVR pipeline was run for all seasonal trials and global means of agronomic traits and spectral phenotypes separately. Like for MLM, the goal is to identify assocaitions that remain consistent across environments. Therefore, the following criteria were applied to SNPs that remained after running the GA-wrapper:

1. The association appeared in the final set for at least two environments (seasons) of the seasonal trials run

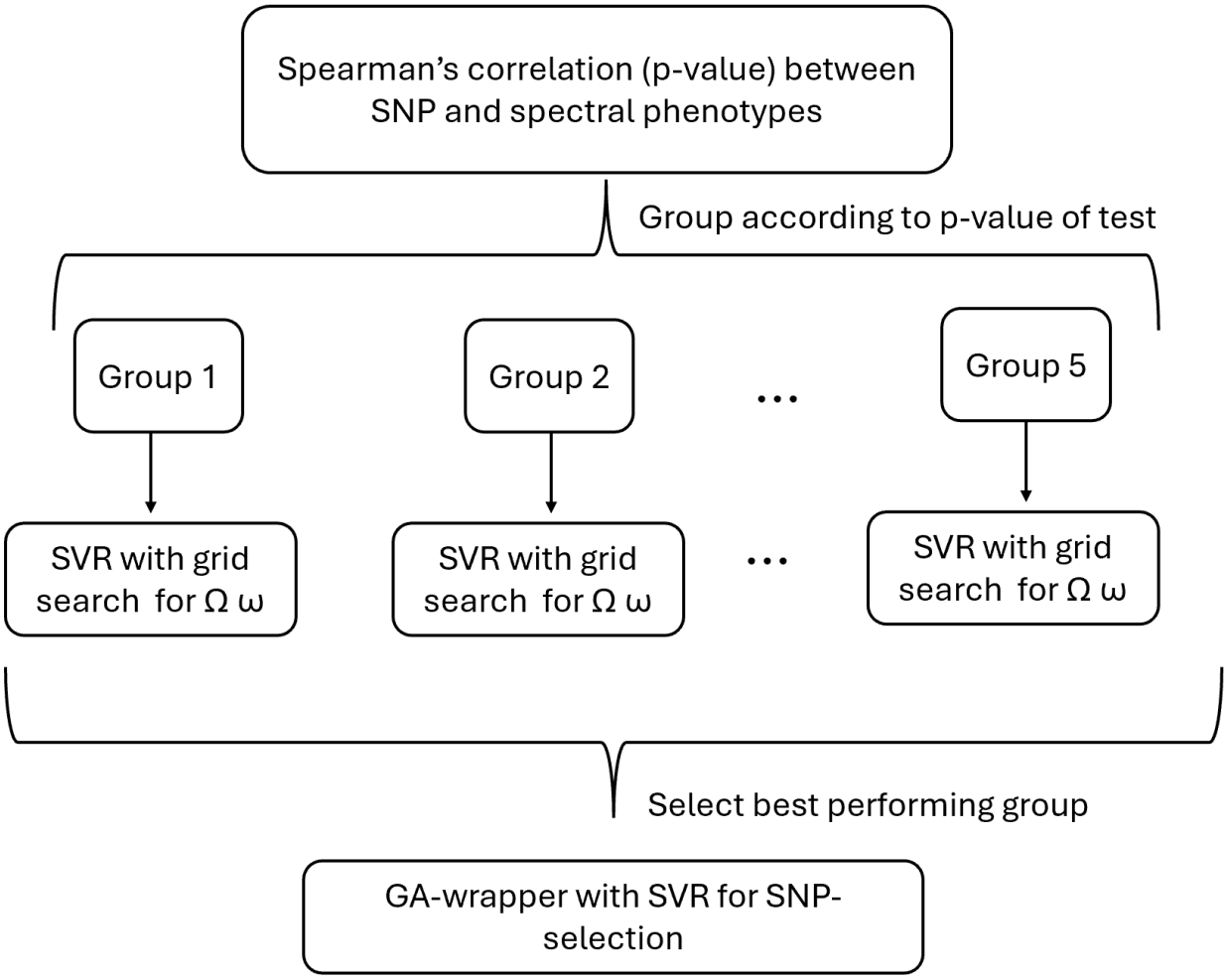

Figure 3: Illustration of the SVR-GA pipeline.

2. The association appeared in the final set of the global means run

The region around consistent peaks (identified by the criteria outlined above) were expanded using the same procedure described in section 3.4

3.6 Stacking of GWAS Results

Once QTL had been identified for both spectral phenotypes and for agronomic traits, we performed a comparative analysis to identify overlapping QTL. The procedure was implemented for QTL identified using MLM and the GA-SVR pipeline seperately. The following procedure was used to identify agronomic QTL that overlap with spectral QTL:

1. For a given agronomic QTL, create a window of 40 Mbp (+/- 20 Mbp) around the region the QTL spans
2. Identify spectral QTL (bands, VIs or AUC QTL) that are within the defined window created in 1.
3. Report location of overlapping spectral and agronomic QTL

3.7 Code Availability

All code used to produce the results presented in this thesis is published on the public GitLab repository: `https://gitlab.com/awoarab/master_thesis.git`. Data sets and result sets have not been published in this repository.

4 Results

4.1 Heritability

Flight Trials

Starting with the heritability computed for flight trial means, we see that all years show high to moderate heritability for spectral bands, having values between 0.60-0.92, with an exception for year 2020 (see Figure 4). The spectral bands with the lowest heritability were NIR in most seasons (2019, 2020, 2021). For VIs, there is no clear pattern, and they appear to be alternating with respect to heritability through time-points and seasons. In year 2020, the lowest heritability was observed for all spectral bands and VIs, with values ranging from 0.57-0.10. Time-point 2 stands out in particular for in year 2020, heritability in this season ranging from 0.37-0.10 for spectral bands and VIs. In this season, the blue and red bands show the most stability having heritability between 0.47-0.57 across all time-points. Interestingly, we observe the lowest heritability of VIs and spectral bands for time-point T2 in both years 2019 and 2020, whereas in 2021-2022 the lowest heritability appears in the last time-point, T6. Despite heritability being lower in T6 compared to other time-points for seasons 2021-2022, it is still moderate to high having values between 0.67-0.93.

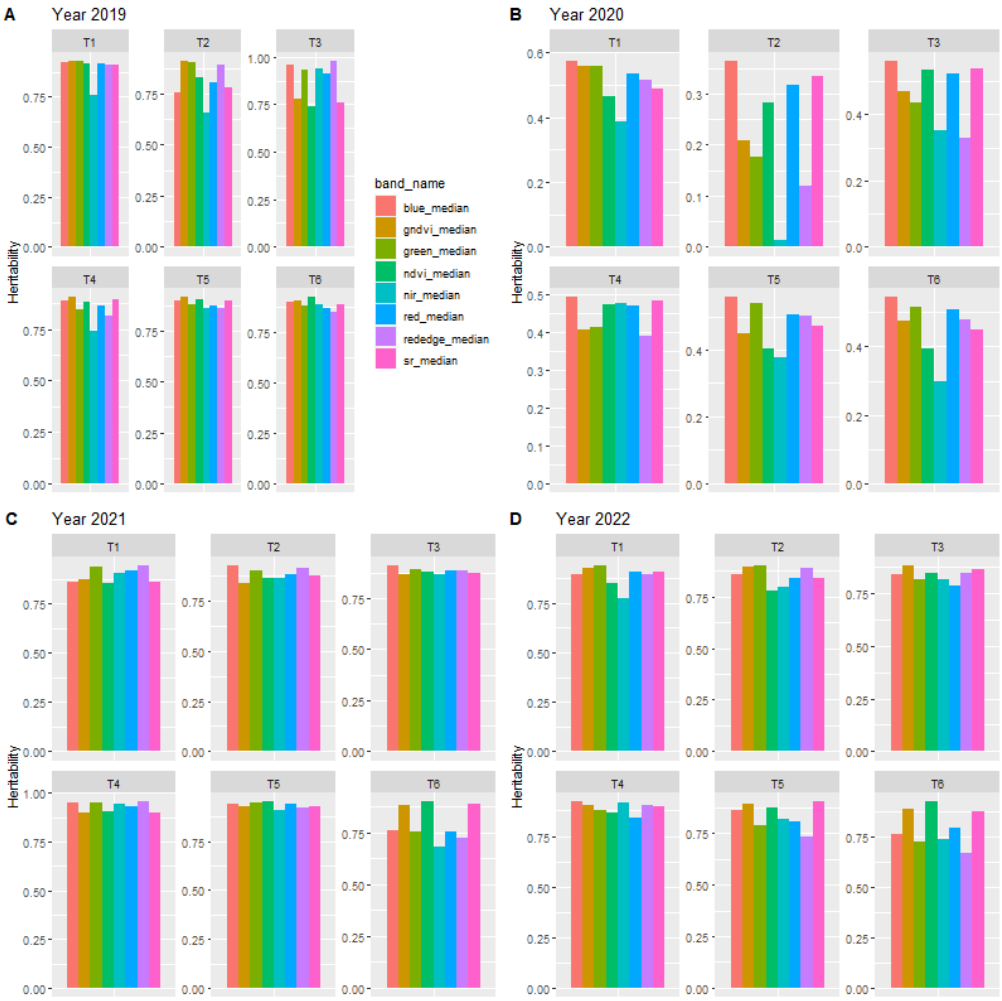

Figure 4: A-D for respective years. Plot of heritability of bands and VIs for flight trials

Seasonal Trials (AUC-values)

Heritability of AUC-values for VIs show more stability over years, including the year 2020. We see the same pattern as in Figure 5, being that heritability in year 2020 is considerably lower compared to the other seasons, having values from 0.41-0.50 (indicating low heritability). In year 2020, SR had a higher heritability value than any of the other VIs, although the difference between VIs is quite small. Excluding year 2020, heritability for ranges from 0.88-0.96. There is no particular pattern with one AUC-value of VI having consistently higher/lower AUC-value, and the differences are minimal.

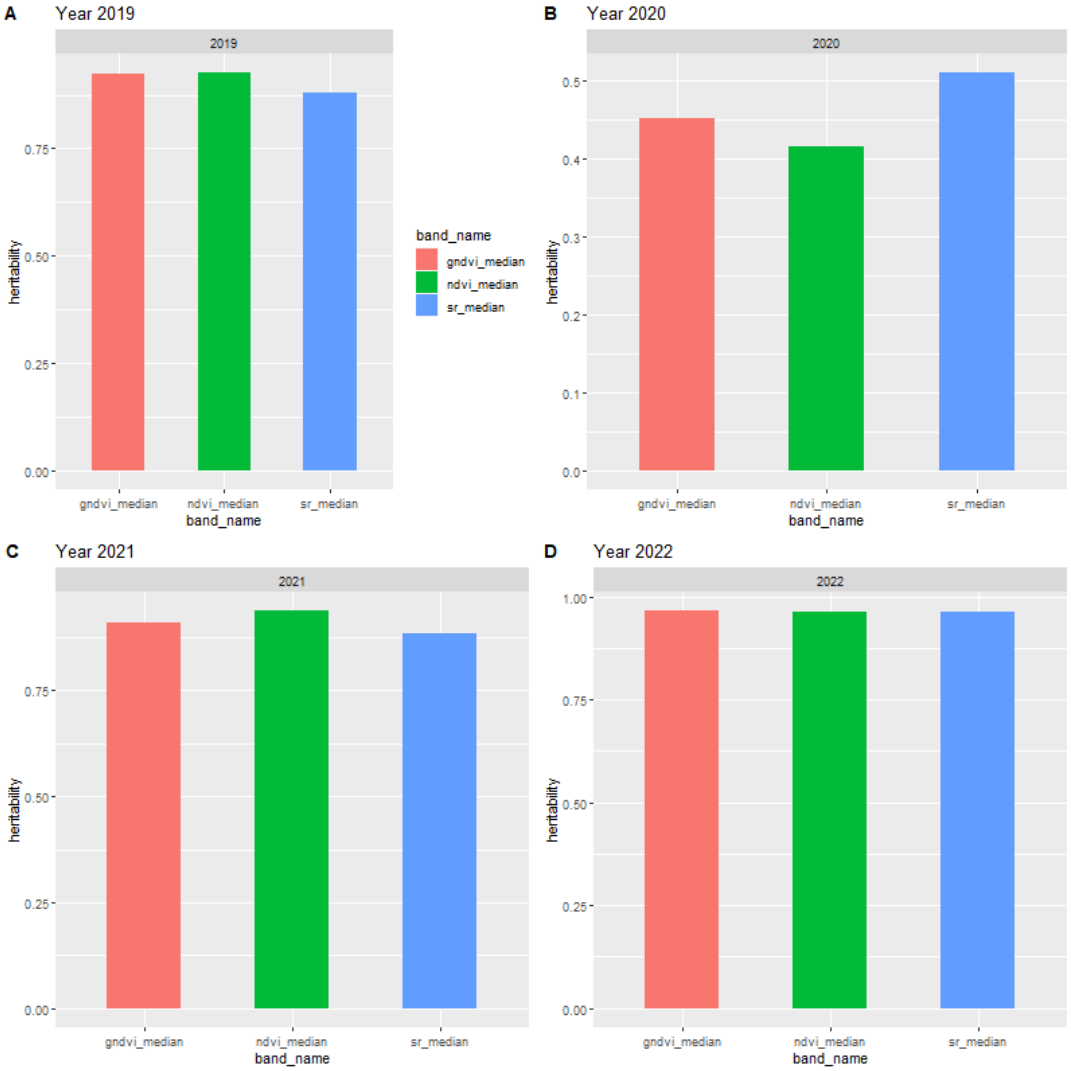

Figure 5: A-D for respective years. Plot of heritability of AUC-values of VIs for seasonal trials

Seasonal Trials (Agronomic Traits)

The heritability of agronomic traits is summarized in Figure 6, and across all seasons we observe high heritability (between 0.76-0.96) for all traits. In general the three traits PH, GPC and GY appear to be producing the highest heritability estimates across all seasons, while DM and DH appear to be slightly lower than the three in all seasons (except in 2022). The greatest estimated heritability appear for GPC in year 2021, while the lowest heritability estimate also appear for GPC in season 2022. Second to GPC is both GY and PH which produce similar estimated heritability throughout all seasons, with 2021 being the season with highest heritability estimates for the two traits ($H^2 \approx 0.94$ for both). For DH the greatest heritability estimate appears in 2021 ($H^2 \approx 0.92$), while for DM this value appear in 2019 ($H^2 \approx 0.88$). Lowest values for DH and DM appear in seasons 2019 for DH ($H^2 \approx 0.88$) and in 2022 for DM ($H^2 \approx 0.81$).

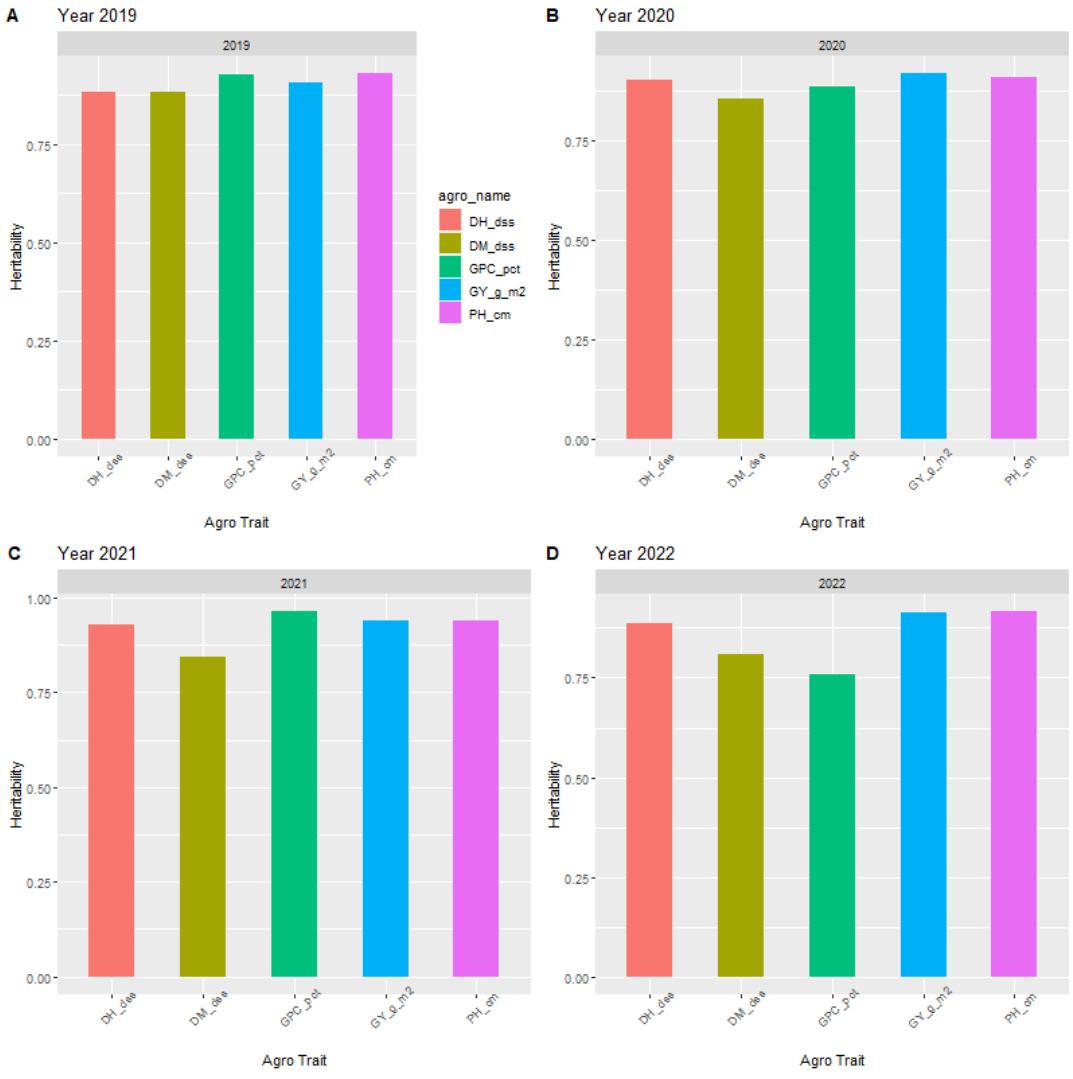

Figure 6: A-D for respective years. Plot of heritability of agronomic traits for seasonal trials

4.2 BLUEs Estimation

Trial Means and Global Means of Spectral Bands/VIs

As described in section 3.3, genotype was modelled as a random effect prior to fitting BLUEs for all models (including trial means and global means). This was to estimate the the amount of variance attributed to genotype (σ_g^2) compared to the random error term (σ_e^2).

Over all years for trial means the estimated error ($\hat{\sigma}_e$) is greater than or of the same size as estimated standard deviation of genotype ($\hat{\sigma}_g$). To illustrate this pattern, we have included the results for trial means in 2019, where genotype is modelled as a random effect in the appendix (see Table A1). Note in Table A1 that random error term for NDVI is estimated as = 0.138, while the estimated standard deviation of genotype is estimated as $\hat{\sigma}_g = 0.068$. This is the greatest difference between $\hat{\sigma}_e$ and $\hat{\sigma}_g$ that appears in table A1, but the general patterns holds for all other bands and VIs. A similar pattern appears in global means as well (see table A2), where the estimated error ($\hat{\sigma}_e$) is significantly larger than the estimated standard deviation of genotype ($\hat{\sigma}_g$). Overall, this pattern indicates that there is a large portion of variability in the spectral phenotypes that remains unexplained.

Global Means for AUC-values of VIs and Agronomic Traits

We also modelled genotype as a random effect before fitting BLUEs for AUC-values and agronomic traits. For the global means of AUC-values and agronomic traits, a different pattern appeared when comparing estimated variance components ($\hat{\sigma}_e$ vs. $\hat{\sigma}_g$) compared to the results in the section above.

For both the AUC-values and agronomic traits, the global means resulted in estimated variance components of genotype that were considerably larger than those estimated for the random error term. Table A3-A4 display the BLUEs estimated for global trials (AUC-values and agronomic traits respectively) where genotype is modelled as a random effect.

In A3, we see how for example the AUC-value of GNDVI resulted in standard deviation of $\hat{\sigma}_g = 0.765$ while the random error term was estimated to $\hat{\sigma}_e = 0.359$. This pattern holds for all global means for VIs. In A4, we see how for example GY resulted in estimated variance for $\hat{\sigma}_g = 74.739$ while the random error term was estimated to $\hat{\sigma}_e = 29.880$.

Unlike the genotype effect estimated for spectral time-series data, it appears that models for AUC-values and agronomic traits estimate larger genotype effetcs (i.e. larger $\hat{\sigma}_g$) compared to the estimated random error ($\hat{\sigma}_e$).

4.3 Correlation Between Spectral Data and Agronomic Traits

Spectral Bands and VIs

Correlations between spectral bands/VIs at each time-point and agronomic traits are summarized in Figure 7. Starting with the first trait DH, the correlations at the initial time points (T1-T2) is near 0.0-0.1 for all spectral bands/VIs for all years except in year 2020. There is a general trend where the VIs (GNDVI, NDVI and SR) increases over time, and reach a maximum value at the latest time-point (T6) with values between 0.4-0.5. The spectral bands show a opposite trend of decreasing over time in all seasons, with red for example reaching the largest negative values at the last time-points (T5-T6) with value between

-0.4 and -0.6. The remaining bands' correlation with DH tend to fluctuate or decrease throughout the season, where for example NIR reaches a maximum the middle of the season (T3-T4) of 0.4-0.5, before it decreases. This pattern for NIR appears for all seasons except in 2019.

DM is among the traits that produce the largest correlations in terms of absolute value (between -0.7 and 0.8). The spectral bands and VIs follow as similar pattern as described for DH. We observe that the VIs (GNDVI, NDVI, and SR) begin with values close to 0.0-0.1 initially (T1-T2) and produce large positive correlation in later time-points (T5-T6) between 0.6 and 0.8. The spectral band show an opposite pattern (except red-edge), in particular the red band, which start with very low correlations initially and reaches negative correlations of between -0.5 and -0.7 at later time-points (T5-T6). Red-edge appears to be quite in 2022, and fluctuates in the remaining seasons with correlation between -0.1 to 0.3.

Next, we consider correlation between spectral data and GPC, where we observe large fluctuations in correlations in seasons 2021 and 2019, and in seasons 2020 and 2022 we observe more stable patterns. We observe moderate correlations with bands/VIs with values between -0.4 and 0.4 in seasons 2020 and 2022, while the correlation in 2019 and 2021 are lower (between -0.2 and 0.2). The red band tends to show the largest positive correlation with GPC in most seasons, with initial correlation of 0.0-0.4 in T1-T2 and correlations of 0.2-0.4 in T5-T6. The VIs (NDVI, GNDVI and SR) tend to show the largest negative correlations with GPC in 2020 and 2022 with correlations between -0.3 4and -0.4 throughout the seasons.

Next, we consider correlation between spectral bands and GY. GY (like DM) shows the greater correlations with bands and VIs compared to other traits in terms of absolute value (between -0.6 and 0.7). For GY there is a clear pattern where VIs (NDVI, GNDVI, and SR) show large positive correlation with GY across most time-points across all seasons (between 0.3-0.7). The greatest correlation for VIs occurs in the mid time-points (T3-T4) for all seasons except in 2020. In 2020 the largest correlation for VIs appears in T6 with values between 0.4-0.7. For the spectral bands, an opposite pattern appears, and this is particularly clear with the red band. The red band produces the largest negative correlations with values between -0.3 and -0.6 throughout the season. For the mid time-points (T3-T4) the largest negative values are produced with values between -0.4 and -0.6.

Lastly, we look into the correlations produces for PH, which produces fluctuating correlations throughout the seasons. where we observe moderate correlations between -0.3 and 0.5 in seasons 2019 and 2022. In seasons 2021 and 2020 the correlations are somewhat larger (absolute values) with values -0.5 and 0.6. Furthermore the red-edge band tends to increase over time in most seasons, starting with initial values of 0.0 reaching maximum value in T5-T6, with values between 0.3 and 0.6. GNDVI has an opposite pattern starting near 0 and reaching its largest negative values at the last time-point (T6) for most seasons, with value between -0.3 and -0.4. However, in 2020, GNDVI shows a high, consistent correlation with PH with values between 0.4 and 0.5 throughout the season.

AUC-values of VIs

Correlations between AUC-values of VIs and agronomic traits are summarized in Figure 8. We observe a positive correlation between AUC-values of VIs and agronomic traits DH, DM and GY across all seasons with correlation coefficients ranging from 0.2-0.8. There's a negative correlation between AUC-values and GPC (between -0.4 and -0.2). For PH, the correlation with AUC-values ranges from moderately (between -0.4 and -0.2) negative to near zero and moderately positive (0.1-0.2), with an exception for 2020. In year 2020, we observe the greatest positive correlation between VIs and PH (0.5-0.6).

All VIs show the greatest correlation with the trait DM across all seasons, with values ranging from 0.4-0.8.

The AUC-value of NDVI appears to have the greatest correlation with DM (0.7-0.8) throughout all seasons. For GY, GNDVI shows the greatest correlation throughout all seasons (0.6-0.7).

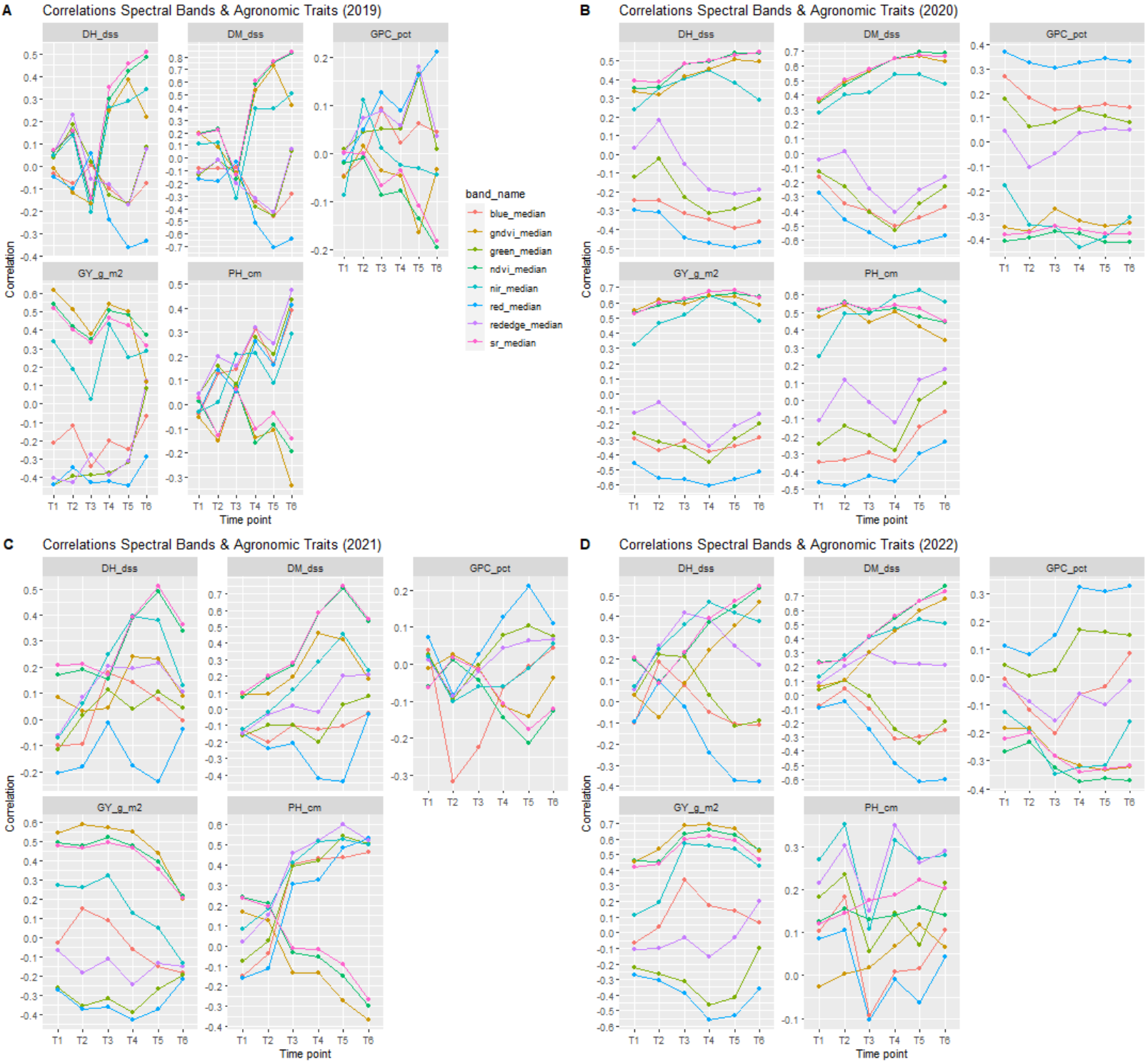

Figure 7: A-D for respective years. Plot of Pearson's correlation between agronomic traits and spectral reflectance values /VIs at different time-points (T1-T6).

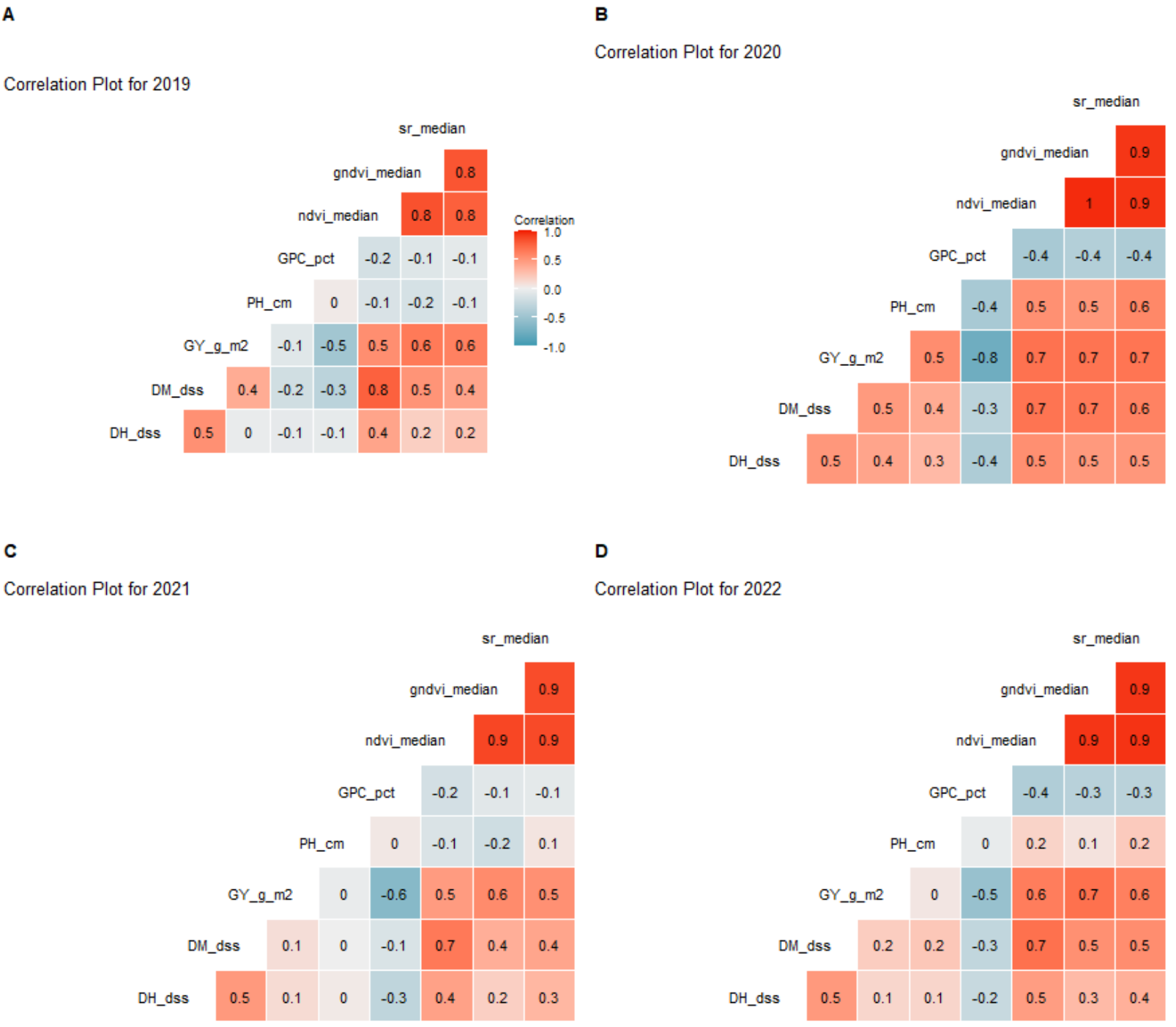

Figure 8: A-D for respecive years. Plot of Pearson's correlation between agronomic traits and AUC-values for VIs.

4.4 GWAS Results with MLM

4.4.1 Flight Trials

We first look into results for flight trials. No significant associations (peaks) identified for flight trials were replicated across seasons when using Bonferroni correction. This may be due to the stringent correction of p-values. When using the alternative p-value threshold ($p < 0.001$), 354 associations were replicated across seasons. Keep in mind that environments for flight-trials were defined in terms of both seasons and time-bins (meaning that time-points were assigned to either HEAD or GF time-bin).

Furthermore, the alternative p-value threshold identified a considerably greater number of significant peaks compared to Bonferroni correction, as seen in Table 6. Regardless of which criteria we use, we detect most associations in season 2021. In 2021 we detected 23 associations (13 unique SNPs) with Bonferroni correction, while with the p-value threshold we detected 1877 associations (474 unique SNPs).

In addition, flight trial phenotypes contain information about developmental stage (HEAD vs GF), and Table 6 shows the number of peaks identified within each time-bin for Bonferroni correction and alternative p-value threshold. We observe that most significant associations are identified for the GF-stage. For Bonferroni correction, there are no associations that appear for spectral phenotypes recorded in the HEAD-stage in seasons 2020 and 2022. We observe a similar pattern for peaks identified with the alternative p-value, where for example in 2021 there are only 259 peaks identified in the HEAD-stage, while the GF-stage contains 1618 associations (see Table 6).

We may look further into the specific positions of these associations identified with the $p < 0.001$. For the GF-stage, most significant associations appear on chromosomes 2A, 5A and 4B (598, 393 and 334 respectively). On chromosome 2A, most peaks appear in the region 74-78 Mbp. On 5A, most peaks appear on 438 Mbp, while on chromosome 4B most peaks appear in the region 20-79 Mbp.

For HEAD-stage, most significant associations appear on 3B, 3A and 5A (151, 141 and 121 respectively). On chromosome 3B, the peaks appear in the region 563-576 Mbp. On 3A the peaks appear in 445 Mbp and between 615-620 Mbp, while on 5A peaks appear mostly in the region 617-646 Mbp.

Table 6: Summary of GWAS-results for flight trials

Season	# peaks Bonferroni (unique SNPs)	# peaks Alt p-val (unique SNPs)	# peaks Bonferroni HEAD/GF	# peaks Alt p-val HEAD/GF
2019	7 (5)	1366 (514)	4/3	437/929
2020	2 (2)	684 (293)	0/2	210/474
2021	23 (13)	1877 (474)	3/20	259/1618
2022	6 (3)	1261 (492)	0/6	397/864

4.4.2 Trial Means

GWAS for trial means produced no or only one significant peak in all seasons, with an exception for 2021 when using Bonferroni correction (see Table 7). When considering the alternative p-value, we identify more peaks for all seasons compared to Bonferroni correction. Season 2021 produced the greatest number of peaks for the alternative threshold with 446 associations (197 unique SNPs). Furthermore, no associations were replicated across seasons with the Bonferroni corrected results. On the other hand, 74 associations were replicated when using the alternative threshold.

Next, we consider the associations identified with $p < 0.001$. The majority of associations appeared for the blue and green bands, and for GNDVI in all seasons. Since most assocaitions are appearing for these bands, we may look into the specific positions of these associations. Starting with the blue and green bands, most associations appear on chromosome 2A, 7A, 5A when all seasons are considered. For the GNDVI most associations appear on 2A, 5A and 5B.

Table 7: Summary GWAS-results for trial means

Season	# peaks Bonferroni (unique SNPs)	# peaks Alt p-val (unique SNPs)
2019	1	201 (114)
2020	0	132 (66)
2021	7 (4)	446 (197)
2022	0	223 (151)

4.4.3 Global Means of Spectral Bands/VIs

First, we summarize the differences in significant peaks when using Bonferroni-correction and the alternative p-value threshold. The number of associations detected using $p < 0.001$ is significantly greater than that of Bonferroni corrected results. As we can see in Table 8, the alternative threshold produced 318 significant associations, where 222 of these were replicated in at least 2 environments. Bonferroni correction produced only 8 significant peaks, with only two of them being replicated in 2 or more environments. For Bonferroni corrected markers, most associations appear on chromosome 2A. The remaining associations appear on 1A and 3D.

Table 8: Summary GWAS-results for global means

Correction method	# peaks (unique SNPs)	# replicated in 2 environments (unique SNPs)
Bonferroni	8 (7)	2 (2)
$p < 0.001$	318 (183)	222 (138)

Since the alternative p-value threshold produced a greater number of associations, these results were used to identify replicated peaks and expand the regions around such peaks to find QTL (see section 3.4). The identified QTL for the spectral time-series data is given in the appendix (see Table A5). Most associations appeared for the spectral phenotypes red-edge, green and NIR. The VIs NDVI and GNDVI produced the fewest number of QTL. Furthermore, most QTL appeared on chromosomes 2A , 3B and 4B. For all these chromosomes, most associations were related to the red-edge, green and NIR bands. Furthermore, there are multiple QTL that overlap for different phenotypes. For example, in the region 591-592 Mbp of chromosome 1A, QTL were found for all spectral bands (blue, green, NIR, red, and red-edge). Also, the QTL spanning 31-59 Mbp on 4B appears for both the red-edge and red band.

4.4.4 Seasonal Trials of AUC-values for VIs

With Bonferroni correction the seasonal trials did not produce any significant peaks. The alternative p-value threshold produced some results which are summarized in Table 9 for the different VIs. There

are a significant number of associations in 2019 (90 peaks) and 2021 (78). For all seasons, except 2022, AUC-values for GNDVI produce more peaks compared to the other two VIs. We see this particularly in 2019 where GNDVI produced 50 peaks, whereas NDVI and SR produced 22 and 18 respectively. The difference in number of significant peaks between phenotypes in the remaining seasons is quite small.

Table 9: Summary of GWAS-results for seasonal trials of AUC-values

Season	# Peaks Total (Unique SNPs)	# Peaks NDVI	# Peaks GNDVI	# Peaks SR
2019	90 (79)	22	50	18
2020	35 (22)	11	12	11
2021	78 (65)	21	29	28
2022	47 (39)	14	15	18

Next, we look into the specific results for seasonal trials. The alternative p-value threshold identified 250 associations on chromosomes 4B (29/250), 7A (29/250), and 4A (25/250). The majority of associations on chromosome 4B were for NDVI (20/29). On 7A, the majority of associations were produced by GNDVI (12/29). On 4A, all VIs were found in the 25 associations with comparable frequency.

4.4.5 Global Means for AUC-values for VIs

A summary of GWAS-results is given in Table 10, which shows both associations identified for global means and associations that are replicated in two environments for seasonal trials. Since no peaks were identified for global means of AUC-values for VIs with Bonferroni correction, the alternative p-value ($p < 0.001$) was used to identify significant markers. Using this alternative threshold, the total number of peaks for global means of AUC-values for VIs is 52. SR produces the greatest number of associations (22/52). Of these 52 associations, only a total of 11 peaks have been replicated in at least two environments in the seasonal trials.

Table 10: Summary of GWAS-results for global means of AUC-values

Phenotype	# Peaks	# replicated in 2 environments
NDVI	15	2
GNDVI	15	5
SR	22	4

Table A6 in the appendix summarizes QTL identified for the AUC-values. QLTs were identified as described earlier (see 3.4). We see that most peaks appeared on chromosome 4B and 6B. Associations on chromosome 4B were related to NDVI, while assocaitions on 6B were related to SR. Most QTL described in Table A6 were related to NDVI, and NDVI produced additional QTL on chromosome 5A and 7A. The QTL identified on chromosome 7A is also related to GNDVI.

4.4.6 Seasonal Trials for Agronomic Traits

A summary of peaks identified for seasonal trials is given in Table 11. As seen earlier, the alternative p-value produces more assocaitions compared to the Bonferroni corrected results. The total number of

associations identified with the alternative threshold is 807 (517 unique SNPs), while with Bonferroni we only identify 79 associations (42 unique SNPs) when all seasons are considered. Common for the two correction methods is that the greatest number of associations occurred in season 2019. Furthermore, in season 2022 we identify the fewest number of assocaitions for both methods.

Table 11: Summary GWAS-results for seasonal trials of agronomic traits

Season	# peaks Bonferroni (unique SNPs)	# peaks Alt p-val (unique SNPs)
2019	43 (37)	313 (255)
2020	5 (5)	174 (154)
2021	18 (18)	163 (151)
2022	12 (13)	157 (149)

Most associations produced with $p < 0.001$ appeared on chromosomes 2A, 7B and 5A (46, 44 and 43 unique SNPs respectively). On 2A peaks appeared for DM, while on 7B and 5A most assocaitions appeared for GY and GPC. Moving on, when considering all associations identified, we see that most associations are produced for GPC, DM and GY (172, 152 and 145 unique SNPs respectively). There were fewer SNP identified for PH and DH (86 and 70 unique SNPs respectively). Furthermore, it should be noted that out of all associations identified with the alternative p-value, 120 assocaitions were replicated across 2 or more seasons.

4.4.7 Global Means for Agronomic Traits

A summary of peaks identified for global means is given in Table 12, which show both associations identified for global means and associations that are also replicated in two environments for seasonal trials. We identify 17 peaks using Bonferroni correction, all of them related to PH and located on chromosomes 4A-4D. On chromosome 4B, the assocaitions span the region 31-79 Mbp.

Using the alternative threshold we identify 169 peaks, which is considerably larger. Most of these associations are related to DM, GY and PH (43, 39 and 35 peaks respectively). The greatest number of associations appear on chromosomes 4B, 2A and 6B. We may look further into the associations appearing on these chromosomes, starting with 4B where most peaks were related to PH and span the region 31-79 Mbp. The remaining assocaitions on 4B were related to DM and GY. On chromosome 2A most assocaitions were related to DM and PH. On chromosome 6B most associations occurred for DM.

Table 12: Summary GWAS-results for agronomic traits

Correction method	# peaks (unique SNPs)	# replicated in 2 environments (unique SNPs)
Bonferroni	17 (17)	17 (17)
$p < 0.001$	169 (148)	80 (74)

The alternative p-value threshold was used to identify QTL, and results are summarized in Table A7. First note that *Q_PH_4B_1*, located in the region 13-79 Mbp, contains the greatest number of peak markers. Many of the identified QTL in A7 are produced by only 1-2 markers with an exception for *Q_PH_4B_1* and *Q_PH_4D_1*, where the first was identified by 18 peak markers while the latter was identified by 3

peak markers. These QTL, in addition to *Q_PH_4A_1*, were significant when using Bonferroni correction as well, hence we can be confident in the significance of these QTL.

4.4.8 Stacking of Agronomic and Spectral GWAS-results

As described in section 3.6, the identified QTL for spectral phenotypes and agronomic traits were stacked to identify overlapping QTL. These results are given in Table 13. There are 29 instances of spectral time series QTL overlapping with agronomic QTL. Furthermore, we see that most overlapping spectral QTL overlap with regions identified for DM and PH. We may look further into the results for each phenotype.

Starting with DH, we see that there are 5 unique QTL for DH that overlap with regions identified for the spectral time-series. Note that although they overlap, they share only 1 peak marker. Spectral phenotype that overlap with DH are NIR, NDVI and SR. Interestingly, the QTL for NDVI and SR (*Q_NDVI_7A_2*, *Q_sr_7A_2*) appear on the same location and overlap with *Q_DH_7A_1*.

For DM, there are 13 unique spectral QTL that overlap with genomic regions identified for this trait. The spectral QTL *Q_green_2A_1*, *Q_NIR_2A_1* and *Q_rededge_2A_1* span a larger region, and they are within the 40 Mbp window defined for the DH related region *Q_DM_2A_1*. Next, we see how on chromosome 4A, *Q_NDVI_4A_1* and *Q_red_4A_1* are located in the exact same positions as *Q_DM_4A_1*. Moving regions on chromosome 4B for the spectral phenotypes NDVI, SR, red-edge and red (located on 20-32 Mbp and 31-59 Mbp) overlap with *Q_DM_4B_1*. This particular overlap is interesting, and will be further discussed in 5.2. Lastly, a single overlap appears on chromosome 5A between a QTL identified for the blue band and DM (548-549 Mbp).

Next, for GPC we see co-localized QTL on chromosome 1B and 5A. On 1B the overlap is in the region 662-672 Mbp, and appears for the spectral phenotypes green and red-edge. On 5A, a QTL for NIR is near a QTL identified for GPC appearing in the region 2-10 Mbp.

For GY, we observe overlapping QTL on chromosome 2A and 7A. On chromosome 2A the region spans 758-773 Mbp. The overlap appears for three spectral phenotypes (red, red-edge, and green bands), while on 7A only 1 phenotype overlaps with GY QTL.

For PH we identify overlapping QTL on 4B chromosome in the region 20-59 Mbp. The number of peak markers is greater than 2 for both the PH QTL and spectral QTL with an exception for *Q_sr_4B_1*. The band red-edge and red bands produce the greatest number of peaks compared to the remaining spectral phenotype. The importance of this region for PH will be further discussed in section 5.2.

Table 13: Results for agronomic QTL that overlap with spectral time-series QTL (bands and VIs)

Spectral QTL	Agronomic QTL	Agronomic Trait	Span (Spectral)	Span (Agronomic)	# Markers (Spectral)	# Markers (Agronomic)
Q_NIR_3A_1	Q_DH_3A_1	DH_dss	267	267	1	1
Q_NIR_5A_1	Q_DH_5A_1	DH_dss	10	10	1	1
Q_NDVI_7A_2	Q_DH_7A_1	DH_dss	669	669	1	1
Q_SR_7A_2	Q_DH_7A_1	DH_dss	669	669	1	1
Q_NIR_7B_1	Q_DH_7B_1	DH_dss	62	62	1	1
Q_green_2A_1	Q_DM_2A_1	DM_dss	74-78	63	6	1
Q_NIR_2A_1	Q_DM_2A_1	DM_dss	74-77	63	13	1
Q_rededge_2A_1	Q_DM_2A_1	DM_dss	74-78	63	18	1
Q_NDVI_4A_1	Q_DM_4A_1	DM_dss	25	25	1	1

Table 13 continued: Results for agronomic QTL that overlap with spectral time-series QTL (bands and VIs)

Spectral QTL	Agronomic QTL	Agronomic Trait	Span (Spectral)	Span (Agronomic)	# Markers (Spectral)	# Markers (Agronomic)
Q_red_4A_1	Q_DM_4A_1	DM_dss	25	25	1	1
Q_NDVI_4B_1	Q_DM_4B_1	DM_dss	20-32	32	3	1
Q_red_4B_1	Q_DM_4B_1	DM_dss	31-59	32	6	1
Q_rededge_4B_1	Q_DM_4B_1	DM_dss	31-59	32	8	1
Q_SR_4B_1	Q_DM_4B_1	DM_dss	20	32	1	1
Q_blue_5A_2	Q_DM_5A_1	DM_dss	549	548	1	1
Q_green_5A_3	Q_DM_5A_1	DM_dss	549	548	1	1
Q_NIR_5A_2	Q_DM_5A_1	DM_dss	549	548	1	1
Q_rededge_5A_2	Q_DM_5A_1	DM_dss	549	548	1	1
Q_green_1B_1	Q_GPC_1B_2	GPC_pct	672	662	2	1
Q_rededge_1B_1	Q_GPC_1B_2	GPC_pct	668	662	1	1
Q_NIR_5A_1	Q_GPC_5A_1	GPC_pct	10	2	1	1
Q_green_2A_3	Q_GY_2A_1	GY_g_m2	773	758	1	2
Q_red_2A_2	Q_GY_2A_1	GY_g_m2	773	758	1	2
Q_rededge_2A_3	Q_GY_2A_1	GY_g_m2	770	758	1	2
Q_green_7A_2	Q_GY_7A_1	GY_g_m2	51-92	112	4	2
Q_NDVI_4B_1	Q_PH_4B_1	PH_cm	20-32	13-79	3	18
Q_red_4B_1	Q_PH_4B_1	PH_cm	31-59	13-79	6	18
Q_rededge_4B_1	Q_PH_4B_1	PH_cm	31-59	13-79	8	18
Q_SR_4B_1	Q_PH_4B_1	PH_cm	20	13-79	1	18

Moving on, we look into overlapping QTL for agronomic traits and AUC-values of VIs. Table 14 summarizes these results. There is only one AUC-QTL for NDVI which overlaps with DM and PH. It is the previously described region on chromosome 4B (13-79 Mbp).

Table 14: Results for agronomic QTL that overlap with spectral time-series QTL (bands and VIs)

AUC QTL	Agronomic QTL	Agronomic Trait	Span (AUC)	Span (Agronomic)	# Markers (AUC)	# Markers (Agronomic)
Q_NDVI_4B	Q_DM_4B_1	DM_dss	20-32	32	3	1
Q_NDVI_4B	Q_PH_4B_1	PH_cm	20-32	13-79	3	18

4.5 GWAS-Results with GA-SVR Pipeline

4.5.1 Grouping of SNPs: AUC-values

Grouping of SNPs was done as described in section 3.5 using using the p-value derived from Spearman's correlation coefficient. The purpose was to test the correlation between AUC-values of VIs and individual SNPs. Starting with the results for seasonal trials of AUC-values given in Table A10, we see that group size decreases as the p-value threshold decreases for all seasons and all phenotypes. Also, there are large differences in group sizes across seasons. For example, in years 2020-2021 we observe generally smaller groups across all p-value thresholds. In 2020 NDVI produced the largest groups with 78 SNPs ($p < 10^{-5}$),

and in 2021 SR produced the largest groups with 169 SNPs ($p < 10^{-5}$). All p-value groups are significantly larger in 2022 for all phenotypes, especially for groups with the lower p-value thresholds. The largest group for 2022 appears for GNDVI with 774 SNPs ($p < 10^{-5}$). When we consider the group with the lowest p-value threshold ($p < 10^{-9}$) in year 2022, we see that we have 33 SNPs and the group is for GNDVI.

Similar grouping was done for the global means of AUC-values as well (see table A11). We observe a similar pattern with respect to group size and p-value thresholds. The larger groups are the ones with the highest p-value thresholds. Moreover, GNDVI produced larger groups when compared to the other VIs, which was also the case for seasonal trials. Unlike seasonal trials, the group sizes for the lowest p-value thresholds are larger.

4.5.2 Grouping of SNPs: Agronomic Traits

Next we look into the grouping of SNPs done for agronomic traits, starting with the results for seasonal trials. As seen earlier for the AUC-values, group size decreases as p-value threshold decreases for all seasons and all phenotypes (as seen in Table A12).

Season 2019 produced the smallest groups for all phenotype across all thresholds. Furthermore, we see that GY and GPC produces the largest groups for all years. For example in 2019, GY produced 167 SNPs and GPC produced 26 SNPs for the highest p-value group ($p < 1 \times 10^{-5}$). In the remaining seasons, the two phenotypes produced considerably larger groups. For example in 2022 GY produced 4973 SNPs for the highest p-value threshold ($p < 1 \times 10^{-5}$), while GPC in 2020 produced 2922 SNPs for the highest p-value threshold ($p < 1 \times 10^{-5}$).

The phenotypes DH, DM and PH generally had smaller groups compared to GY and GPC for most seasons. This is particularly true for DH, which had only 11 SNPs for the highest p-value threshold ($p < 1 \times 10^{-5}$) in 2019. In season 2022, DH had 182 SNPs for the highest p-value threshold. On the other hand, DM produced 1755 in the same season (2022) for the highest p-value threshold ($p < 1 \times 10^{-5}$). PH produced its greatest number of SNPs in season 2021, with 247 SNPs for the highest p-value threshold ($p < 1 \times 10^{-5}$).

For the global means of agronomic traits, we observe a similar pattern (Table A13). The larger groups are the ones with the highest p-value thresholds. Furthermore, GY and GPC produced the largest groups across all p-value groups.

4.5.3 Cross-Validation Results for SVR-Tuning: AUC-values

Starting with seasonal trials, Table 15 contains results for the best-performing group after fitting SVR with 10-fold CV to each group identified in the previous step. The best performing group (in terms of Pearson's correlation) for seasons 2019-2021 is group 1 or 2 ($p < 10^{-5}, 10^{-6}$). For 2022, groups with lower p-value thresholds have better performance. For example for GNDVI in 2022, the best performing group is group 4 ($p < 10^{-8}$). For NDVI and SR in 2022, the the best performing group is group 3 ($p < 10^{-7}$). This difference between seasons is not surprising, since the groups in year 2022 is much larger than groups in 2019-2021. Therefore, groups that have lower p-value thresholds in 2022 may still contain sufficient number of SNPs to perform well with SVR.

Table 15: Results for cross-validation for seasonal trials of AUC-values.

Year	Phenotype	Group No.	p-threshold	Pearson's correlation
2019	GNDVI	2	1×10^{-6}	0.980
2019	NDVI	1	1×10^{-5}	0.988
2019	SR	2	1×10^{-6}	0.934
2020	GNDVI	1	1×10^{-5}	0.836
2020	NDVI	1	1×10^{-5}	0.886
2020	SR	1	1×10^{-5}	0.607
2021	GNDVI	1	1×10^{-5}	0.629
2021	NDVI	1	1×10^{-5}	0.939
2021	SR	2	1×10^{-6}	0.954
2022	GNDVI	4	1×10^{-8}	0.989
2022	NDVI	3	1×10^{-7}	0.988
2022	SR	3	1×10^{-7}	0.796

For the global means, we see that the groups with the lower p-value thresholds ($p < 10^{-7}, 10^{-8}$) perform best (see Table 16). Again, this may be due to these groups generally being large, hence the reduction in SNPs may have improved performance of the SVR-model as it may have removed redundant SNPs. This in combination with hyperparameter tuning may have resulted in better models.

Table 16: Results for cross-validation for global trials of AUC-values

	Phenotype	Group No.	p-threshold	Pearon's correlation
1	GNDVI	4	1×10^{-8}	0.972
2	NDVI	3	1×10^{-7}	0.971
3	SR	3	1×10^{-7}	0.985

4.5.4 Cross-Validation Results for SVR-Tuning: Agronomic Traits

In Table 17 is the cross-validation results for SVR-tuning done for seasonal trials (agronomic traits). The best performing group is generally either group 1 ($p < 10^{-5}$) or 2 ($p < 10^{-6}$). We see that for some years and phenotypes, the lower p-value thresholds have the best performance, like for GY and GPC in years 2020-2021 where the best performing group $p < 10^{-9}$ (strictest threshold). We observe the same thing in years 2021-2022 for DM, where the best performing groups have threshold $p < 10^{-9}$.

As discussed for earlier for AUC-values, large groups in these seasons may allow for the elimination of SNPs without affecting the overall correlation with phenotype. For DH (which had small groups), we observe that the first or second group ($p < 10^{-5}$ and $p < 10^{-6}$) has the best performance across all seasons. DH has few SNPs in its largest group to begin with. Therefore, there might not be any redundant SNPs to remove before the correlation with the phenotype is negatively impacted.

Table 17: Results for cross-validation for seasonal trials of agronomic traits

Year	Phenotype	Group No.	p-threshold	Pearson's correlation
2019	DH_dss	1	1×10^{-5}	0.395
2019	DM_dss	1	1×10^{-5}	0.914

Table 17 continued: Results for cross-validation for seasonal trials of agronomic traits

Year	Phenotype	Group No.	p-threshold	Pearson's correlation
2019	GPC_pct	2	1×10^{-6}	0.675
2019	GY_g_m2	1	1×10^{-5}	0.770
2019	PH_cm	2	1×10^{-6}	0.917
2020	DH_dss	1	1×10^{-5}	0.789
2020	DM_dss	2	1×10^{-6}	0.979
2020	GPC_pct	5	1×10^{-9}	0.857
2020	GY_g_m2	5	1×10^{-9}	0.779
2020	PH_cm	1	1×10^{-5}	0.874
2021	DH_dss	1	1×10^{-5}	0.770
2021	DM_dss	5	1×10^{-9}	0.983
2021	GPC_pct	5	1×10^{-9}	0.998
2021	GY_g_m2	5	1×10^{-9}	0.719
2021	PH_cm	2	1×10^{-6}	0.940
2022	DH_dss	2	1×10^{-6}	0.941
2022	DM_dss	5	1×10^{-9}	0.989
2022	GPC_pct	2	1×10^{-6}	0.955
2022	GY_g_m2	5	1×10^{-9}	0.706
2022	PH_cm	1	1×10^{-5}	0.962

In Table 18 we have the cross-validation results for global means. We see that overall significant correlation between the best-performing groups and the different phenotypes. We observe a similar pattern as earlier for seasonal trials for agronomic traits.

Table 18: Results for cross-validation for global means of agronomic traits

Phenotype	Group No.	p-threshold	Pearson's correlation
DH_dss	1	1×10^{-5}	0.878
DM_dss	3	1×10^{-7}	1.000
GPC_pct	5	1×10^{-9}	0.857
GY_g_m2	5	1×10^{-9}	0.780
PH_cm	1	1×10^{-5}	0.952

4.5.5 Performance of GA-Wrapper: AUC-values

Keep in mind that the purpose of the GA-wrapper was to select a subset of SNPs. The SNPs inputted were the best performing groups (see 4.5.3). Table 19 contains the performance of tuned SVR-models before and after feature-selection with GA (for seasonal trials). We see that GA reduced the number of features (SNPs) by almost half for the largest groups, like for GNDVI, NDVI and SR in year 2022. The number of features also decreased somewhat in the remaining seasons, although not by half. For example GNDVI has 15 SNPs in 2020 initially, but after running the GA-wrapper, 11 SNPs remains. The group is small prior to feature selection, hence the small change in features is not unexpected. However, it is interesting to see that model performance either remains the same or slightly increases despite the elimination of features via the GA-wrapper.

Table 19: Results for feature selection with GA-wrapper for seasonal trials (AUC-values)

Year	Phenotype	# Features before GA	# Features after GA	Pearson's correlation before GA	Pearson's correlation after GA
2019	GNDVI	37	29	0.980	0.980
2019	NDVI	73	47	0.988	0.989
2019	SR	29	21	0.934	0.934
2020	GNDVI	15	11	0.836	0.836
2020	NDVI	78	50	0.886	0.895
2020	SR	20	12	0.607	0.619
2021	GNDVI	26	16	0.629	0.665
2021	NDVI	23	16	0.939	0.931
2021	SR	71	36	0.954	0.959
2022	GNDVI	78	32	0.989	0.988
2022	NDVI	68	41	0.988	0.988
2022	SR	49	27	0.796	0.810

For the global means of AUC-values, we observe in Table 20 a similar pattern as for seasonal trials. The performance of the SVR-models remain unchanged despite reducing the number of features considerably. The GA-wrapper eliminates between 15-32 features for the different spectral phenotypes.

Table 20: Results for feature selection with GA-wrapper for global trials (AUC-values)

Phenotype	# Feature before GA	# Feature after GA	Pearson's correlation before GA	Pearson's correlation after GA
GNDVI	34	19	0.972	0.973
NDVI	42	30	0.971	0.971
SR	68	36	0.985	0.985

4.5.6 Performance of GA-Wrapper: Agronomic Traits

The performance of GA-wrapper for agronomic traits is summarized in Table 21. Starting with seasonal trials, the GA-wrapper reduced the number of features (SNPs) by almost half or more for the largest groups, like for GY and GPC, in all seasons. For example in season 2020, GY initially had 1172 SNPs, and only 568 SNPs remained after feature selection with GA. Also, for smaller groups the number of SNPs eliminated was large. For example for DH in 2019 the number of SNPs initially was 11, however, after feature selection the number of SNPs was reduced to 4. However, for GPC in the same season, number of SNPs remained the same before and after feature selection (5 SNPs).

Table 21: Results for feature selection with GA-wrapper for seasonal trials (agronomic traits)

Year	Phenotype	# Features before GA	# Features after GA	Pearson's correlation before GA	Pearson's correlation after GA
2019	DH_dss	11	4	0.395	0.396
2019	DM_dss	53	25	0.914	0.918
2019	GPC_pct	5	5	0.675	0.675
2019	GY_g_m2	167	78	0.770	0.781
2019	PH_cm	53	35	0.917	0.938
2020	DH_dss	23	16	0.789	0.790
2020	DM_dss	182	90	0.979	0.980
2020	GPC_pct	644	282	0.857	0.865
2020	GY_g_m2	1172	568	0.779	0.782
2020	PH_cm	29	18	0.874	0.876
2021	DH_dss	55	33	0.770	0.772
2021	DM_dss	72	42	0.983	0.982
2021	GPC_pct	291	150	0.998	0.998
2021	GY_g_m2	1056	482	0.719	0.724
2021	PH_cm	83	46	0.940	0.942
2022	DH_dss	57	31	0.941	0.940
2022	DM_dss	142	78	0.989	0.989
2022	GPC_pct	33	21	0.955	0.961
2022	GY_g_m2	1470	679	0.706	0.709
2022	PH_cm	65	39	0.962	0.963

We observe a similar pattern for the global means results as well, as can been seen in Table 22.

Note that for both seasonal trials and for global means, the performance of the SVR-models remain mostly unchanged before and after feature selection with GA.

Table 22: Results for feature selection with GA-wrapper for global trials (agronomic traits)

Phenotype	# Feature before GA	# Feature after GA	Pearson's correlation before GA	Pearson's correlation after GA
DH_dss	56	33	0.878	0.879
DM_dss	595	278	1.000	1.000
GPC_pct	483	214	0.857	0.863
GY_g_m2	1786	835	0.780	0.781
PH_cm	88	42	0.952	0.961

4.5.7 Final Selection of SNPs: AUC-values

As Table 23 shows, there were 338 associations in total for the final set of selected SNPs for seasonal trials. The greatest number associations appear in year 2019 and 2022. Unlike for the seasonal trials with MLM, GNDVI produced the greatest number assocaitions only in 2022. For the remaining seasons, NDVI and SR had the greatest number of assocaitions. Next, we may look into the resulting set of selected SNPs. Most associations appear on chromosomes 4A (63/338), 6B (45/338) and 3A (35/338). On these chromosomes,

NDVI accounts for most associations on all three of these chromosomes (38/65 on 4A, 27/45 on 6B and 14/35 on 3A).

Table 23: Resultssummarizing the final SNP-set for seasonal trials (AUC-values)

Season	# Peaks (Unique SNPs)	# SNPs GNDVI	# SNPs NDVI	# SNPs SR
2019	97 (87)	29	47	21
2020	73 (63)	11	50	12
2021	68 (59)	16	16	36
2022	100 (78)	32	41	27

For global means, NDVI and SR account for most SNPs selected using the GA/SVR-pipeline (see Table 24). Despite there being in total 85 SNPs identified in the global means, only 20 SNPs were also replicated in the seasonal trials. Similarly for the MLM-results, the majority of assocaitions that were significant for global means of AUC-values were not replicated in the seasonal trials.

Table 24: Resultssummarizing the final SNP-set for global means (AUC-values)

Phenotype	# Peaks	# Replicated in 2 environments
GNDVI	19	6
NDVI	30	9
SR	36	5

As done for MLM, we expanded the regions around identified peaks to find QTL (see section 3.5). For the QTL identified using the GA-SVR pipeline (see table A8), we see most QTL appeared on chromosomes 4A (5/20), 1A(3/20) and 3A (3/20). On chromosome 4A, all three VIs had QTL appearing. On 1A, all QTL were related to NDVI. On chromosome 3A, there were QTL for GNDVI (2/3) and SR (1/3).

When comparing the final set of SNPs identified using GA-SVR with MLM for AUC-values (Tables A8 vs. A6), we see that the ML-method identified more QTL. Also, some of the regions identified with GA-SVR does overlap with QTL identified with MLM (see chromosome 4A and 7A). Otherwise, the GA-SVR identified different regions (and chromosomes) compared to MLM approach. For instance, the GA-SVR found QTL on chromosomes 1A, 5B, 1B and 3A, while the MLM approach did not identify any significant QTL on these chromosomes.

4.5.8 Final Selection of SNPs: Agronomic Traits

As seen in Table 25, there are 2722 assocaitions (1708 unique SNPs) identified for seasonal trials of agronomic traits across all seasons. The greatest number of associations was for seasons 2020 and 2022. Similarly as when using MLM on agronomic traits, most assocaitions across all seasons appeared for phenotypes GY, GPC and DM (1807, 458, and 235 unique SNPs) (see Table 26). Also, most assocaitions appeared on chromosomes 7B, 3B and 7A (202, 150 and 137 unique SNPs). On these chromosomes most assocaitions were related to GY.

Table 25: Results summarizing the final SNP-set for seasonal trials (agronomic traits)

Season	# Peaks (Unique SNPs)
2019	147 (140)
2020	974 (847)
2021	753 (688)
2022	848 (836)

These results mostly agree with the ones we got with MLM, however, the number of assocaitions and unique SNPs identified is greater. We identified a considerably smaller number of significant SNPs with MLM, even with the lowered p-value threshold. Furthermore, with MLM most significant peaks were located on chromosome 2A. For the GA-SVR a different set of chromosomes produced the greatest number of assocaitions, namely 7B, 3B and 7A. Also, the number of replicated associations (across seasons) was greater for GA-SVR compared that of MLM, as seen in Table 26. In total we have 1249 assocaitions that are replicated for GA-SVR, which is much greater than number replicated associations identified using MLM, which was 80. When we consider only SNPs that were replicated across seasons, then we see that GY, GPC and PH (948, 129, and 90 unique SNPs) had the greatest number of SNPs (see Table 26).

Table 26: Results summarizing the final SNP-set for global means (agronomic traits)

Phenotype	# Peaks	# Replicated in 2 environments
DH	84	11
DM	235	71
GPC	458	129
GY	1807	948
PH	138	90

For the GA-SVR pipeline, we identified 149 unique agronomic QTL using the criteria outlined in section 3.5 (significant in global means and replicated in 2 environments for seasonal trials). These QTL are summarized in A9. In total, we identified more QTL using the GA-SVR pipeline compared to MLM. Most QTL are on chromosomes 7B (16), 3B (12) and 5A (10).

We may look into results for each phenotype as well, starting with DH where we have identified only two QTL on chromosomes 4A and 7B. Both QTL identified consists of 1-2 peak markers. For DM there were considerably more QTL (14 in total), however, even these QTL contain 1-2 peaks. For GPC we identified 21 QTL, and some of the QTL span larger regions, like *Q_GPC_3B_1* (562-587 Mbp), *Q_GPC_7B_1* (519-541 Mbp). Similarly, there were more QTL in total for GY (76 QTL), with the larger ones located on 5A (687-708 Mbp), 7B (124-191 Mbp and 539-584 Mbp). For PH, we identified fewer QTL (8 in total), however the identified QTL span larger regions. For example, *Q_PH_4B_1* spans 31-59 Mbp, and *Q_PH_4D_1* which spans 19-26 Mbp.

4.5.9 Stacking of GA-SVR Results

As we did earlier for spectral and agronomic QTL identified using MLM, we stacked the QTL identified using the alternative ML-pipeline. The procedure for this is outlined in section 3.6, and results are summarized in Table 27. First, note that GA-SVR identified far more overlapping QTL compared to MLM.

For MLM, we identified only two AUC-QTL overlapping with agronomic QTL. Next, unlike earlier with MLM, we identified far more QTL that are related to GY, GPC and DH. In fact, most overlapping QTL identified with GA-SVR are related to GY and GPC. There are no DM QTL identified, and only one which overlaps with a PH QTL (on 3A). Keep in mind that with MLM, there was only one AUC-QTL (NDVI) on 4B which overlapped with both DM and PH-related QTL. It is therefore interesting to see that this QTL does not appear for the stacked ML-results.

Next, we look into the specific results for GY and GPC. For GY, two overlapping QTL related to GNDVI and SR appeared on chromosomes 1A and 5B. For the remaining GY QTL, only 1 AUC QTL overlapped with them. The largest QTL which is close to a AUC QTL is *Q_GY_3A_3* which is near *Q_NDVI_3A_1*. For GPC, we observe similarly GNDVI and SR QTL overlapping with *Q_GPC_1A_1*. The GNDVI QTL contains the entirety of *Q_GPC_1A_1*, while the SR QTL only shares one position with *Q_GPC_1A_1*. The remaining overlapping QTL for GPC share only 1 overlapping marker with AUC QTL, and appear on chromosomes 5A and 7A.

Table 27: Results for agronomic QTL that overlap with AUC-values

AUC QTL	Agronomic QTL	Agronomic Trait	Span (AUC)	Span (Agronomic)	# Markers (AUC)	# Markers (Agronomic)
Q_NDVI_3A_1	Q_DM_3A_1	DM_dss	603-615	603	3	1
Q_NDVI_7A_1	Q_DM_7A_1	DM_dss	11	27	1	1
Q_GNDVI_1A_1	Q_GPC_1A_1	GPC_pct	29-31	26-27	2	2
Q_SR_1A_1	Q_GPC_1A_1	GPC_pct	29	26-27	1	2
Q_GNDVI_5A_1	Q_GPC_5A_3	GPC_pct	570	585-587	1	4
Q_NDVI_7A_1	Q_GPC_7A_1	GPC_pct	11	8	1	1
Q_GNDVI_1A_1	Q_GY_1A_1	GY_g_m2	29-31	27-33	2	2
Q_SR_1A_1	Q_GY_1A_1	GY_g_m2	29	27-33	1	2
Q_NDVI_3A_1	Q_GY_3A_3	GY_g_m2	603-615	572-589	3	2
Q_NDVI_4A_1	Q_GY_4A_2	GY_g_m2	97	103-105	2	2
Q_GNDVI_5A_1	Q_GY_5A_4	GY_g_m2	570	570-586	1	2
Q_GNDVI_5B_1	Q_GY_5B_1	GY_g_m2	36	36	1	1
Q_SR_5B_1	Q_GY_5B_3	GY_g_m2	686	687	1	1
Q_NDVI_7A_1	Q_GY_7A_1	GY_g_m2	11	4-27	1	3
Q_SR_7B_1	Q_GY_7B_11	GY_g_m2	707	713	1	1
Q_NDVI_3A_1	Q_PH_3A_2	PH_cm	603-615	599	3	1

5 Discussion

5.1 Correlations and Heritability Estimates

Spectral Data and Correlation with Agronomic Traits

As discussed previously, spectral data may be used as proxies for agronomic traits (Shafiee et al., 2023). We see in Figures 7-8 that GNDVI, NDVI, and SR (both AUC-values of VIs and time-series VIs) and the red and NIR bands were the bands/VIs that showed moderate to high correlation with DM and GY. Starting with GY, the study by Burud et al. (2017) also demonstrated high correlation between GY and NDVI. High correlations between spectral bands/VIs and GY may stem from the fact that GY is affected by a wide range of underlying factors, such as biomass and plant height (Li et al. 2019). As summarized by Hatfield et al. (2008), bands and VIs derived from the red and near-infrared region tend to correlate with agronomic traits such as green biomass. Hence, time-series and AUC-values of bands/VIs may be able to capture development in biomass, which may somewhat explain why GY is among the traits that produce the highest correlations with spectral bands/VIs in our results.

Next, the high correlation between DM and spectral phenotypes may be explained by changes in photosynthetic activity and chlorophyll content as crop reach maturity. As previously mentioned (see 2.1), spectral data can capture changes in both these biophysical properties, as well as apparent changes in color that occur during senescence (Hatfield et al. 2008). In the study by Hassan et al. (2021), they used NDVI collected over time to quantify senescence related QTL, which they succeeded at. Their work demonstrates that temporal spectral data can capture physiological changes in wheat, in particular changes that appear in later stages.

Also, we observe that the correlations change over time for the spectral time-series data. As discussed earlier, spectral data captured at different developmental stages contains information specific to that stage (Wang et al. 2021). For example spectral reflectance data captured at grain-filling stages has shown higher correlation with or resulted in better predictions for traits like GY compared to reflectance captured at earlier stages (Fei et al. 2022, Han et al. 2020). Observing temporal changes in correlation were expected, in particular for traits such as GY, PH and DM. This is because as these traits develop, there are apparent, physical changes linked to these traits, such as gain in biomass or apparent changes in colour, that can be captured by spectral reflectance data.

Furthermore, we see that accumulated VIs (AUC-values) tend to produce higher correlations with agronomic traits (in particular GY and DM) in comparison to VIs captured at single time-points. Also, we observe that the correlations between traits and VIs in the spectral time-series fluctuates considerably in certain seasons (see Figure 7, seasons 2019 and 2022). Unlike VIs captured at single time-points, AUC-values summarize VIs for an entire season, hence they may be more robust to variations in reflectance appearing in only some flight missions. This may explain why accumulated VIs produce comparable or higher correlations. Moreover, the accumulated VIs may show higher correlation because they capture growth dynamics better (like faster gain in biomass for some lines). Previous studies have shown that summary metrics (over a temporal window) or modelling of spectral time-series can be used to detect phenological stages (Liu et al. 2022, Hill & Donald 2003). Examples of metrics which have been used to identify phenological stages is finding the time when a VI exceeds a given threshold, finding the largest slopes/derivatives in a spectral time-series, and finding inflection points (Zeng et al. 2020, Hill & Donald 2003). A review of the literature shows that AUC-values are typically not used to study phenological development. However, the work by Tangpattanakul et al. (2015) show that AUC-values derived from the VI Excessive Green (ExG) can be used to identify stages like seedling, heading and maturity in rice. The

study demonstrates that AUC-values of VIs may indicate crop maturity, explaining why we see AUC-values being highly correlated with late stage traits like DM and GY in our results.

BLUEs Estimation for Spectral Data and Differences in Heritability

Interestingly, when genotype was modelled as a random effect in the spectral time-series it resulted in larger estimated errors compared to estimated errors for the AUC-values (see Tables A1-A4). This holds especially true for the trial means and global means equations for the spectral time-series. On the other hand, for flight trials the estimated error and overall heritability is comparable to that of seasonal trials for AUC-values (Figures 4-5). While heritability was not computed for trial means and global means of the spectral time-series, the results in A1-A2 suggest heritability would be low because the estimated genotypic effect is considerably smaller than the estimated error.

The computation of BLUEs for flight trials in our study was similar to that of Shafiee et al. (2024) and Krause et al. (2019). For our study, the main difference between the flight trial models and models for trial and global means (Equations 2-3) is the use of nesting. In the trial means model all effects except genotypic effects are nested under time-points, and for global means there is nesting under season as well. Although such nesting was done by Krause et al. (2019) as well, whether it is correct is debatable. This is because in their research they also computed BLUEs for developmental stages as well, which entail more than one mission (see Table 3). It could be worth looking into such an approach as one flight mission might not contain enough information about crop status, whereas integration over individual developmental stages (like VEG, HEAD and GF) that have multiple flight missions may contain enough relevant information.

Another alternative explanation is that there are other sources of variance in the spectral data that we have not accounted for, like interactions between genotypic effects and time-points. For the flight trials model, we are fitting BLUEs within each time-point, hence no such interaction can occur. However, for the trial means and global means model, we are modelling time-point as a random effect, hence it may be worth exploring if there are significant interactions between time-points and genotypic effects. Such interaction are likely to be present for the spectral time-series, since studies have demonstrated that such data captures temporal genetic controls (Wang et al. 2021). In other words, the effect of different genotypes on spectral data may depend on the time in which spectral data was recorded. Also, as discussed earlier, spectral time-series are useful in identifying different phenological stages, making it plausible that interactions between genetic effects and time of flight missions exist.

Furthermore, our models may have large estimated errors because we fail to account for environmental factors such weather conditions. As discussed in the section 2.1, spectral reflectance can easily be affected by changing solar illumination or recent rainfall. We attempted to identify flight missions affected by rainfall in the days prior to the flight by cross-referencing weather data provided in the supplementary material by Mroz et al. (2023). However, we may have overlooked other weather related factors that could have an impact on the included flight missions.

An alternative explanation for the large estimated error is that the BLUEs equations are mis-specified. Alternative BLUEs were explored for both trial means and global means, such as having time-point as a fixed effect, and not nesting effects under time-points. However, such models produced equally large estimated error terms. Furthermore, the alternative models did not make sense with respect to the goal of the analysis and when comparing them to the models found in literature (Krause et al. 2019, Shafiee et al. 2024).

Next, we address the differences in heritability when comparing AUC of VIs and VIs from time series, where

AUC-values produced considerably larger heritability estimates (Figures 4-5). Again, this may show that accumulated VIs computed over entire seasons are more stable and contain less noise compared to spectral data recorded for individual flight missions. Overall, the differences in estimated error and heritability for spectral bands/VIs time-series and seasonal AUC demonstrates the potential usefulness of deriving summary metrics from spectral time-series. It may reduce the influence of noise factors and contain more information relating to growth dynamics. Individual time-points and developmental stages can still be useful, as seen in the research by Wang et al. (2021) and Gao et al. (2023), as they may reveal temporal control patterns that are difficult to detect using summary statistics alone. Hence the two approaches for dealing with spectral time-series data may complement each other.

Lastly, it is worth noting that in the work by Krause et al. (2019), they developed BLUEs for both individual flight missions and growth stages (VEG, HEAD, and GF). For our work, the trial means and global means for spectral time-series nest all effects under time-point (excluding genotype), which effectively removes any temporal effects spectral bands/VIs may have on genotype. This also removes the opportunity to study temporal QLTs effectively, since BLUEs for trial means and global means are mean estimates across all time-points.

5.2 GWAS-Results with MLM

GWAS on Spectral Phenotypes

In contrast to the GWAS-results for AUC-values of VIs, the spectral time-series data detected more significant SNPs and QTL. As discussed earlier, GWAS is successful only if a large population is studied with enough diversity (phenotypic and genetic) (Sukumaran et al. 2022, Xiao et al. 2022). Different plots may not have shown enough phenotypic variation with respect to AUC-values (see Figure A3). Distribution of NDVI and GNDVI AUC-values are narrow in all seasons, while SR is wider. Additionally, the computation of AUC-values for each plot could have affected the GWAS results. This report used a trapezoid method derived from the median spectral reflectance. Other methods (including Simpson integration) can also be used, but we have not explored them. Also, all QTL identified for AUC-values overlaps with the ones identified for the spectral time-series. This raises the question of whether accumulated VIs are useful or not compared to spectral time series. For our report, it seems like AUC-values of VIs do not capture anything different from spectral time-series.

Next, we need to consider that the time-series contained six spectral phenotypes organized into two developmental bins (HEAD and GF). This provides a unique opportunity to study dynamic changes in significant peaks. GF-stage shows the greatest number of peaks for flight trials. There may be two reasons why we detect more peaks in GF compared to HEAD. First, the HEAD-bin contains fewer flight missions (T1-T2) compared to GF-stage (T3-T6). Time points were binned using the definitions of developmental stages discussed in Krause et al. (2019) and seen in Table 3. The HEAD-bin contains fewer flight missions because we do not have many flight missions early in the season. The second reason may be biological, meaning that the spectral reflectance data contains more biologically relevant information in the GF-bin compared to HEAD-bin.

As well as observing more significant peaks in the GF-stage than the HEAD-stage, we discovered that some peaks are time-bin specific. GF, for instance, shows significant peaks on chromosomes 4B (20-79 Mbp) and 2A (74-78 Mbp) but these peaks were not replicated the HEAD-stage. Also, some identified regions appeared in both time-bins like on chromosome 5A (549 Mbp). This may indicate that there are temporal genetic controls which can be identified using multispectral time-series. The GF-specific region

on 4B has been reported previously to be related to PH, while the region on 2A has been reported to be related to flowering (anthesis) in spring wheat. It should therefore not be surprising that these regions appear significant for spectral data captured later in the season.

Next, our results demonstrate that it is difficult to identify replicated associations when using a Bonferroni correction scheme on multispectral time-series. There were no association in flight trials and trial means that were replicated when using Bonferroni correction, while with the lowered p-value threshold we identified replicated peaks across seasons. One possible explanation is that spectral phenotypes are highly quantitative, meaning that they depended on multiple small-effects loci. For this reason, it may be difficult to replicate associations between seasons with the MLM-method. Therefore, using a less stringent p-value may be reasonable to identify replicated associations. Bonferroni correction is a correction method which is poorly suited for detecting small-loci effects and multi-locus interactions, as it depends on markers displaying large effects individually (Zhang et al. 2010, Saini et al. 2021).

To summarize, we identified significantly more QTL using the spectral time-series compared to accumulated VIs. The spectral time-series also provided a more interesting study, as it identified the exact same QTL as the accumulated VIs, but it also enabled us to identify temporal genetic controls. Also, with a lower p-value threshold we were able to identify more significant peaks that were replicated across seasons.

Overlapping QTL: Spectral and Agronomic QTL

We observed multiple spectral QTL which overlapped with agronomic QTL (see 4.4.8, Tables 13-14). The most interesting ones are the ones that span a large region or contain genes that have been previously reported. Since the time-series QTL contain all QTL identified for AUC-values, we will only be considering the results summarized in Table 35, which contains agronomic QTL and time-series QTL that overlap.

Starting with PH, *Q_PH_4B_1*, which spans 13-79 Mbp, contains an important height related gene, namely *Rht-B1*. Both this gene and *Rht-D1*, are semi-dwarfing genes in wheat which together results in a reduction of plant height, while increasing yield by allowing for more tillers (Jobson et al. 2019). Breeding for these genes played a significant role in the Green Revolution, which refers to a period between 1960-1970s when more productive crop varieties were developed (Jobson et al. 2019, Zhang et al. 2006). The presence of specific alleles of these genes (*Rht-B1b* and *Rht-D1b*) has in one study shown to reduce PH significantly (by up to 41%) (Flintham et al. 1997). The presence of just one of the alleles (like *Rht-B1b*) has also shown to result in a reduction of PH (Flintham et al. 1997). It is interesting to see that GWAS on multispectral time-series is able to capture PH-related genes. This is despite most spectral bands, AUC-values of VIs and VIs showing little to moderate correlation with PH (see Figures 7-8). The bands and VIs with QLTs which overlap with this region containing Rht-B1 are red , red-edge, NDVI, and SR. The red-region is well suited for capturing differences in canopy coverage and plant height (Payero et al. 2004, Tenreiro et al. 2021). Therefore, it should not be surprising that bands and VIs derived from this region are capturing physical properties related PH and canopy coverage, and thus acting as proxies for these properties. In the study by Hassan et al. (2019), they also identified *Rht-B1* and *Rht-D1* using imaging data collected by UAVs. Gao et al. (2023) also identified a PH QTL containing this genomic region using imaging data (*qPH_4B_1*). Both these studies show and our own results showcase the potential of using imaging data as a proxy for PH or PH-related features. Keep in mind though that the spectral QTL and agronomic QTL we identified in this region are quite large. The spectral phenotypes lie in the region 20-59 Mbp, while the agronomic QTL lies in the region 13-79 Mbp. Hence, there may be other genomic factors in these regions which may effect PH which we have not described here.

Next, we also observed many DM QTL overlapping with spectral QTL. DM QTL were co-localized with

spectral QTL on chromosomes 2A (74-78 Mbp), 4B (20-59 Mbp) and 5A (548-549 Mbp) (Table 13). The gene discussed earlier on chromosome 4B (*Rht-B1*) may also play role in the photosynthetic activity, as the variant *Rht-B1b* reduces both photosynthetic activity and chlorophyll content during anthesis, as shown in Jobson et al. (2019). The findings in this study should be interpreted carefully, however, it does somewhat coincide with our results since spectral imaging should be able to capture differences in chlorophyll content. We may therefore speculate that the overlapping QTL which appear between DM and spectral phenotypes on 4B is due to its effect chlorophyll and photosynthetic activity content during the later developmental stages.

Next, we consider the QTL on 5A. There are numerous studies that have identified QTL related to senescence in spring wheat on chromosome 5A, as seen in the study by Hassan et al. (2021) were they used remote spectral imaging to find senescence and GY related QTL. Their study identified a senescence related QTL (*QTL-caas.5A_1)* which does not overlap with our QTL for DM. However, it may be close enough to speculate that the spectral QTL is close because it captures information related to the senescence stage. Senescence refers to the final developmental stages where nutrients are mobilized from the plant and into the developing grain (Janusauskaite 2022). During senescence photosynthetic activity is reduced quickly, and the leaves gradually turn yellow. Spectral imaging data should be able to capture changes in color which appear during the senescence process, hence it should not be surprising that we identify both DM QTL and spectral QTL (for the green, NIR, red-edge and blue) which are somewhat near QTL reported for senescence. The particular bands too which overlap with DM are also interesting, since as leaves turn yellow, they reflect less light in the green, NIR and red-edge regions. All these bands are indicative of plant health and vigor (Wang et al. 2021), hence it may explain why QTL identified for these bands are co-localized with DM and senescence QTL.

Another study which identified maturity time related QTL on chromosome 5A was Semagn et al. (2021), where they found QTL for maturity that overlap with the ones we identified for DM (*QMat.dms-5A.1* located on 569-570 Mbp and *QMat.dms-5A.2* located on 587 Mbp). In their study, they performed mapping of QTL related to various developmental stages like flowering, heading and maturity. Their identified QTL do not directly overlap with the DM QTL on 5A in our study, however, we may consider them to be somewhat close. They found that one of the QTL *(QMat.dms-5A.1)* contained the gene *Vrn-A1*, and our QTL (*Q_DM_5A_1*) is the near the region containing this gene. *Vrn-A1* is among the genes which regulate how wheat crop respond to prolonged periods of lower temperatures (Zhang et al. 2008). Together with other genetic factors, they regulate flowering time, and this gene has been shown to effect the maturity time of wheat crop (Zhang et al. 2008, Chen et al. 2010).

Also, we observed multiple spectral QTL co-localized with DM QTL on chromosome 2A (*Q_DM_2A_1*, 74-78 Mbp). This region is overlaps with meta-QTL identified by Shariatipour et al. (2021) related to green-leaf area (50% green leaf area and 75% green leaf area). As discussed earlier, DM is a late-season trait where the crop undergoes colour changes (yellowing). Hence identifying previously reported QTL related to leaf green area should not be surprising, and it makes sense that the spectral phenotypes green, NIR and red-edge are co-localized with green-leaf area QTL. As mentioned earlier, these are spectral bands which capture variations in green colour as well as the yellowing process which occurs in the later development stages of wheat.

Furthermore, we observed some spectral QTL co-localized with GY and GPC QTL. As reported in Table 13, we identify very few of these overlapping regions. This is despite the fact that we identified multiple QTL related to these two phenotypes in the MLM-results for agronomic traits (see Table A7). Both GY and GPC are complex, physiological traits which depend on multiple loci. Unlike PH and DM, which are agronomic traits that when recorded over time will display apparent changes in the crop, GY and GPC are traits which do not necessarily give rise to apparent changes. PH results in changes of biomass or

canopy cover, and crop become yellow as they reach maturity. Therefore, both PH and DM are visually observable changes, while GY and GPC are not as apparent. This may explain why we have not identified many spectral QTL co-localized with GY and GPC.

Starting with GY, we identified QTL on 2A overlapping with spectral QTL for the red-edge, green and red bands (758-773 Mbp), and on 7A co-localized with a QTL for the green band (51-112 Mbp). Starting with 2A, Li et al. (2019) reported GY related QTL in regions near or overlapping with our reported GY QTL. In their study they reported thousand kernel weight (TKW), kernel length (KL), and kernel weight (KW) QTL in regions 760, 740 and 758-760 Mbp respectively on chromosome 2A. TKW, KL and KW are all traits underlying GY, since they effect the final yield. They also reported a QTL for TKW on chromosome 7A (49.1-50.0 Mbp) which overlaps with our identified QTL on the same chromosome. It is difficult to explain exactly what the spectral bands red-edge, green and red capture which results in them being co-localized with reported GY related QTL and our own identified regions. However, previous studies have shown that genomic prediction using spectral data predicts GY with high accuracy (**?**Mróz et al. 2024). Also, we have shown that spectral imaging correlates well with end-of-season yield (Figures 7-8). Therefore, although the exact genetic information which spectral imaging data may be capturing remains unknown and warrants further investigation, spectral imaging may still be useful as it provides a non-invasive method for predicting and selecting high yielding varieties. For this report, we have only uncovered previously reported GY QTL which are co-localized with some of our spectral QTL and GY QTL. We have not, however, described candidate genes that directly affect GY in our GY QTL.

Next, we may look into GPC QTL which overlap with spectral QTL. We identified only two GPC QTL located on chromosome 1B (662-672 Mbp) and 5A (2-10 Mbp) that overlap with spectral QTL for the green, red-edge and NIR bands. Starting with 1B, Shariatipour et al. (2021) identified one meta QTL (*MQTL_1B_3* on 678.45–681.00 Mbp) which is related to grain-filling duration (GFD), among other traits. GFD is related to GPC, as GFD is an important developmental stage in wheat crop where the size and weight of the grain increases, and its protein content is determined (Kartseva et al. 2023). During this period, proteins like gluten proteins are synthesized and deposited in the endosperm (Shewry 2023). Therefore, the length of GFD can significantly affect the final GPC (Kartseva et al. 2023, Uhlen et al. 1998). However, it is important to note that while there is a relationship between the GFD and GPC, it is complex and influenced by many other factors (Uhlen et al. 1998). It is still interesting to identify a region related to GPC co-localized with GFD QTL given the known relationship between the two. For the remaining QTL on 5A, we found no reported QTL related to GPC or traits which affect GPC.

To summarize, the spectral QTL found in our study does overlap with some agronomic QTL previously reported in the literature. Not all spectral QTL contain or are close to genes that fully explain their relation to the agronomic QTL they overlap with. For instance, we did not find spectral QTL overlapping with GY and GPC QTL that contain or are near genes that explain their relation to GY or GPC. On the other hand, for spectral QTL shared with PH and DM we identified genes (*Rht-B1*, *Vrn-A1*) that may explain their relation to PH and DM. Overall, our findings demonstrate that multispectral data may be able to genetically dissect simple traits (like height and maturity time), but fails for more complex traits (like yield and protein content).

5.3 GWAS-Resutls for GA-SVR

General Results and Differences in No. of Hits

It is important to note that the GA-SVR pipeline was applied only to the agronomic traits (see A9) and AUC values of VIs (see A8). Interestingly, the GA-SVR pipeline identified more QTL than the MLM approach for both agronomic traits and AUC values.

As highlighted in section 2.4, there are fundamental differences between SVR and MLM in terms of identifying significant associations. MLM is a single-locus model which is typically effective in detecting associations between markers and traits when the effects of markers is large (Zhang et al. 2010, Saini et al. 2021). MLM is not suitable for detecting minor-effect loci. Therefore, MLM may fail to capture significant genomic regions if a trait is influenced by multiple loci, and if each locus contributes with small effects.

On the contrary, SVR addresses limitations inherent to MLM, since it is well-suited for tackling multi-regression problems. GWAS can be viewed as multi-regression problem, because the goal is to identify a set of markers that influence or correlate with an observed phenotype, and also quantify their influence (effects) as well. Unlike MLM, SVR considers multiple loci simultaneously when determining the best separating margin. This allows SVR to capture more complex patterns in the data, potentially making it more effective in modelling multi-locus effects. This is particularly true when SVR is paired with non-linear kernels, enabling it to discover non-linear relationships between markers and the phenotype under study. Despite this advantage SVR has over MLM, it remains challenging to account for population structure and familial relatedness when implementing ML-methods. ML are often considered a 'black-box' with no apparent variance-structure or fixed effects in which confounding variables like kinship can be modelled. This holds true for SVR, since it is difficult to explain or interpret patterns in data the model learns. In addition, it is difficult to assess how confounding variables (such as familial relatedness and population structure) influence the model's performance.

As discussed earlier, MLM accounts for these confounding variables in its model definition. However, in this report, we attempted to consider population structure by adding columns from the Q-matrix to the SVR model's feature set. The idea was that PCs (o Q-matrix columns) would act as additional dimensions in the feature space. In these additional dimensions, samples could be more easily separated based on common ancestry, as related samples will lie more closely in space compared non-related samples. Whether this is an efficient way of accounting for population structure when using SVR is difficult to say. It is also difficult to say if there is a need to account for such confounding variables as the studies by de Oliveira et al. (2014) and Díez Díaz et al. (2021) made no attempt in correcting for them when using SVR for GWAS. It may therefore be worth investigating whether spurious correlations are occurring as a result of failing to account for confounding variables when implementing ML-alternatives for GWAS.

The GA-SVR pipeline, as discussed in the study by de Oliveira et al. (2014), indeed presents a significant computational challenge, particularly when it comes to the calculation of p-value groups. The SVR models are fitted within groups of SNPs that pass a specific p-value threshold, which is determined by Spearman's correlation coefficient. In our results, we noticed considerable variations in the sizes of the p-value groups, depending on both the spectral phenotype and the set p-value threshold. This approach of fitting SVR models only within p-value groups is computationally efficient, considering that fitting SVR models to large predictor sets is both computationally demanding and memory-intensive. This method also conveniently allows for the initial elimination of any redundant markers before the fitting of SVR models, as discussed by de Oliveira et al. (2014). However, the use of p-groups introduces a challenge that would not exist if all SNPs were used to fit the SVR model. As previously discussed, SVR models are better equipped to

capture multi-locus effects. However, by dividing the markers into multiple groups and fitting SVR models only within these groups, we risk missing interactions between loci if they occur in different p-value groups. Unfortunately, the potential impact of separating markers into p-value groups is not sufficiently addressed in the work by (de Oliveira et al. 2014).

Identified QTL: MLM vs. GA-SVR

Table 27 contains the stacked GWAS-results for AUC-values and agronomic data when using GA-SVR. Interestingly, we identified more overlapping QLTs using the GA-SVR pipeline compared to using MLM for AUC-values of VIs (see Table 14). When using the MLM approach, however, we identified overlapping QTL in a region that has a well-known gene that affects crop height (*Rht-B1* on 4B). In general, we identified more PH and DM related QTL with MLM when considering the stacked results (Tables 13-14). In contrast, the GA-SVR pipeline identified a greater number of spectral QTL overlapping with the more complex traits GY and GPC. In fact, the majority of the overlapping QTL identified were for GY and GPC. It is important to note that SVR does not account for familial relatedness, and the implications of including a Q-matrix into the model's feature set have not been discussed in existing literature. Therefore, the results presented in Table 27 should be interpreted with caution. However, the fact that the GA-SVR method produced more overlapping spectral QTL in regions where we have identified GY and GPC QTL may suggest that the model is capable of capturing the complex relationships between markers and traits underlying GY and GPC.

Nevertheless, it is somewhat strange the peak-markers on chromosome 4B (13-79 Mbp) were not captured by the GA-SVR approach. This region was significant even with Bonferroni-correction for MLM. We can therefore be confident that the association identified on 4B has a significant influence on crop height, and failing to identify this with GA-SVR may indicate that the method is somewhat flawed. Furthermore, when comparing results in Table 14 and 27, we see that there are no overlapping spectral or agronomic QTL for MLM and GA-SVR.

Also identifying GY and GPC QTL with GA-SVR that lie in the exact same regions may indicate that there are some problems with the method. It has been documented that yield and protein content tend to be negatively correlated (Kibite & Evans 1984, Sandhu et al. 2021). Figure 8 shows that there is negative correlation between GPC and GY for all seasons (in particular in 2020). The reason these traits tend to show such correlation is because both GY and GPC are influenced by nitrogen utilization and excess nitrogen content in the soil (Ayadi et al. 2022). Typically, nitrogen concentrations in the soil is kept high as it results in higher yield. However, any excess nitrogen not absorbed by the crop accumulates in the soil, leading to delayed senescence, which in turn shortens the grain filling rate and reduces protein content. For example Ayadi et al. (2022) put durum wheat lines under contrasting fertilization regimes, and they observed a general trend of low GPC under high nitrogen treatment, while GY remained high. To avoid spurious associations, it is important to control for this effect when identifying GPC-related markers. To account for this correlation, Rapp et al. (2018) showed that grain protein deviation (GPD), which subtracts the effect GY has from GPC, identified GPC-related QTL. GPD showed little correlation with GY, which demonstrates the metric removes the influence of GY on GPC effectively. For the GA-SVR implementation in this study, we have not made such adjustments. Hence it may both explain why we identify most QTL for GY and GPC, and also why they appear to be co-localized. For example, *Q_GPC_1A_1*, *Q_GPC_5A_3* and *Q_GPC_7A_1* are all located in regions identified for GY (see Table 27). The exact overlap indicates the GA-SVR analysis might be identifying QTL related to GY instead of GPC.

However, as documented by Shariatipour et al. (2021), observing co-localization of GPC and GY QTL

does not always indicate failure to account for this relation between the two. In their study, they identified numerous GPC meta-QTL which were co-localized with GY related traits like TKW (frequency of co-localization 63%). Overall they found that numerous GY related and GPC related meta-QTL appeared to be co-localized. This was done by aggregating data from numerous GWA-studies using met-aQTL analysis, which enabled the researchers to study the genetic correlation between traits. Therefore the identified QTL for GPC with SVR-GA pipeline may truly affect GPC, while still being co-localized with GY related QTL.

6 Conclusion

Overall, our results demonstrate that phenotypes derived from multispectral time-series data may provide valuable insight into the genetic controls underlying important agronomic traits. We identified that spectral bands and VIs recorded over time correlated well with some agronomic traits (like GY), and showed high heritability. Additionally, simultaneous GWAS on both agronomic traits data and spectral phenotypes helped uncover known and basic genetic controls underlying traits like PH and DM. Seeing that QTL for spectral bands overlapped with or were near genes like *Rht-B1* and *Vrn-A1*, and that we identified these regions for the agronomic traits data as well demonstrates that the spectral data might capture simple traits like height and maturity time.

Also, uncovering large effects for regions containing or near *Rht-B1* and *Vrn-A1* for GWAS on spectral time-series provides a sanity check on whether multispectral data contains sufficient biologically relevant information to reveal genetic architecture of important traits. Despite these interesting findings for PH and DM, GWAS on spectral data did not uncover as many significant markers in regions related to GY and GPC. This may be for various reasons, including that the selected model (MLM) is not suitable for complex traits affected by many small-effect loci. It would therefore be interesting to explore multi-locus model alternatives like MLMM, Fixed and Random Model Circulating Probability Unification (FarmCPU) or Bayesian-information and Linkage-disequilibrium Iteratively Nested Keyway (BLINK). For future GWA-studies using spectral time-series, these multi-locus models should be explored as they may help uncover interactions between markers and small-effect markers.

Furthermore, the spectral phenotypes derived from the time-series should be further refined into their respective developmental stages. In this thesis, the trial means and global means models provide mean genotypic values across the entire season. However, as seen in our results, the information contained within spectral bands and VIs changes over the season. Additionally, their correlation and explainability of agronomic traits changes over the season. Therefore, for future work, the BLUEs for trial means and global means need to be defined so that they account for these differences in developmental stages. GWAS on spectral phenotypes specific to developmental stages may also provide a more interesting study, as they may uncover more temporal genetic control. We attempted to uncover such temporal effects using GWAS on flight missions, which was partially successfully.

Lastly, it is interesting to see that the implemented ML-alternative resulted in different peak markers and genomic regions compared to MLM. Overall, GA-SVR is a feasible alternative, because it produced some QTL overlapping with those identified with MLM. However, the regions identified with the alternative pipeline need to be further studied. For this report, we did not review the literature for the QTL found with GA-SVR. We simply compared these regions with those found using MLM. In future studies, this should be done, as it will reveal if GA-SVR detects genetic elements relevant to the phenotype under study. The implications of confounding variables (population structure, kinship, and correlation between GY and GPC) should also be addressed before any conclusions on QTL identified for GA-SVR are made.

References

Ang, K. L. M. & Seng, J. K. P. (2021), 'Big data and machine learning with hyperspectral information in agriculture', *IEEE Access* **9**, 36699–36718.

Asíns, M. J. (2002), 'Present and future of quantitative trait locus analysis in plant breeding', *Plant Breeding* **121**(4), 281–291.
URL: *https://onlinelibrary.wiley.com/doi/abs/10.1046/j.1439-0523.2002.730285.x*

Ayadi, S., Jallouli, S., Chamekh, Z., Zouari, I., Landi, S., Hammami, Z., Ben Azaiez, F. E., Baraket, M., Esposito, S. & Trifa, Y. (2022), 'Variation of grain yield, grain protein content and nitrogen use efficiency components under different nitrogen rates in mediterranean durum wheat genotypes', *Agriculture* **12**(7), 916.
URL: *https://www.mdpi.com/2077-0472/12/7/916*

Azim, M., Islam, M., Rahman, M. & Jahan, F. (2021), 'An effective feature extraction method for rice leaf disease classification', *TELKOMNIKA (Telecommunication Computing Electronics and Control)* **19**, 463–470.
URL: *http://telkomnika.uad.ac.id/index.php/TELKOMNIKA/article/download/16488/9867*

Birth, G. S. & McVey, G. R. (1968), 'Measuring the color of growing turf with a reflectance spectrophotometer1', *Agronomy Journal* **60**(6), 640–643.
URL: *https://acsess.onlinelibrary.wiley.com/doi/abs/10.2134/agronj1968.00021962006000060016x*

Burud, I., Lange, G., Lillemo, M., Bleken, E., Grimstad, L. & From, P. J. (2017), 'Exploring robots and uavs as phenotyping tools in plant breeding', *IFAC-PapersOnLine* **50**(1), 11479–11484.

Buschmann, C. & Nagel, E. (1993), 'In vivo spectroscopy and internal optics of leaves as basis for remote sensing of vegetation', *International Journal of Remote Sensing* **14**(4), 711–722.
URL: *https://doi.org/10.1080/01431169308904370*

Chang-Brahim, I., Koppensteiner, L. J., Beltrame, L., Bodner, G., Saranti, A., Salzinger, J., Fanta-Jende, P., Sulzbachner, C., Bruckmüller, F., Trognitz, F., Samad-Zamini, M., Zechner, E., Holzinger, A. & Molin, E. M. (2024), 'Reviewing the essential roles of remote phenotyping, gwas and explainable ai in practical marker-assisted selection for drought-tolerant winter wheat breeding', *Frontiers in Plant Science* **15**.
URL: *https://www.frontiersin.org/journals/plant-science/articles/10.3389/fpls.2024.1319938*

Chen, Y., Carver, B. F., Wang, S., Cao, S. & Yan, L. (2010), 'Genetic regulation of developmental phases in winter wheat', *Molecular Breeding* **26**(4), 573–582.
URL: *https://doi.org/10.1007/s11032-010-9392-6*

Chen, Z., Boehnke, M., Wen, X. & Mukherjee, B. (2021), 'Revisiting the genome-wide significance threshold for common variant gwas', *G3 Genes—Genomes—Genetics* **11**(2).
URL: *https://doi.org/10.1093/g3journal/jkaa056*

Chlingaryan, A., Sukkarieh, S. & Whelan, B. (2018), 'Machine learning approaches for crop yield prediction and nitrogen status estimation in precision agriculture: A review', *Computers and electronics in agriculture* **151**, 61–69.

de Oliveira, F. C., Borges, C. C. H., Almeida, F. N., e Silva, F. F., da Silva Verneque, R., da Silva, M. V. G. B. & Arbex, W. (2014), 'Snps selection using support vector regression and genetic algorithms in

gwas', *BMC Genomics* **15**(7), S4.
URL: *https://doi.org/10.1186/1471-2164-15-S7-S4*

Deering, D. W. (1978), Rangeland reflectance characteristics measured by aircraft and spacecraft sensors, Phd diss., Texas A&M Univ.
URL: *https://hdl.handle.net/1969.1/DISSERTATIONS-253780*

Díez Díaz, F., Sánchez Lasheras, F., Moreno, V., Moratalla-Navarro, F., Molina de la Torre, A. J. & Martín Sánchez, V. (2021), 'Gasvem: A new machine learning methodology for multi-snp analysis of gwas data based on genetic algorithms and support vector machines', *Mathematics* **9**(6), 654.
URL: *https://www.mdpi.com/2227-7390/9/6/654*

Engelhardt, B. E. & Stephens, M. (2010), 'Analysis of population structure: A unifying framework and novel methods based on sparse factor analysis', *PLOS Genetics* **6**(9), e1001117.
URL: *https://doi.org/10.1371/journal.pgen.1001117*

Fei, S., Hassan, M. A., Xiao, Y., Rasheed, A., Xia, X., Ma, Y., Fu, L., Chen, Z. & He, Z. (2022), 'Application of multi-layer neural network and hyperspectral reflectance in genome-wide association study for grain yield in bread wheat', *Field Crops Research* **289**, 108730.
URL: *https://www.sciencedirect.com/science/article/pii/S037842902200301X*

Feng, H., Guo, Z., Yang, W., Huang, C., Chen, G., Fang, W., Xiong, X., Zhang, H., Wang, G., Xiong, L. & Liu, Q. (2017), 'An integrated hyperspectral imaging and genome-wide association analysis platform provides spectral and genetic insights into the natural variation in rice', *Scientific Reports* **7**(1), 4401.
URL: *https://doi.org/10.1038/s41598-017-04668-8*

Flintham, J. E., Angus, W. J. & Gale, M. D. (1997), 'Heterosis, overdominance for grain yield, and alpha-amylase activity in f1 hybrids between near-isogenic rht dwarf and tall wheats', *The Journal of Agricultural Science* **129**(4), 371–378.
URL: *https://www.cambridge.org/core/product/2FB820EF8B3E33F3F801863DB6C84131*

Gao, J., Hu, X., Gao, C., Chen, G., Feng, H., Jia, Z., Zhao, P., Yu, H., Li, H., Geng, Z., Fu, J., Zhang, J., Cheng, Y., Yang, B., Pang, Z., Xiang, D., Jia, J., Su, H., Mao, H., Lan, C., Chen, W., Yan, W., Gao, L., Yang, W. & Li, Q. (2023), 'Deciphering genetic basis of developmental and agronomic traits by integrating high-throughput optical phenotyping and genome-wide association studies in wheat', *Plant Biotechnol J* **21**(10), 1966–1977.
URL: *https://www.ncbi.nlm.nih.gov/pubmed/37392004*

Gillani, S. S. M., Tahir, M. N., Anwar, A., Ul-Haq, S. I., Awais, M., Iqbal, M., Iqbal, J., Malik, H. A., Naqvi, S. M. Z. A. & Ullah, R. (2023), 'Real time estimation of wheat chlorophyll content retrieve from landsat 8 imagery under rainfed condition'.

Gitelson, A. A. & Merzlyak, M. N. (1996), 'Signature analysis of leaf reflectance spectra: Algorithm development for remote sensing of chlorophyll', *Journal of Plant Physiology* **148**(3), 494–500.
URL: *https://www.sciencedirect.com/science/article/pii/S0176161796802847*

Gitelson, A. & Merzlyak, M. N. (1994), 'Quantitative estimation of chlorophyll-a using reflectance spectra: Experiments with autumn chestnut and maple leaves', *Journal of Photochemistry and Photobiology B: Biology* **22**(3), 247–252.
URL: *https://www.sciencedirect.com/science/article/pii/1011134493069634*

González-Camacho, J. M., Ornella, L., Pérez-Rodríguez, P., Gianola, D., Dreisigacker, S. & Crossa, J. (2018), 'Applications of machine learning methods to genomic selection in breeding wheat for rust resistance', *The Plant Genome* **11**(2), 170104.
URL: *https://acsess.onlinelibrary.wiley.com/doi/abs/10.3835/plantgenome2017.11.0104*

Guo, Z., Yang, W., Chang, Y., Ma, X., Tu, H., Xiong, F., Jiang, N., Feng, H., Huang, C., Yang, P., Zhao, H., Chen, G., Liu, H., Luo, L., Hu, H., Liu, Q. & Xiong, L. (2018), 'Genome-wide association studies of image traits reveal genetic architecture of drought resistance in rice', *Mol Plant* **11**(6), 789–805.

Han, J., Zhang, Z., Cao, J., Luo, Y., Zhang, L., Li, Z. & Zhang, J. (2020), 'Prediction of winter wheat yield based on multi-source data and machine learning in china', *Remote Sensing* **12**(2), 236.

Hassan, M. A., Yang, M., Fu, L., Rasheed, A., Zheng, B., Xia, X., Xiao, Y. & He, Z. (2019), 'Accuracy assessment of plant height using an unmanned aerial vehicle for quantitative genomic analysis in bread wheat', *Plant Methods* **15**, 37.

Hassan, M. A., Yang, M., Rasheed, A., Tian, X., Reynolds, M., Xia, X., Xiao, Y. & He, Z. (2021), 'Quantifying senescence in bread wheat using multispectral imaging from an unmanned aerial vehicle and qtl mapping', *Plant physiology* **187**(4), 2623–2636.

Hatfield, J. L., Gitelson, A. A., Schepers, J. S. & Walthall, C. L. (2008), 'Application of spectral remote sensing for agronomic decisions', *Agronomy Journal* **100**(S3), S–117–S–131.
URL: *https://acsess.onlinelibrary.wiley.com/doi/abs/10.2134/agronj2006.0370c*

Hedrick, P. W. (2011), *Linkage Disequilibrium and Recombination*, 4th ed. edn, Jones and Bartlett Publishers, Boston, pp. 525–596.

Hill, M. & Donald, G. (2003), 'Estimating spatio-temporal patterns of agricultural productivity in fragmented landscapes using avhrr ndvi time series', *Remote Sensing of Environment* **84**, 367–384.

James, G., Witten, D., Hastie, T. & Tibshirani, R. (2013), *Support Vector Machines*, Springer New York, New York, NY, pp. 337–372.
URL: *https://doi.org/10.1007/978-1-4614-7138-7_9*

Jang, G., Kim, J., Yu, J.-K., Kim, H.-J., Kim, Y., Kim, D.-W., Kim, K.-H., Lee, C. W. & Chung, Y. S. (2020), 'Review: Cost-effective unmanned aerial vehicle (uav) platform for field plant breeding application', *Remote Sensing* **12**(6), 998.
URL: *https://www.mdpi.com/2072-4292/12/6/998*

Jangra, S., Chaudhary, V., Yadav, R. C. & Yadav, N. R. (2021), 'High-throughput phenotyping: A platform to accelerate crop improvement', *Phenomics* **1**(2), 31–53.
URL: *https://doi.org/10.1007/s43657-020-00007-6*

Janusauskaite, D. (2022), 'Leaf senescence of winter wheat and spring wheat as influenced by tillage and fertilization management', *Acta Physiologiae Plantarum* **44**(7), 74.
URL: *https://doi.org/10.1007/s11738-022-03399-2*

Jobson, E. M., Johnston, R. E., Oiestad, A. J., Martin, J. M. & Giroux, M. J. (2019), 'The impact of the wheat rht-b1b semi-dwarfing allele on photosynthesis and seed development under field conditions', *Frontiers in Plant Science* **10**.
URL: *https://www.frontiersin.org/journals/plant-science/articles/10.3389/fpls.2019.00051*

Kartseva, T., Alqudah, A. M., Aleksandrov, V., Alomari, D. Z., Doneva, D., Arif, M. A. R., Börner, A. & Misheva, S. (2023), 'Nutritional genomic approach for improving grain protein content in wheat', *Foods* **12**(7), 1399.
URL: *https://www.mdpi.com/2304-8158/12/7/1399*

Kibite, S. & Evans, L. E. (1984), 'Causes of negative correlations between grain yield and grain protein concentration in common wheat', *Euphytica* **33**(3), 801–810.
URL: *https://doi.org/10.1007/BF00021906*

Krause, M. R., González-Pérez, L., Crossa, J., Pérez-Rodríguez, P., Montesinos-López, O., Singh, R. P., Dreisigacker, S., Poland, J., Rutkoski, J., Sorrells, M., Gore, M. A. & Mondal, S. (2019), 'Hyperspectral reflectance-derived relationship matrices for genomic prediction of grain yield in wheat', *G3 (Bethesda)* **9**(4), 1231–1247.

Kumar, A., Bharti, B., Kumar, J., Bhatia, D., Singh, G. P., Jaiswal, J. P. & Prasad, R. (2020), 'Improving the efficiency of wheat breeding experiments using alpha lattice design over randomised complete block design', *Cereal Research Communications* **48**(1), 95–101.
URL: *https://doi.org/10.1007/s42976-020-00014-3*

Lambora, A., Gupta, K. & Chopra, K. (2019), Genetic algorithm- a literature review, *in* '2019 International Conference on Machine Learning, Big Data, Cloud and Parallel Computing (COMITCon)', pp. 380–384.

Li, F., Wen, W., Liu, J., Zhang, Y., Cao, S., He, Z., Rasheed, A., Jin, H., Zhang, C., Yan, J., Zhang, P., Wan, Y. & Xia, X. (2019), 'Genetic architecture of grain yield in bread wheat based on genome-wide association studies', *BMC Plant Biology* **19**(1), 168.
URL: *https://doi.org/10.1186/s12870-019-1781-3*

Liu, L., Cao, R., Chen, J., Shen, M., Wang, S., Zhou, J. & He, B. (2022), 'Detecting crop phenology from vegetation index time-series data by improved shape model fitting in each phenological stage', *Remote Sensing of Environment* **277**, 113060.
URL: *https://www.sciencedirect.com/science/article/pii/S0034425722001742*

lme4 Convergence Warnings: Troubleshooting (2024), `https://rstudio-pubs-static.s3.amazonaws.com/33653_57fc7b8e5d484c909b615d8633c01d51.html`. Accessed: February 01, 2024.

Lozano, A. C., Ding, H., Abe, N. & Lipka, A. E. (2023), 'Regularized multi-trait multi-locus linear mixed models for genome-wide association studies and genomic selection in crops', *BMC Bioinformatics* **24**(1), 399.
URL: *https://www.ncbi.nlm.nih.gov/pubmed/37884874*

Mathews, K. L. & Crossa, J. (2022), *Experimental Design for Plant Improvement*, Springer International Publishing, Cham, pp. 215–235.
URL: *https://doi.org/10.1007/978-3-030-90673-3_13*

Mooney, M., Wilmot, B., Bipolar Genome Study, T. & McWeeney, S. (2012), 'The ga and the gwas: using genetic algorithms to search for multilocus associations', *IEEE/ACM Trans Comput Biol Bioinform* **9**(3), 899–910.

Mroz, T., Dieseth, J. A. & Lillemo, M. (2023), 'Grain yield and adaptation of spring wheat to norwegian growing conditions is driven by allele frequency changes at key adaptive loci discovered by genome-wide association mapping', *Theor Appl Genet* **136**(9), 191.

Mróz, T., Shafiee, S., Crossa, J., Montesinos-Lopez, O. A. & Lillemo, M. (2024), 'Multispectral-derived genotypic similarities from budget cameras allow grain yield prediction and genomic selection augmentation in single and multi-environment scenarios in spring wheat', *Mol Breed* **44**(1), 5.

Mu, H., Zhou, L., Dang, X. & Yuan, B. (2019), Winter wheat yield estimation from multitemporal remote sensing images based on convolutional neural networks, *in* '2019 10th International Workshop on the Analysis of Multitemporal Remote Sensing Images (MultiTemp)', pp. 1–4.

Myles, C. & Wayne, M. (2008), 'Quantitative trait locus (qtl) analysis', *Nature Education 1 (1)* **208**.

Nannuru, V. K. R., Windju, S. S., Belova, T., Dieseth, J. A., Alsheikh, M., Dong, Y., McCartney, C. A., Henriques, M. A., Buerstmayr, H., Michel, S., Meuwissen, T. H. E. & Lillemo, M. (2022), 'Genetic architecture of fusarium head blight disease resistance and associated traits in nordic spring wheat', *Theor Appl Genet* **135**(7), 2247–2263.

Nazzicari, N. & Biscarini, F. (2022), *GROAN: an R package for testing genomic regression accuracy on (optionally noisy) phenotypes*, R package version 1.3.
URL: *https://cran.r-project.org/web/packages/GROAN/index.html*

Nowak, B. (2021), 'Precision agriculture: Where do we stand? a review of the adoption of precision agriculture technologies on field crops farms in developed countries', *Agricultural Research* **10**(4), 515–522.
URL: *https://doi.org/10.1007/s40003-021-00539-x*

Pang, Y., Liu, C., Wang, D., St Amand, P., Bernardo, A., Li, W., He, F., Li, L., Wang, L., Yuan, X., Dong, L., Su, Y., Zhang, H., Zhao, M., Liang, Y., Jia, H., Shen, X., Lu, Y., Jiang, H., Wu, Y., Li, A., Wang, H., Kong, L., Bai, G. & Liu, S. (2020), 'High-resolution genome-wide association study identifies genomic regions and candidate genes for important agronomic traits in wheat', *Mol Plant* **13**(9), 1311–1327.

Payero, J. O., Neale, C. & Wright, J. L. (2004), 'Comparison of eleven vegetation indices for estimating plant height of alfalfa and grass', *Applied Engineering in Agriculture* **20**.

Pedregosa, F., Varoquaux, G., Gramfort, A., Michel, V., Thirion, B., Grisel, O., Blondel, M., Prettenhofer, P., Weiss, R., Dubourg, V., Vanderplas, J., Passos, A., Cournapeau, D., Brucher, M., Perrot, M. & Duchesnay, E. (2011), 'Scikit-learn: Machine learning in python', *J. Mach. Learn. Res.* **12**, 2825–2830.

Phillips, R. L. (2017), 'Scikit-learn puk kernel implementation', https://github.com/rlphilli/sklearn-PUK-kernel. Accessed: February 12, 2024.

Piepho, H. P., Büchse, A. & Truberg, B. (2006), 'On the use of multiple lattice designs and -designs in plant breeding trials', *Plant Breeding* **125**(5), 523–528.
URL: *¡Go to ISI¿://WOS:000240440600019*

Qifu, Z., Haifeng, H., Youzheng, Z. & Guodong, S. (2009), Support vector machine based on universal kernel function and its application in quantitative structure - toxicity relationship model, *in* '2009 International Forum on Information Technology and Applications', Vol. 3, pp. 708–711.

Rahman, M. & Robson, A. (2016), 'A novel approach for sugarcane yield prediction using landsat time series imagery: A case study on bundaberg region', *Advances in Remote Sensing* **5**, 93–102.

Rapp, M., Lein, V., Lacoudre, F., Lafferty, J., Müller, E., Vida, G., Bozhanova, V., Ibraliu, A., Thorwarth, P., Piepho, H. P., Leiser, W. L., Würschum, T. & Longin, C. F. H. (2018), 'Simultaneous improvement of

grain yield and protein content in durum wheat by different phenotypic indices and genomic selection', *Theoretical and Applied Genetics* **131**(6), 1315–1329.
URL: *https://doi.org/10.1007/s00122-018-3080-z*

Raschka, S. & Mirjalili, V. (2019*a*), *Maximum margin classification with support vector machines*, Packt Publishing Ltd, pp. 76–81.

Raschka, S. & Mirjalili, V. (2019*b*), *Solving nonlinear problems using a kernel SVM*, Packt Publishing Ltd, pp. 76–81.

Rodrigues, F. A., J., Blasch, G., Defourny, P., Ortiz-Monasterio, J. I., Schulthess, U., Zarco-Tejada, P. J., Taylor, J. A. & Gérard, B. (2018), 'Multi-temporal and spectral analysis of high-resolution hyperspectral airborne imagery for precision agriculture: Assessment of wheat grain yield and grain protein content', *Remote Sens (Basel)* **10**(6), 930.

Saini, D. K., Chopra, Y., Singh, J., Sandhu, K. S., Kumar, A., Bazzer, S. & Srivastava, P. (2021), 'Comprehensive evaluation of mapping complex traits in wheat using genome-wide association studies', *Molecular Breeding* **42**(1), 1.
URL: *https://doi.org/10.1007/s11032-021-01272-7*

Sandhu, N., Sethi, M., Kumar, A., Dang, D., Singh, J. & Chhuneja, P. (2021), 'Biochemical and genetic approaches improving nitrogen use efficiency in cereal crops: A review', *Frontiers in Plant Science* **12**.
URL: *https://www.frontiersin.org/journals/plant-science/articles/10.3389/fpls.2021.657629*

Sarić, R., Nguyen, V. D., Burge, T., Berkowitz, O., Trtílek, M., Whelan, J., Lewsey, M. G. & Čustović, E. (2022), 'Applications of hyperspectral imaging in plant phenotyping', *Trends in plant science* .

Schmidt, P., Hartung, J., Bennewitz, J. & Piepho, H.-P. (2019), 'Heritability in plant breeding on a genotype-difference basis', *Genetics* **212**(4), 991–1008.
URL: *https://doi.org/10.1534/genetics.119.302134*

Scrucca, L. (2013), 'Ga: A package for genetic algorithms in r', *Journal of Statistical Software* **53**(4), 1 – 37.
URL: *https://www.jstatsoft.org/index.php/jss/article/view/v053i04*

Segura, V., Vilhjalmsson, B. J., Platt, A., Korte, A., Seren, U., Long, Q. & Nordborg, M. (2012), 'An efficient multi-locus mixed-model approach for genome-wide association studies in structured populations', *Nat Genet* **44**(7), 825–30.
URL: *https://www.ncbi.nlm.nih.gov/pubmed/22706313*

Semagn, K., Iqbal, M., Chen, H., Perez-Lara, E., Bemister, D. H., Xiang, R., Zou, J., Asif, M., Kamran, A., N'Diaye, A., Randhawa, H., Pozniak, C. & Spaner, D. (2021), 'Physical mapping of qtl in four spring wheat populations under conventional and organic management systems. i. earliness', *Plants (Basel)* **10**(5).

Shafiee, S., Montesinos-López, O. A., Crossac, J., Burud, I., Dieseth, J. A., Alsheikh, M. & Lillemo, M. (2024), 'Integrating genomic and phenomic data from multi-temporal uav imagery enhances prediction accuracy of wheat late season traits', *Manuscript, unpublished* .

Shafiee, S., Mroz, T., Burud, I. & Lillemo, M. (2023), 'Evaluation of uav multispectral cameras for yield and biomass prediction in wheat under different sun elevation angles and phenological stages', *Computers and Electronics in Agriculture* **210**, 107874.
URL: *https://www.sciencedirect.com/science/article/pii/S0168169923002624*

Shariatipour, N., Heidari, B., Tahmasebi, A. & Richards, C. (2021), 'Comparative genomic analysis of quantitative trait loci associated with micronutrient contents, grain quality, and agronomic traits in wheat (triticum aestivum l.)', *Frontiers in Plant Science* **12**.
URL: *https://www.frontiersin.org/journals/plant-science/articles/10.3389/fpls.2021.709817*

Shewry, P. (2023), 'Wheat grain proteins: Past, present, and future', *Cereal Chem* **100**(1), 9–22.

Silleos, G., Alexandridis, T., Gitas, I. & Perakis, K. (2006), 'Vegetation indices: Advances made in biomass estimation and vegetation monitoring in the last 30 years', *Geocarto International* **21**, 21–28.

Sukumaran, S., Rebetzke, G., Mackay, I., Bentley, A. R. & Reynolds, M. P. (2022), *Pre-breeding Strategies*, Springer International Publishing, Cham, pp. 451–469.
URL: *https://doi.org/10.1007/978-3-030-90673-3_25*

Tangpattanakul, P., Soontranon, N., Lawawirojwong, S., Rakwatin, P. & Pannangpetch, K. (2015), A study of rice phenological development stages estimation from field server images, pp. 1–4.

Tenreiro, T. R., García-Vila, M., Gómez, J. A., Jiménez-Berni, J. A. & Fereres, E. (2021), 'Using ndvi for the assessment of canopy cover in agricultural crops within modelling research', *Computers and Electronics in Agriculture* **182**, 106038.
URL: *https://www.sciencedirect.com/science/article/pii/S0168169921000569*

Uhlen, A., Hafskjold, R., Kalhovd, A. H., Sahlstrøm, S., Longva, Å. & Magnus, E. (1998), 'Effects of cultivar and temperature during grain filling on wheat protein content, composition, and dough mixing properties', *Cereal Chemistry - CEREAL CHEM* **75**.

van Dijk, A. D. J., Kootstra, G., Kruijer, W. & de Ridder, D. (2021), 'Machine learning in plant science and plant breeding', *Iscience* **24**(1).

Verrelst, J., Camps-Valls, G., Muñoz-Marí, J., Rivera, J. P., Veroustraete, F., Clevers, J. G. P. W. & Moreno, J. (2015), 'Optical remote sensing and the retrieval of terrestrial vegetation bio-geophysical properties – a review', *ISPRS Journal of Photogrammetry and Remote Sensing* **108**, 273–290.
URL: *https://www.sciencedirect.com/science/article/pii/S0924271615001422*

Virtanen, P., Gommers, R., Oliphant, T. E., Haberland, M., Reddy, T., Cournapeau, D., Burovski, E., Peterson, P., Weckesser, W., Bright, J., van der Walt, S. J., Brett, M., Wilson, J., Millman, K. J., Mayorov, N., Nelson, A. R. J., Jones, E., Kern, R., Larson, E., Carey, C. J., Polat, İ., Feng, Y., Moore, E. W., VanderPlas, J., Laxalde, D., Perktold, J., Cimrman, R., Henriksen, I., Quintero, E. A., Harris, C. R., Archibald, A. M., Ribeiro, A. H., Pedregosa, F., van Mulbregt, P. & SciPy 1.0 Contributors (2020), 'Scipy 1.0: Fundamental algorithms for scientific computing in python', *Nature Methods* **17**, 261–272.

Wang, J., Li, X., Guo, T., Dzievit, M. J., Yu, X., Liu, P., Price, K. P. & Yu, J. (2021), 'Genetic dissection of seasonal vegetation index dynamics in maize through aerial based high-throughput phenotyping', *Plant Genome* **14**(3), e20155.
URL: *https://www.ncbi.nlm.nih.gov/pubmed/34596348*

Xiao, Q., Bai, X., Zhang, C. & He, Y. (2022), 'Advanced high-throughput plant phenotyping techniques for genome-wide association studies: A review', *J Adv Res* **35**, 215–230.

Xu, S. (2022), *Genome-Wide Association Studies*, Springer International Publishing, Cham, pp. 347–366.
URL: *https://doi.org/10.1007/978-3-030-83940-6_19*

Yang, M., Hassan, M. A., Xu, K., Zheng, C., Rasheed, A., Zhang, Y., Jin, X., Xia, X., Xiao, Y. & He, Z. (2020), 'Assessment of water and nitrogen use efficiencies through uav-based multispectral phenotyping in winter wheat', *Frontiers in Plant Science* **11**.
URL: *https://www.frontiersin.org/journals/plant-science/articles/10.3389/fpls.2020.00927*

Yoosefzadeh-Najafabadi, M., Eskandari, M., Torabi, S., Torkamaneh, D., Tulpan, D. & Rajcan, I. (2022), 'Machine-learning-based genome-wide association studies for uncovering qtl underlying soybean yield and its components', *Int J Mol Sci* **23**(10).

Yu, J., Pressoir, G., Briggs, W. H., Vroh Bi, I., Yamasaki, M., Doebley, J. F., McMullen, M. D., Gaut, B. S., Nielsen, D. M., Holland, J. B., Kresovich, S. & Buckler, E. S. (2006), 'A unified mixed-model method for association mapping that accounts for multiple levels of relatedness', *Nat Genet* **38**(2), 203–8.
URL: *https://www.ncbi.nlm.nih.gov/pubmed/16380716*

Zeng, L., Wardlow, B. D., Xiang, D., Hu, S. & Li, D. (2020), 'A review of vegetation phenological metrics extraction using time-series, multispectral satellite data', *Remote Sensing of Environment* **237**, 111511.
URL: *https://www.sciencedirect.com/science/article/pii/S0034425719305309*

Zhang, X. K., Xiao, Y. G., Zhang, Y., Xia, X. C., Dubcovsky, J. & He, Z. H. (2008), 'Allelic variation at the vernalization genes vrn-a1, vrn-b1, vrn-d1, and vrn-b3 in chinese wheat cultivars and their association with growth habit', *Crop Science* **48**(2), 458–470.
URL: *https://acsess.onlinelibrary.wiley.com/doi/abs/10.2135/cropsci2007.06.0355*

Zhang, X., Yang, S., Zhou, Y., He, Z. & Xia, X. (2006), 'Distribution of the rht-b1b, rht-d1b and rht8 reduced height genes in autumn-sown chinese wheats detected by molecular markers', *Euphytica* **152**(1), 109–116.
URL: *https://doi.org/10.1007/s10681-006-9184-6*

Zhang, Z., Ersoz, E., Lai, C. Q., Todhunter, R. J., Tiwari, H. K., Gore, M. A., Bradbury, P. J., Yu, J., Arnett, D. K., Ordovas, J. M. & Buckler, E. S. (2010), 'Mixed linear model approach adapted for genome-wide association studies', *Nat Genet* **42**(4), 355–60.

Zhao, K., Aranzana, M. J., Kim, S., Lister, C., Shindo, C., Tang, C., Toomajian, C., Zheng, H., Dean, C., Marjoram, P. & Nordborg, M. (2007), 'An arabidopsis example of association mapping in structured samples', *PLOS Genetics* **3**(1), e4.
URL: *https://doi.org/10.1371/journal.pgen.0030004*
ΩÜstün et al.

Üstün, B., Melssen, W. J. & Buydens, L. M. C. (2006), 'Facilitating the application of support vector regression by using a universal pearson vii function based kernel', *Chemometrics and Intelligent Laboratory Systems* **81**(1), 29–40.
URL: *https://www.sciencedirect.com/science/article/pii/S0169743905001474*

7 Appendix

7.1 Variance Components Estimation: Trials Means and Global Means for Bands/VIs

Table A1: Results for trial means in 2019 when genotype is modelled as a random effect. SD refers to $\hat{\sigma}$. See equation 2.

	blue	green	red	red-edge	NIR	NDVI	GNDVI	SR
(Intercept)	-0.001	0.000	0.000	0.000	0.000	0.000	0.000	-0.001
	(0.373)	(0.390)	(0.423)	(0.405)	(0.437)	(0.432)	(0.419)	(0.427)
SD (Intercept Time Pointrepblock)	0.246	0.221	0.148	0.169	0.142	0.170	0.220	0.214
SD (Intercept Time Pointcolumn)	0.065	0.067	0.049	0.067	0.018	0.000	0.025	0.038
SD (Intercept Line Number)	0.291	0.258	0.148	0.217	0.068	0.108	0.172	0.113
SD (Intercept Time Pointrep)	0.151	0.117	0.052	0.110	0.056	0.033	0.030	0.105
SD (Intercept Time Point)	0.905	0.949	1.034	0.989	1.069	1.057	1.026	1.043
SD (Residuals)	0.376	0.337	0.235	0.305	0.138	0.162	0.198	0.137
R2 Cond.	0.875	0.901	0.953	0.920	0.984		0.966	0.984
AIC	3467.1	2905.8	933.9	2269.6	-1616.9	-695.1	544.6	-995.3
BIC	3508.2	2946.9	975.0	2310.7	-1575.8	-654.0	585.7	-954.2
ICC	0.9	0.9	1.0	0.9	1.0		1.0	1.0
RMSE	0.33	0.30	0.21	0.27	0.12	0.14	0.17	0.12

Table A2: Global means for bands/VIs time-series when genotype is modeled as a random effect. SD refers to $\hat{\sigma}$. See equation 3.

	blue	green	red	red-edge	NIR	NDVI	GNDVI	SR
(Intercept)	0.000	0.022	0.009	0.019	0.005	−0.003	−0.011	−0.004
	(0.162)	(0.175)	(0.192)	(0.169)	(0.184)	(0.197)	(0.197)	(0.198)
SD (Intercept Seasontime Pointrepblock)	0.244	0.198	0.178	0.244	0.326	0.195	0.192	0.232
SD (Intercept Seasontime Pointcolumn)	0.036	0.046	0.032	0.044	0.029	0.000	0.000	0.027
SD (Intercept Line Number)	0.342	0.329	0.186	0.327	0.175	0.140	0.181	0.145
SD (Intercept Seasontime Pointrep)	0.111	0.082	0.041	0.114	0.112	0.049	0.047	0.113
SD (Intercept Seasontime Point)	0.783	0.848	0.940	0.818	0.894	0.965	0.961	0.963
SD (Intercept Season)	0.000	0.000	0.000	0.000	0.000	0.000	0.002	0.000
SD (Residuals)	0.494	0.428	0.295	0.459	0.302	0.207	0.206	0.165
R2 Cond.			0.916	0.801			0.959	
AIC	20 784.7	17 186.9	8532.8	19 221.5	11 071.5	1208.1	1193.7	−2561.1
BIC	20 844.2	17 246.3	8592.3	19 280.9	11 130.9	1267.6	1253.1	−2501.7
ICC			0.9	0.8			1.0	
RMSE	0.46	0.40	0.27	0.43	0.27	0.19	0.19	0.15

7.2 Variance Components Estimation: Global Means of AUC-values and Agronomic Traits

Table A3: Global means for AUC-values when genotype is modeled as a random effect. SD refers to $\hat{\sigma}$. See equation 5.

	NDVI	GNDVI	SR
(Intercept)	−0.027	−0.048	−0.033
	(0.059)	(0.058)	(0.076)
SD (Intercept seasonrepblock)	0.614	0.610	0.670
SD (Intercept line_number)	0.730	0.765	0.677
SD (Intercept seasoncolumn)	0.082	0.097	0.116
SD (Intercept seasonrep)	0.068	0.040	0.149
SD (Intercept season)	0.000	0.000	0.000
SD (Residuals)	0.342	0.359	0.350
R2 Cond.	0.888		
AIC	4103.5	4329.8	4264.6
BIC	4144.6	4371.0	4305.7
ICC	0.9		
RMSE	0.29	0.31	0.30

Table A4: Global means for agronomic traits when genotype is modeled as a random effect. SD refers to $\hat{\sigma}$. See equation 5.

	DH_dss	DM_dss	GY_g_m2	PH_cm	GPC_pct
(Intercept)	64.975	109.864	604.971	88.236	10.979
	(1.544)	(2.820)	(28.499)	(2.680)	(0.171)
SD (Intercept seasonrepblock)	0.379	1.344	43.204	3.183	0.370
SD (Intercept line_number)	1.378	2.503	74.739	7.092	0.874
SD (Intercept seasoncolumn)	0.109	0.252	5.637	0.174	0.054
SD (Intercept seasonrep)	0.172	0.291	1.309	0.951	0.201
SD (Intercept season)	3.080	5.626	56.128	5.242	0.290
SD (Residuals)	0.614	1.608	29.880	2.943	0.445
R2 Cond.	0.968	0.939	0.923	0.911	0.839
AIC	5544.6	9603.4	22 734.3	12 571.4	4215.9
BIC	5584.3	9643.0	22 774.0	12 611.1	4255.5
ICC	1.0	0.9	0.9	0.9	0.8
RMSE	0.53	1.37	24.82	2.49	0.38

7.3 DH and DM Distribution with Selected Time-Points

Figure A1 shows the distribution of days to heading (DH) and days to maturity (DM) within each season relative to sowing dates. The figure also contains black horizontal lines signifying the time-points sampled from the multispectral time-series for downstream analysis. Furthermore, the colored lined refer to different developmental stages, and are based on the definitions of (Krause et al. 2019). The green line refers to the vegetative stage (VEG), the orange line signifies the heading stage (HEAD) and the red line signifies the grain filling stages (GF). All observations falling to the left of a coloured line belong to the given stage.

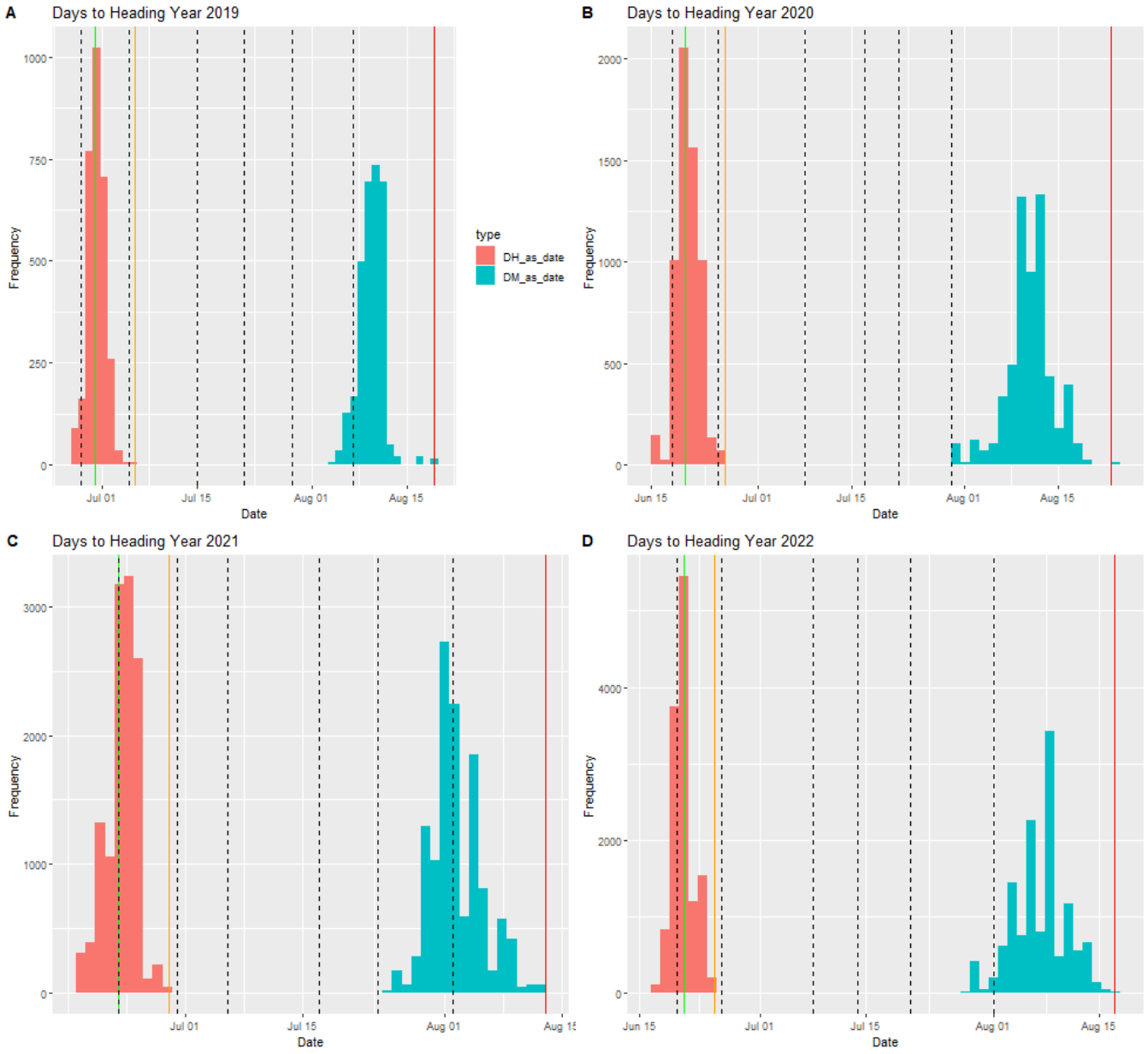

Figure A1: A-D show the distribution of DH and DM within the respective seasons. Black lines are the selected time points (T1-T6). Coloured lines signify the growth stages (green = VEG, orange = HEAD, red = GF)

7.4 Time-Series Data After Frequency Adjustment

Figure A2 showcases the averaged time-series for each spectral band and VI after we have sampled 6 flight missions (T1-T6) within each season. Average values for each band/VIs was derived by averaging over all plots within each time-point.

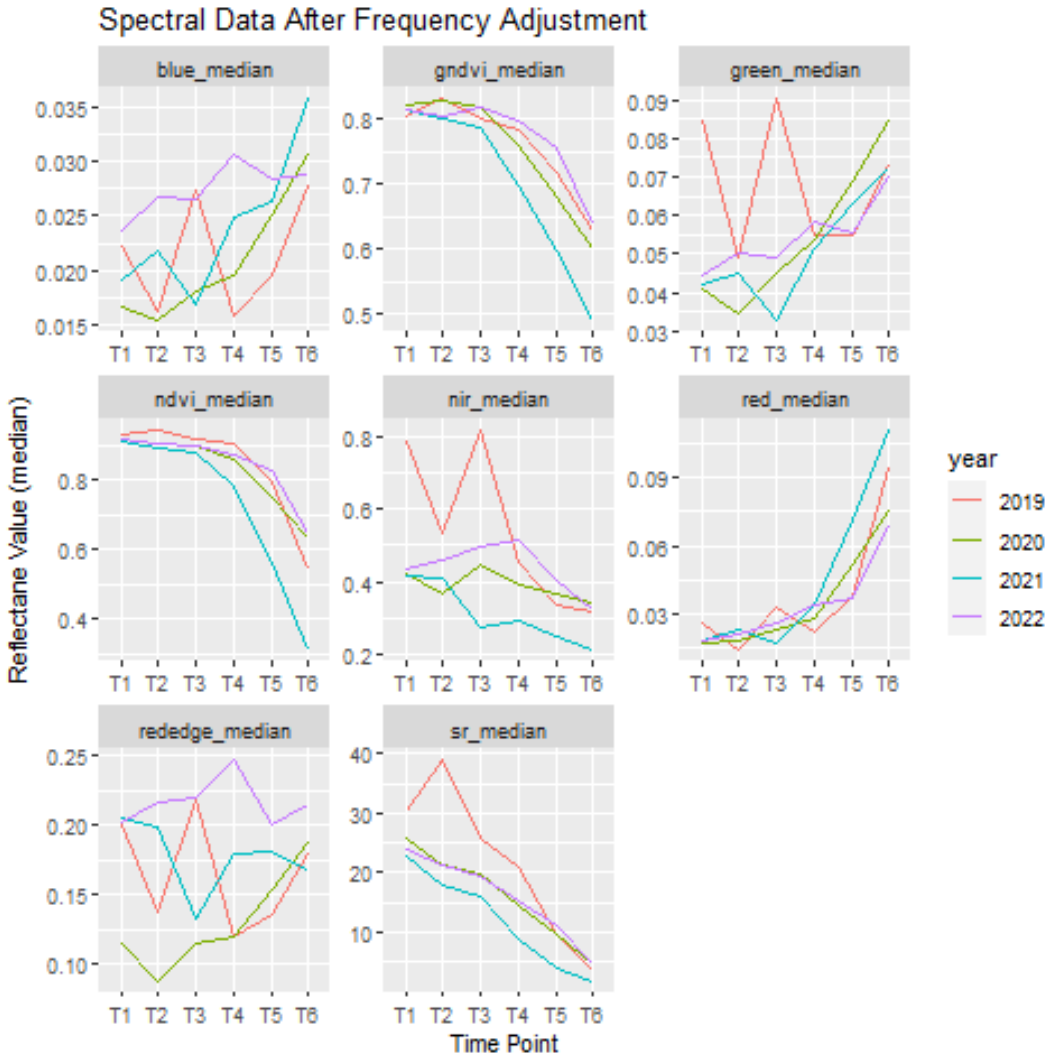

Figure A2: The averaged spectral reflectance value for bands and VIs across the selected time points

7.5 Distribution of AUC-values of VIs

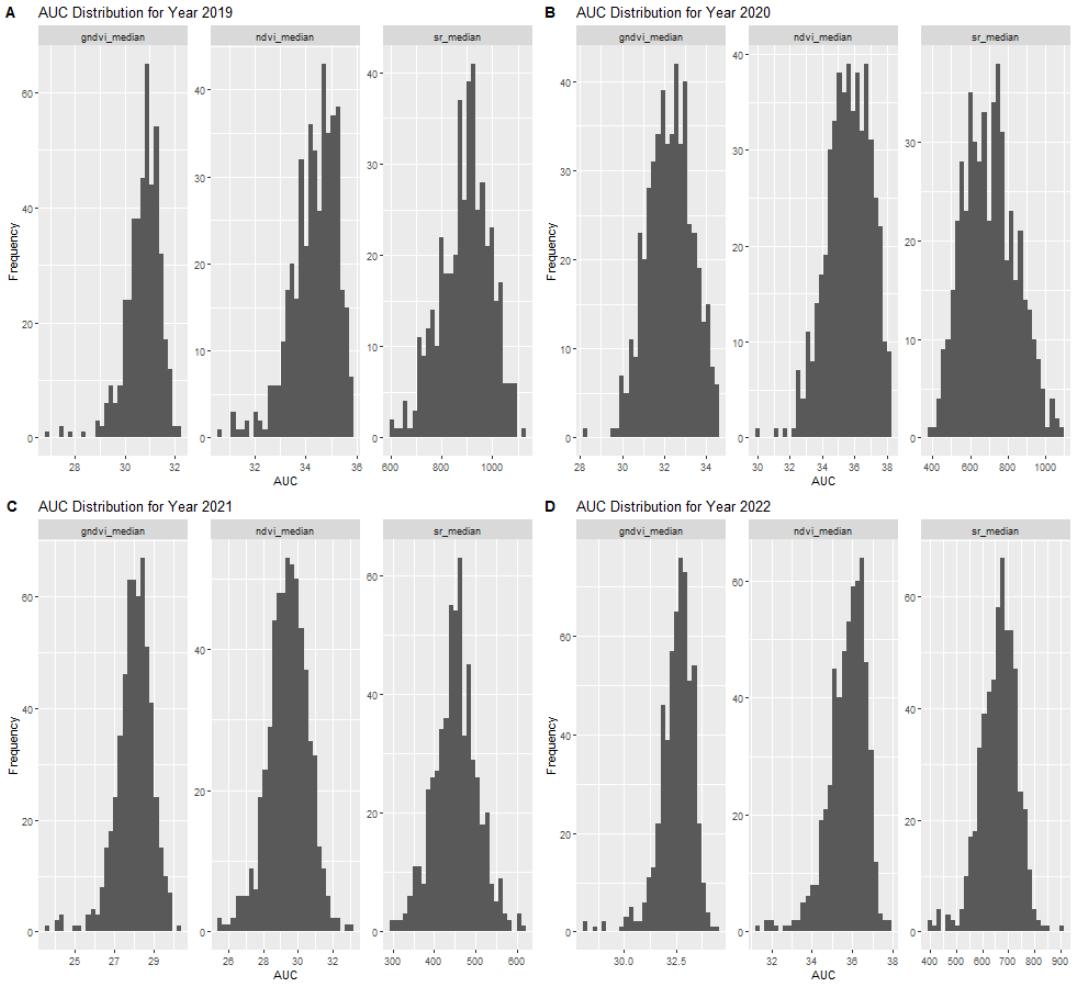

Figure A3: A-D show the distribution of AUC-values for plots within respective seasons.

7.6 QTL Identified for Spectral Time-Series Using MLM

Table A5: QTL identified for spectral time-series ($p < 0.001$)

Phenotype	QTL	Chr	Span	# Markers	Peak-marker	P.value	MAF	Effect
blue	Q_blue_1A_1	1A	591-592	2	RAC875_c85550_73	0.00042	0.066	-0.15
blue	Q_blue_1A_1	1A	591-592	2	BS00021780_51	0.00042	0.066	-0.15
blue	Q_blue_2A_1	2A	127	1	Kukri_c441_891	0.00013	0.076	-0.17
blue	Q_blue_3A_1	3A	594	1	Kukri_c7087_896	0.00043	0.066	0.19
blue	Q_blue_3B_1	3B	571-576	2	AX-158557916	0.00088	0.14	0.14
blue	Q_blue_3B_1	3B	571-576	2	AX-158541479	0.00018	0.093	0.19
blue	Q_blue_3B_2	3B	800	1	RAC875_c39339_400	4.4e-05	0.055	-0.22
blue	Q_blue_4A_1	4A	623	1	Excalibur_c25699_113	0.001	0.16	-0.1
blue	Q_blue_4A_2	4A	673	1	Excalibur_c53864_331	2e-05	0.067	0.21
blue	Q_blue_5A_1	5A	36	1	wsnp_Ku_c4389_7970859	0.0002	0.18	-0.12
blue	Q_blue_5A_2	5A	549	1	AX-94501987	5.8e-06	0.074	0.22
blue	Q_blue_5A_3	5A	599	1	BS00000929_51	0.00084	0.12	0.15
blue	Q_blue_6B_1	6B	714	1	GENE-4008_395	0.00035	0.1	0.16
blue	Q_blue_7A_1	7A	59	1	Excalibur_c57078_255	0.00017	0.074	0.18
blue	Q_blue_Unkown_1	Unkown	144	1	BobWhite_c12261_130	0.00059	0.1	0.15
GNDVI	Q_GNDVI_2A_1	2A	127	1	Kukri_c441_891	0.00099	0.076	0.07
GNDVI	Q_GNDVI_3A_1	3A	594	1	Kukri_c7087_896	0.00061	0.066	-0.091
GNDVI	Q_GNDVI_4A_1	4A	512	1	RAC875_c91464_170	0.00019	0.062	0.087
GNDVI	Q_GNDVI_5A_1	5A	687	1	Ku_c19516_384	0.0009	0.13	0.068
GNDVI	Q_GNDVI_5B_1	5B	50	1	RAC875_c16827_292	0.00083	0.13	0.056
GNDVI	Q_GNDVI_7A_1	7A	51	1	AX-94617750	1.6e-05	0.061	0.11
GNDVI	Q_GNDVI_7A_2	7A	482	1	Kukri_c52429_81	0.00033	0.059	0.087
green	Q_green_1A_1	1A	403	1	AX-110387060	0.001	0.087	-0.14
green	Q_green_1A_2	1A	591-592	2	RAC875_c85550_73	4.2e-06	0.066	-0.18
green	Q_green_1A_2	1A	591-592	2	BS00021780_51	4.2e-06	0.066	-0.18
green	Q_green_1B_1	1B	672	2	AX-158521058	0.00052	0.061	-0.23
green	Q_green_1B_1	1B	672	2	BS00023105_51	0.00052	0.061	-0.23
green	Q_green_2A_1	2A	74-78	6	BS00036767_51	4.3e-05	0.073	-0.21
green	Q_green_2A_1	2A	74-78	6	Kukri_rep_c83485_398	4.3e-05	0.073	-0.21
green	Q_green_2A_1	2A	74-78	6	AX-110428187	7.9e-05	0.08	-0.18
green	Q_green_2A_1	2A	74-78	6	BS00039983_51	7.9e-05	0.08	-0.18
green	Q_green_2A_1	2A	74-78	6	Kukri_rep_c104727_91	7.4e-05	0.054	-0.24
green	Q_green_2A_1	2A	74-78	6	wsnp_Ex_rep_c68113_66877517	2.3e-05	0.054	-0.26
green	Q_green_2A_2	2A	105-127	7	wsnp_Ex_c1782_3365844	0.00045	0.22	-0.1
green	Q_green_2A_2	2A	105-127	7	wsnp_Ex_rep_c101866_87158671	0.00062	0.21	-0.1
green	Q_green_2A_2	2A	105-127	7	AX-158546418	0.00061	0.21	-0.1
green	Q_green_2A_2	2A	105-127	7	TA003045-1227	0.00061	0.21	-0.1
green	Q_green_2A_2	2A	105-127	7	wsnp_Ex_rep_c69124_68035485	0.00061	0.21	-0.1
green	Q_green_2A_2	2A	105-127	7	AX-94457129	0.00038	0.27	-0.097
green	Q_green_2A_2	2A	105-127	7	Kukri_c441_891	4.5e-07	0.076	-0.21
green	Q_green_2A_3	2A	773	1	BS00091763_51	5.2e-05	0.09	-0.15
green	Q_green_3A_1	3A	594	1	Kukri_c7087_896	0.00056	0.066	0.18
green	Q_green_3A_2	3A	743	1	AX-95254393	0.0006	0.25	-0.1
green	Q_green_3B_1	3B	473-474	4	AX-110403928	7.5e-05	0.095	-0.15
green	Q_green_3B_1	3B	473-474	4	RAC875_c50787_146	8.6e-05	0.097	-0.15
green	Q_green_3B_1	3B	473-474	4	AX-110958104	0.00089	0.087	-0.13
green	Q_green_3B_1	3B	473-474	4	AX-158538397	0.00052	0.08	-0.13
green	Q_green_3B_2	3B	501	1	RAC875_c2044_170	0.00043	0.16	0.14

Table A5 continued: QTL identified for spectral time-series ($p < 0.001$)

Phenotype	QTL	Chr	Span	# Markers	Peak-marker	P.value	MAF	Effect
green	Q_green_3B_3	3B	576	1	AX-158541479	0.00037	0.093	0.17
green	Q_green_3B_4	3B	627	1	AX-158598230	0.00013	0.19	0.13
green	Q_green_3B_5	3B	800	1	RAC875_c39339_400	2e-05	0.055	-0.21
green	Q_green_4A_1	4A	512	1	RAC875_c91464_170	0.00012	0.062	-0.17
green	Q_green_4A_2	4A	673	1	Excalibur_c53864_331	4.4e-05	0.067	0.19
green	Q_green_4B_1	4B	644	1	AX-89771703	0.00011	0.067	-0.18
green	Q_green_5A_1	5A	35-36	2	AX-94958984	0.00048	0.092	-0.16
green	Q_green_5A_1	5A	35-36	2	wsnp_Ku_c4389_7970859	0.00042	0.18	-0.11
green	Q_green_5A_2	5A	445	1	AX-158542603	0.00038	0.19	-0.11
green	Q_green_5A_3	5A	549	1	AX-94501987	3.8e-05	0.074	0.18
green	Q_green_5A_4	5A	680	1	BobWhite_c8906_83	0.00047	0.1	-0.16
green	Q_green_6A_1	6A	616	1	BS00082460_51	0.00026	0.059	-0.17
green	Q_green_6B_1	6B	644	1	TA004372-0730	0.00026	0.12	-0.14
green	Q_green_7A_1	7A	14	1	BS00068863_51	0.00035	0.16	-0.11
green	Q_green_7A_2	7A	51-92	4	AX-94617750	0.00027	0.061	-0.17
green	Q_green_7A_2	7A	51-92	4	Excalibur_c57078_255	0.00013	0.074	0.17
green	Q_green_7A_2	7A	51-92	4	BS00091891_51	0.00071	0.064	-0.17
green	Q_green_7A_2	7A	51-92	4	BobWhite_c24295_777	0.00091	0.12	-0.12
green	Q_green_Unkown_1	Unkown	796	1	IAAV1529	0.00011	0.057	-0.18
green	Q_green_Unkown_2	Unkown	1081	1	Kukri_c3570_1817	0.00011	0.055	-0.19
green	Q_green_Unkown_3	Unkown	1127	1	Kukri_c7914_99	4.3e-05	0.073	-0.21
green	Q_green_Unkown_4	Unkown	1335	1	RAC875_rep_c71921_672	9.4e-05	0.066	-0.15
green	Q_green_Unkown_5	Unkown	1376	1	RFL_Contig5758_757	0.00043	0.17	0.14
NDVI	Q_NDVI_4A_1	4A	25	1	wsnp_Ex_c22913_32130617	0.00042	0.062	0.059
NDVI	Q_NDVI_4B_1	4B	20-32	3	Kukri_rep_c74376_188	0.00071	0.29	-0.032
NDVI	Q_NDVI_4B_1	4B	20-32	3	AX-94685504	0.00037	0.48	0.034
NDVI	Q_NDVI_4B_1	4B	20-32	3	AX-89380014	0.00042	0.39	0.036
NDVI	Q_NDVI_5A_1	5A	300	1	AX-110003331	3.8e-05	0.21	0.045
NDVI	Q_NDVI_7A_1	7A	49-51	2	AX-95133112	0.00077	0.09	0.059
NDVI	Q_NDVI_7A_1	7A	49-51	2	AX-94617750	0.00014	0.061	0.075
NDVI	Q_NDVI_7A_2	7A	669	1	BS00021261_51	0.00083	0.078	-0.065
NIR	Q_NIR_1A_1	1A	591-592	2	RAC875_c85550_73	9.2e-05	0.066	-0.091
NIR	Q_NIR_1A_1	1A	591-592	2	BS00021780_51	9.2e-05	0.066	-0.091
NIR	Q_NIR_2A_1	2A	74-77	13	AX-110998568	0.0002	0.099	-0.087
NIR	Q_NIR_2A_1	2A	74-77	13	BS00036766_51	0.00042	0.11	-0.08
NIR	Q_NIR_2A_1	2A	74-77	13	BS00036767_51	0.00012	0.073	-0.11
NIR	Q_NIR_2A_1	2A	74-77	13	Kukri_rep_c83485_398	0.00012	0.073	-0.11
NIR	Q_NIR_2A_1	2A	74-77	13	Tdurum_contig9731_121	0.00011	0.083	-0.11
NIR	Q_NIR_2A_1	2A	74-77	13	Excalibur_c15733_252	0.00011	0.083	-0.11
NIR	Q_NIR_2A_1	2A	74-77	13	Excalibur_rep_c111743_194	0.00064	0.073	-0.098
NIR	Q_NIR_2A_1	2A	74-77	13	GENE-1365_255	0.00011	0.083	-0.11
NIR	Q_NIR_2A_1	2A	74-77	13	RAC875_c20700_853	0.00011	0.083	-0.11
NIR	Q_NIR_2A_1	2A	74-77	13	Tdurum_contig48302_532	0.00011	0.083	-0.11
NIR	Q_NIR_2A_1	2A	74-77	13	Tdurum_contig5311_67	0.00011	0.083	-0.11
NIR	Q_NIR_2A_1	2A	74-77	13	AX-110428187	0.00026	0.08	-0.097
NIR	Q_NIR_2A_1	2A	74-77	13	BS00039983_51	0.00026	0.08	-0.097
NIR	Q_NIR_2B_1	2B	114	1	Excalibur_c37649_125	0.00024	0.1	-0.083
NIR	Q_NIR_3A_1	3A	267	1	BS00110129_51	0.00044	0.42	-0.05
NIR	Q_NIR_3A_2	3A	445	1	IAAV4343	0.00045	0.18	0.057
NIR	Q_NIR_3A_3	3A	466-484	3	wsnp_JD_rep_c64325_41024646	0.001	0.37	-0.046
NIR	Q_NIR_3A_3	3A	466-484	3	wsnp_JD_c5699_6859527	0.00091	0.1	0.071

Table A5 continued: QTL identified for spectral time-series ($p < 0.001$)

Phenotype	QTL	Chr	Span	# Markers	Peak-marker	P.value	MAF	Effect
NIR	Q_NIR_3A_3	3A	466-484	3	wsnp_RFL_Contig2011_1216801	0.0009	0.11	0.071
NIR	Q_NIR_3A_4	3A	511	1	AX-95205191	0.00014	0.16	0.085
NIR	Q_NIR_3B_1	3B	473	2	AX-110403928	0.00014	0.095	-0.084
NIR	Q_NIR_3B_1	3B	473	2	RAC875_c50787_146	0.00032	0.097	-0.078
NIR	Q_NIR_3B_2	3B	497-507	12	AX-109475553	5e-05	0.16	0.09
NIR	Q_NIR_3B_2	3B	497-507	12	IAAV4105	5e-05	0.16	0.09
NIR	Q_NIR_3B_2	3B	497-507	12	Tdurum_contig12941_1413	5e-05	0.16	0.09
NIR	Q_NIR_3B_2	3B	497-507	12	Excalibur_c14999_712	5e-05	0.16	0.09
NIR	Q_NIR_3B_2	3B	497-507	12	BobWhite_c45623_215	5e-05	0.16	0.09
NIR	Q_NIR_3B_2	3B	497-507	12	RAC875_c2044_170	1.6e-05	0.16	0.096
NIR	Q_NIR_3B_2	3B	497-507	12	RAC875_c32792_231	5e-05	0.16	0.09
NIR	Q_NIR_3B_2	3B	497-507	12	Tdurum_contig9132_102	5e-05	0.16	0.09
NIR	Q_NIR_3B_2	3B	497-507	12	AX-158555838	5e-05	0.16	0.09
NIR	Q_NIR_3B_2	3B	497-507	12	AX-110527999	0.00017	0.2	0.078
NIR	Q_NIR_3B_2	3B	497-507	12	AX-94407975	5e-05	0.16	0.09
NIR	Q_NIR_3B_2	3B	497-507	12	Tdurum_contig10107_580	2.9e-05	0.16	0.095
NIR	Q_NIR_3D_1	3D	86	1	IAAV2729	2.1e-06	0.11	0.09
NIR	Q_NIR_4A_1	4A	673	1	Excalibur_c53864_331	0.00025	0.067	0.097
NIR	Q_NIR_5A_1	5A	10	1	tplb0029e02_1186	0.00012	0.23	0.057
NIR	Q_NIR_5A_2	5A	549	1	AX-94501987	3.5e-05	0.074	0.1
NIR	Q_NIR_5B_1	5B	421	1	AX-95099091	0.00086	0.069	-0.079
NIR	Q_NIR_7A_1	7A	59	1	Excalibur_c57078_255	0.00013	0.074	0.1
NIR	Q_NIR_7B_1	7B	62	1	Kukri_c14766_484	8.1e-06	0.055	0.13
NIR	Q_NIR_Unkown_1	Unkown	1127	1	Kukri_c7914_99	0.00012	0.073	-0.11
NIR	Q_NIR_Unkown_2	Unkown	1376	1	RFL_Contig5758_757	3.5e-05	0.17	0.091
red	Q_red_1A_1	1A	591-592	2	RAC875_c85550_73	0.00064	0.066	-0.076
red	Q_red_1A_1	1A	591-592	2	BS00021780_51	0.00064	0.066	-0.076
red	Q_red_2A_1	2A	127	1	Kukri_c441_891	5e-06	0.076	-0.1
red	Q_red_2A_2	2A	773	1	BS00091763_51	0.00015	0.09	-0.081
red	Q_red_3A_1	3A	594	1	Kukri_c7087_896	0.00018	0.066	0.11
red	Q_red_4A_1	4A	25	1	wsnp_Ex_c22913_32130617	0.00069	0.062	-0.078
red	Q_red_4B_1	4B	31-59	6	TG0010a	0.00078	0.28	0.056
red	Q_red_4B_1	4B	31-59	6	TG0010b	0.00078	0.28	0.056
red	Q_red_4B_1	4B	31-59	6	AX-89380014	0.00066	0.39	-0.048
red	Q_red_4B_1	4B	31-59	6	AX-158564633	0.0005	0.42	0.048
red	Q_red_4B_1	4B	31-59	6	IAAV971	0.00027	0.26	0.065
red	Q_red_4B_1	4B	31-59	6	Excalibur_c56787_95	0.0008	0.24	0.058
red	Q_red_5A_1	5A	505	1	Excalibur_c6567_845	0.00033	0.29	-0.063
red	Q_red_7A_1	7A	51	1	AX-94617750	0.00043	0.061	-0.096
rededge	Q_rededge_1A_1	1A	591-592	2	RAC875_c85550_73	1.2e-06	0.066	-0.2
rededge	Q_rededge_1A_1	1A	591-592	2	BS00021780_51	1.2e-06	0.066	-0.2
rededge	Q_rededge_1B_1	1B	668	1	AX-158540222	0.00021	0.064	-0.2
rededge	Q_rededge_1D_1	1D	324	1	AX-94922494	0.00017	0.09	-0.15
rededge	Q_rededge_2A_1	2A	74-78	18	AX-110998568	0.00023	0.099	-0.15
rededge	Q_rededge_2A_1	2A	74-78	18	BS00036766_51	0.00062	0.11	-0.14
rededge	Q_rededge_2A_1	2A	74-78	18	BS00036767_51	2.1e-06	0.073	-0.25
rededge	Q_rededge_2A_1	2A	74-78	18	Kukri_rep_c83485_398	2.1e-06	0.073	-0.25
rededge	Q_rededge_2A_1	2A	74-78	18	Tdurum_contig9731_121	1.4e-05	0.083	-0.22
rededge	Q_rededge_2A_1	2A	74-78	18	Excalibur_c15733_252	1.4e-05	0.083	-0.22
rededge	Q_rededge_2A_1	2A	74-78	18	Excalibur_rep_c111743_194	0.00016	0.073	-0.2
rededge	Q_rededge_2A_1	2A	74-78	18	GENE-1365_255	1.4e-05	0.083	-0.22

Table A5 continued: QTL identified for spectral time-series ($p < 0.001$)

Phenotype	QTL	Chr	Span	# Markers	Peak-marker	P.value	MAF	Effect
rededge	Q_rededge_2A_1	2A	74-78	18	RAC875_c20700_853	1.4e-05	0.083	-0.22
rededge	Q_rededge_2A_1	2A	74-78	18	Tdurum_contig48302_532	1.4e-05	0.083	-0.22
rededge	Q_rededge_2A_1	2A	74-78	18	Tdurum_contig5311_67	1.4e-05	0.083	-0.22
rededge	Q_rededge_2A_1	2A	74-78	18	AX-110428187	1.8e-05	0.08	-0.21
rededge	Q_rededge_2A_1	2A	74-78	18	BS00039983_51	1.8e-05	0.08	-0.21
rededge	Q_rededge_2A_1	2A	74-78	18	Kukri_rep_c104727_91	0.0001	0.054	-0.24
rededge	Q_rededge_2A_1	2A	74-78	18	wsnp_CAP11_rep_c8768_3788007	0.0005	0.062	-0.2
rededge	Q_rededge_2A_1	2A	74-78	18	wsnp_CAP12_c901_472535	0.0005	0.062	-0.2
rededge	Q_rededge_2A_1	2A	74-78	18	wsnp_Ex_rep_c68113_66877517	6.9e-05	0.054	-0.25
rededge	Q_rededge_2A_1	2A	74-78	18	wsnp_JD_c12088_12411845	0.0005	0.062	-0.2
rededge	Q_rededge_2A_2	2A	119-127	2	AX-94457129	0.00098	0.27	-0.094
rededge	Q_rededge_2A_2	2A	119-127	2	Kukri_c441_891	2.2e-06	0.076	-0.21
rededge	Q_rededge_2A_3	2A	770	1	AX-109961625	0.00067	0.22	-0.12
rededge	Q_rededge_2B_1	2B	114-129	2	Excalibur_c37649_125	0.00046	0.1	-0.14
rededge	Q_rededge_2B_1	2B	114-129	2	BobWhite_c6166_319	0.00016	0.13	-0.15
rededge	Q_rededge_2B_2	2B	114-139	2	AX-89770172	0.00095	0.32	-0.11
rededge	Q_rededge_2B_2	2B	114-139	2	BS00059315_51	0.00036	0.28	-0.13
rededge	Q_rededge_3A_1	3A	478	1	AX-95247676	9.9e-05	0.12	0.13
rededge	Q_rededge_3A_2	3A	743	1	AX-95254393	6.5e-05	0.25	-0.13
rededge	Q_rededge_3B_1	3B	191-206	2	AX-94853637	0.00052	0.062	-0.17
rededge	Q_rededge_3B_1	3B	191-206	2	CAP7_c3916_256	0.00052	0.062	-0.17
rededge	Q_rededge_3B_2	3B	237	1	AX-89355524	0.00052	0.062	-0.17
rededge	Q_rededge_3B_3	3B	473-474	5	AX-110403928	4.5e-06	0.095	-0.18
rededge	Q_rededge_3B_3	3B	473-474	5	AX-110918031	0.00017	0.09	-0.15
rededge	Q_rededge_3B_3	3B	473-474	5	RAC875_c50787_146	6.9e-06	0.097	-0.17
rededge	Q_rededge_3B_3	3B	473-474	5	AX-110958104	0.00029	0.087	-0.15
rededge	Q_rededge_3B_3	3B	473-474	5	AX-158538397	0.00062	0.08	-0.13
rededge	Q_rededge_3B_4	3B	501-507	2	RAC875_c2044_170	3.1e-05	0.16	0.17
rededge	Q_rededge_3B_4	3B	501-507	2	Tdurum_contig10107_580	5.2e-05	0.16	0.17
rededge	Q_rededge_3B_5	3B	576	1	AX-158541479	0.00019	0.093	0.18
rededge	Q_rededge_3B_6	3B	627	1	AX-158598230	3.3e-05	0.19	0.15
rededge	Q_rededge_3D_1	3D	86	1	IAAV2729	6.3e-05	0.11	0.13
rededge	Q_rededge_4A_1	4A	673	1	Excalibur_c53864_331	6.7e-06	0.067	0.22
rededge	Q_rededge_4B_1	4B	31-59	8	TG0010a	0.0001	0.28	0.12
rededge	Q_rededge_4B_1	4B	31-59	8	TG0010b	0.0001	0.28	0.12
rededge	Q_rededge_4B_1	4B	31-59	8	AX-111081978	0.00038	0.3	0.1
rededge	Q_rededge_4B_1	4B	31-59	8	AX-158564543	0.0006	0.29	0.1
rededge	Q_rededge_4B_1	4B	31-59	8	IAAV971	0.00076	0.26	0.11
rededge	Q_rededge_4B_1	4B	31-59	8	Tdurum_contig81797_369	0.00063	0.093	-0.15
rededge	Q_rededge_4B_1	4B	31-59	8	wsnp_Ex_c8913_14881924	0.00063	0.093	-0.15
rededge	Q_rededge_4B_1	4B	31-59	8	Excalibur_c56787_95	0.00044	0.24	0.11
rededge	Q_rededge_5A_1	5A	445	1	AX-158542603	0.00065	0.19	-0.11
rededge	Q_rededge_5A_2	5A	549	1	AX-94501987	3.8e-06	0.074	0.21
rededge	Q_rededge_5A_3	5A	683	1	Tdurum_contig62286_271	0.00034	0.097	-0.16
rededge	Q_rededge_5B_1	5B	421	2	AX-95099091	0.00065	0.069	-0.14
rededge	Q_rededge_5B_1	5B	421	2	Excalibur_c24638_380	0.00077	0.066	-0.15
rededge	Q_rededge_5B_2	5B	589	1	AX-158525626	0.00073	0.18	-0.11
rededge	Q_rededge_6B_1	6B	644	1	TA004372-0730	0.00073	0.12	-0.13
rededge	Q_rededge_6B_2	6B	701	1	BobWhite_c35035_317	0.00017	0.23	0.1
rededge	Q_rededge_6D_1	6D	2	1	CAP7_c1208_150	0.00057	0.09	0.13
rededge	Q_rededge_6D_2	6D	26	1	D_GB5Y7FA02FHK0M_407	0.00064	0.08	-0.15

Table A5 continued: QTL identified for spectral time-series ($p < 0.001$)

Phenotype	QTL	Chr	Span	# Markers	Peak-marker	P.value	MAF	Effect
rededge	Q_rededge_7A_1	7A	59	1	Excalibur_c57078_255	5.6e-06	0.074	0.22
rededge	Q_rededge_7B_1	7B	658	1	Tdurum_contig43995_370	0.00066	0.087	-0.14
rededge	Q_rededge_Unkown_1	Unkown	1127	1	Kukri_c7914_99	2.1e-06	0.073	-0.25
rededge	Q_rededge_Unkown_2	Unkown	1335	1	RAC875_rep_c71921_672	1.8e-05	0.066	-0.18
rededge	Q_rededge_Unkown_3	Unkown	1376	1	RFL_Contig5758_757	7.8e-05	0.17	0.16
SR	Q_SR_2A_1	2A	4	1	Kukri_c16650_797	0.00038	0.11	0.072
SR	Q_SR_4B_1	4B	20	1	Kukri_rep_c74376_188	0.00079	0.29	-0.033
SR	Q_SR_5A_1	5A	300	1	AX-110003331	0.00013	0.21	0.043
SR	Q_SR_6A_1	6A	615	4	BobWhite_rep_c50324_373	0.0004	0.1	0.073
SR	Q_SR_6A_1	6A	615	4	Kukri_rep_c103067_383	0.0004	0.1	0.073
SR	Q_SR_6A_1	6A	615	4	RAC875_c24832_252	0.00041	0.1	0.074
SR	Q_SR_6A_1	6A	615	4	RAC875_c8088_61	0.00012	0.11	0.077
SR	Q_SR_6B_1	6B	718-721	3	RFL_Contig2615_700	0.00023	0.11	0.072
SR	Q_SR_6B_1	6B	718-721	3	Kukri_c19426_489	0.00038	0.11	0.072
SR	Q_SR_6B_1	6B	718-721	3	Kukri_c64223_135	0.00024	0.11	0.074
SR	Q_SR_6D_1	6D	471-473	3	BobWhite_c13202_312	0.0004	0.1	0.073
SR	Q_SR_6D_1	6D	471-473	3	Kukri_c48283_78	0.00051	0.11	0.072
SR	Q_SR_6D_1	6D	471-473	3	RAC875_rep_c104893_620	0.00051	0.11	0.072
SR	Q_SR_7A_1	7A	51	1	AX-94617750	8.2e-05	0.061	0.079
SR	Q_SR_7A_2	7A	669	1	BS00021261_51	0.0005	0.078	-0.07
SR	Q_SR_Unkown_1	Unkown	1569	1	Tdurum_contig68258_1773	0.00051	0.11	0.072

7.7 QTL Identified for AUC-values of VIs Using MLM

Table A6: QTL identified for AUC-values of VIs ($p < 0.001$)

Phenotype	QTL	Chr	Span	# Markers	Peak marker	P.value	MAF	Effect
GNDVI	Q_GNDVI_4A	4A	512	1	RAC875_c91464_170	9×10^{-5}	0.062	0.38
GNDVI	Q_GNDVI_7A	7A	51	2	AX-94617750	2.5×10^{-5}	0.061	0.43
NDVI	Q_NDVI_4B	4B	20-32	3	Kukri_rep_c74376_188	0.00045	0.29	-0.17
NDVI	Q_NDVI_4B	4B	20-32	3	AX-89747834	0.00052	0.31	-0.18
NDVI	Q_NDVI_4B	4B	20-32	3	AX-89380014	0.00016	0.39	0.2
NDVI	Q_NDVI_5A	5A	300	1	AX-110003331	3.1×10^{-5}	0.21	0.23
NDVI	Q_NDVI_7A	7A	51	2	AX-94617750	0.00014	0.061	0.38
SR	Q_SR_2A	2A	4	1	Kukri_c16650_797	0.00019	0.11	0.35
SR	Q_SR_6A	6A	615	1	RAC875_c8088_61	9.1×10^{-5}	0.11	0.37
SR	Q_SR_6B	6B	718-719	2	RFL_Contig2615_700	0.00012	0.11	0.36
SR	Q_SR_6B	6B	718-719	2	Kukri_c19426_489	0.00019	0.11	0.35

7.8 QTL Identified for Agronomic Traits Using MLM

Table A7: QTL identified for agronomic trait ($p < 0.001$)

Phenotype	QTL	Chr	Span	# Markers	Peak-marker	P.value	MAF	Effect
DH_dss	Q_DH_1A_1	1A	14	1	AX-94741250	0.00073	0.49	-0.34
DH_dss	Q_DH_1B_1	1B	1-2	2	BS00022180_51	0.00036	0.072	-0.91

Table A7 continued: QTL identified for agronomic trait ($p < 0.001$)

Phenotype	QTL	Chr	Span	# Markers	Peak-marker	P.value	MAF	Effect
DH_dss	Q_DH_1B_1	1B	1-2	2	BS00071161_51	6.7e-05	0.079	-0.92
DH_dss	Q_DH_2A_1	2A	733	1	BS00024921_51	0.00031	0.38	-0.38
DH_dss	Q_DH_3A_1	3A	267	1	BS00110129_51	8.7e-05	0.42	-0.41
DH_dss	Q_DH_5A_1	5A	10	1	tplb0029e02_1186	0.00016	0.23	0.4
DH_dss	Q_DH_7A_1	7A	669	1	BS00021261_51	0.00062	0.077	-0.7
DH_dss	Q_DH_7A_2	7A	724	1	wsnp_Ku_c28104_38042857	0.00018	0.076	0.68
DH_dss	Q_DH_7B_1	7B	62	1	Kukri_c14766_484	9.1e-06	0.058	0.89
DH_dss	Q_DH_7B_2	7B	634	1	AX-110369629	0.00092	0.1	0.57
DH_dss	Q_DH_Unkown_1	Unkown	38	1	AX-158598740	0.00021	0.45	0.35
DM_dss	Q_DM_2A_1	2A	63	1	JD_c3930_358	7.8e-05	0.052	-1.6
DM_dss	Q_DM_2A_2	2A	415	1	AX-94499272	1.2e-05	0.076	-1.6
DM_dss	Q_DM_2A_3	2A	504-505	2	Kukri_c15489_626	9.1e-05	0.34	-0.7
DM_dss	Q_DM_2A_3	2A	504-505	2	AX-158540703	1.9e-05	0.24	-0.87
DM_dss	Q_DM_2B_1	2B	441	1	Kukri_c57491_156	0.00014	0.34	-0.67
DM_dss	Q_DM_2D_1	2D	318	1	AX-158572764	1.2e-05	0.076	-1.6
DM_dss	Q_DM_4A_1	4A	25	1	wsnp_Ex_c22913_32130617	3.3e-05	0.065	1.2
DM_dss	Q_DM_4B_1	4B	32	1	AX-89380014	0.00027	0.39	0.62
DM_dss	Q_DM_4B_2	4B	167	1	Excalibur_c52517_464	2e-05	0.41	0.73
DM_dss	Q_DM_4D_1	4D	90	1	AX-95073308	0.00049	0.3	0.63
DM_dss	Q_DM_5A_1	5A	548	1	AX-158585104	0.0001	0.3	-0.7
DM_dss	Q_DM_6A_1	6A	74	1	RAC875_c17297_341	0.00021	0.29	0.66
DM_dss	Q_DM_6A_2	6A	214	1	RAC875_c15872_141	2e-05	0.41	0.73
DM_dss	Q_DM_6B_1	6B	132	2	Kukri_rep_c71420_511	0.00013	0.16	0.84
DM_dss	Q_DM_6B_1	6B	132	2	Tdurum_contig14559_741	0.00021	0.29	0.66
GPC_pct	Q_GPC_1A_1	1A	537	1	AX-158556627	1.9e-05	0.079	-0.4
GPC_pct	Q_GPC_1B_1	1B	472	1	wsnp_RFL_Contig3866_4228783	4.2e-05	0.2	-0.25
GPC_pct	Q_GPC_1B_2	1B	662	1	AX-158570571	1e-04	0.088	-0.34
GPC_pct	Q_GPC_2D_1	2D	62	1	AX-94459264	0.00043	0.086	-0.26
GPC_pct	Q_GPC_3A_1	3A	211	1	AX-108875928	4.2e-05	0.2	-0.25
GPC_pct	Q_GPC_3A_2	3A	402	1	wsnp_Ku_c44089_51445136	4.2e-05	0.2	-0.25
GPC_pct	Q_GPC_4A_1	4A	700	1	wsnp_BG313770B_Ta_1_1	0.00026	0.058	-0.39
GPC_pct	Q_GPC_5A_1	5A	2	1	AX-95114232	4.1e-05	0.21	-0.27
GPC_pct	Q_GPC_6B_1	6B	10	1	AX-158559508	0.00017	0.13	-0.31
GPC_pct	Q_GPC_Unkown_1	Unkown	820	1	IAAV6234	0.00066	0.053	-0.4
GPC_pct	Q_GPC_Unkown_2	Unkown	994	1	Kukri_c2121_2345	5.4e-05	0.13	-0.33
GPC_pct	Q_GPC_Unkown_3	Unkown	1674	1	TGWA25K-TG0223	0.00015	0.06	-0.4
GY_g_m2	Q_GY_1B_1	1B	472	1	wsnp_RFL_Contig3866_4228783	0.00031	0.2	14
GY_g_m2	Q_GY_1B_2	1B	530	1	GENE-0410_71	0.00088	0.31	-16
GY_g_m2	Q_GY_2A_1	2A	758	2	AX-158540701	0.00024	0.086	24
GY_g_m2	Q_GY_2A_1	2A	758	2	Excalibur_c52319_257	6.8e-05	0.084	27
GY_g_m2	Q_GY_2D_1	2D	62	1	AX-94459264	0.00075	0.086	17
GY_g_m2	Q_GY_3A_1	3A	211	1	AX-108875928	0.00031	0.2	14
GY_g_m2	Q_GY_3A_2	3A	402	1	wsnp_Ku_c44089_51445136	0.00031	0.2	14
GY_g_m2	Q_GY_6B_1	6B	7-10	2	BobWhite_c43135_397	7.3e-05	0.14	22
GY_g_m2	Q_GY_6B_1	6B	7-10	2	AX-158559508	0.00021	0.13	20
GY_g_m2	Q_GY_6D_1	6D	54	1	TA001847-0566	0.00028	0.11	-19
GY_g_m2	Q_GY_7A_1	7A	112	2	RAC875_c67063_703	0.00025	0.16	-16
GY_g_m2	Q_GY_7A_1	7A	112	2	RAC875_c67063_984	0.00038	0.16	-15
GY_g_m2	Q_GY_Unkown_1	Unkown	1265	1	RAC875_c48703_189	0.00049	0.055	26
GY_g_m2	Q_GY_Unkown_2	Unkown	1804	1	wsnp_BQ161779D_Ta_2_1	0.00063	0.11	-26
PH_cm	Q_PH_2A_1	2A	528-543	2	AX-158561839	0.0008	0.082	-2.9

Table A7 continued: QTL identified for agronomic trait ($p < 0.001$)

Phenotype	QTL	Chr	Span	# Markers	Peak-marker	P.value	MAF	Effect
PH_cm	Q_PH_2A_1	2A	528-543	2	AX-110399256	0.00083	0.079	-3
PH_cm	Q_PH_4A_1	4A	570-578	2	CAP11_c3631_75	0.00028	0.33	2.4
PH_cm	Q_PH_4A_1	4A	570-578	2	RAC875_c19303_228	3.8e-07	0.33	3.2
PH_cm	Q_PH_4B_1	4B	13-79	18	AX-158583339	0.00026	0.23	2.2
PH_cm	Q_PH_4B_1	4B	13-79	18	BS00037094_51	0.00024	0.24	2.1
PH_cm	Q_PH_4B_1	4B	13-79	18	Tdurum_contig93710_409	4.9e-05	0.23	2.4
PH_cm	Q_PH_4B_1	4B	13-79	18	AX-94685504	5e-06	0.48	-2.4
PH_cm	Q_PH_4B_1	4B	13-79	18	TG0010a	1.7e-10	0.29	4.3
PH_cm	Q_PH_4B_1	4B	13-79	18	TG0010b	1.7e-10	0.29	4.3
PH_cm	Q_PH_4B_1	4B	13-79	18	AX-89380014	0.00016	0.39	-2.1
PH_cm	Q_PH_4B_1	4B	13-79	18	AX-111081978	2.7e-08	0.3	3.5
PH_cm	Q_PH_4B_1	4B	13-79	18	AX-158564543	2.2e-08	0.3	3.6
PH_cm	Q_PH_4B_1	4B	13-79	18	AX-158564633	1.3e-06	0.42	2.6
PH_cm	Q_PH_4B_1	4B	13-79	18	AX-158537142	2.5e-08	0.29	3.5
PH_cm	Q_PH_4B_1	4B	13-79	18	AX-158564542	6.7e-07	0.33	3.1
PH_cm	Q_PH_4B_1	4B	13-79	18	Tdurum_contig33737_157	4.4e-08	0.29	3.5
PH_cm	Q_PH_4B_1	4B	13-79	18	IAAV971	5.8e-08	0.26	3.8
PH_cm	Q_PH_4B_1	4B	13-79	18	AX-158618805	1.2e-05	0.25	2.9
PH_cm	Q_PH_4B_1	4B	13-79	18	Excalibur_c56787_95	8.3e-08	0.24	3.6
PH_cm	Q_PH_4B_1	4B	13-79	18	Excalibur_c17607_542	1.9e-06	0.24	3.2
PH_cm	Q_PH_4B_1	4B	13-79	18	AX-158558529	2.2e-06	0.23	3.2
PH_cm	Q_PH_4D_1	4D	19-26	3	TG0011a	2.8e-10	0.22	4.4
PH_cm	Q_PH_4D_1	4D	19-26	3	TG0011b	8.1e-10	0.25	4.1
PH_cm	Q_PH_4D_1	4D	19-26	3	BobWhite_s64797_152	4.9e-08	0.29	3.5
PH_cm	Q_PH_5D_1	5D	563	1	RAC875_rep_c78258_214	0.00018	0.07	-3.8
PH_cm	Q_PH_7A_1	7A	691	1	Excalibur_c61749_474	0.00014	0.24	2.2
PH_cm	Q_PH_Unkown_1	Unkown	1610	1	TGWA25K-TG0011	6.7e-11	0.21	4.7

7.9 QTL Identified for AUC-values of VIs using GA-SVR

Table A8: QTL identified using GA/SVR-pipeline for AUV-values of VIs

Phenotype (AUC)	QTL	SNP	Chr	Span
GNDVI	Q_GNDVI_1A	RAC875_c14926_589	1A	29-31
GNDVI	Q_GNDVI_1A	AX-94682787	1A	29-31
GNDVI	Q_GNDVI_4A	AX-108900808	4A	543
GNDVI	Q_GNDVI_5A	wsnp_Ex_c22984_32207214	5A	570
GNDVI	Q_GNDVI_5B	AX-158526286	5B	36
GNDVI	Q_GNDVI_6B	wsnp_Ex_c45348_51169164	6B	199
NDVI	Q_NDVI_1B	BobWhite_c11044_322	1B	567
NDVI	Q_NDVI_3A	wsnp_Ex_c18223_27035083	3A	603-615
NDVI	Q_NDVI_3A	AX-94481094	3A	603-615
NDVI	Q_NDVI_3A	AX-89351265	3A	603-615
NDVI	Q_NDVI_4A	Kukri_c6954_320	4A	97
NDVI	Q_NDVI_4A	Excalibur_c25699_113	4A	623
NDVI	Q_NDVI_6B	Ra_c26319_331	6B	606
NDVI	Q_NDVI_7A	RAC875_c11969_384	7A	11

Table A8 continued: Final set of SNPs identified using GA/SVR-pipeline

Phenotype (AUC)	QTL	SNP	Chr	Span
NDVI	Q_NDVI_Unkown	wsnp_Ex_c36701_44603531	Unkown	1934
SR	Q_SR_1A	RAC875_c14926_589	1A	29
SR	Q_SR_4A	AX-158581619	4A	451
SR	Q_SR_4A	tplb0024j12_840	4A	538
SR	Q_SR_5B	wsnp_Ku_c38713_47298856	5B	686
SR	Q_SR_7B	wsnp_Ex_c3738_6809767	7B	707

7.10 QTL Identified for Agronomic Traits Using GA-SVR

Table A9: Final set of QTL identified using GA/SVR-pipeline for agronomic traits

Phenotype (agronmic)	QTL	Chr	Span	Peak Marker(s)
DH_dss	Q_DH_4A_1	4A	684-685	CAP11_c18_238
DH_dss	Q_DH_4A_1	4A	684-685	Excalibur_c4325_1150
DH_dss	Q_DH_7B_1	7B	42	wsnp_Ex_c11106_18002976
DM_dss	Q_DM_1A_1	1A	482	BS00087600_51
DM_dss	Q_DM_1A_2	1A	516	AX-158560524
DM_dss	Q_DM_1B_1	1B	516	AX-158570189
DM_dss	Q_DM_2D_1	2D	9	D_contig17313_245
DM_dss	Q_DM_2D_2	2D	97	AX-94636903
DM_dss	Q_DM_3A_1	3A	603	wsnp_Ex_c18223_27035083
DM_dss	Q_DM_4A_1	4A	38	wsnp_Ex_rep_c67145_65628860
DM_dss	Q_DM_4A_2	4A	597	AX-158524717
DM_dss	Q_DM_4A_2	4A	597	BS00049911_51
DM_dss	Q_DM_4B_1	4B	559	RAC875_c2545_1186
DM_dss	Q_DM_4B_2	4B	647	AX-158550174
DM_dss	Q_DM_5A_1	5A	549	AX-94386305
DM_dss	Q_DM_5B_1	5B	435	AX-110592681
DM_dss	Q_DM_5D_1	5D	4	TG0028
DM_dss	Q_DM_7A_1	7A	27	IAAV6131
GPC_pct	Q_GPC_1A_1	1A	26-27	wsnp_Ku_c42878_50516167
GPC_pct	Q_GPC_1A_1	1A	26-27	Kukri_c7436_2259
GPC_pct	Q_GPC_1A_2	1A	520	IAAV2694
GPC_pct	Q_GPC_1D_1	1D	34	BS00108305_51
GPC_pct	Q_GPC_3A_1	3A	734	RAC875_c61934_186
GPC_pct	Q_GPC_3B_1	3B	562-587	AX-158541608
GPC_pct	Q_GPC_3B_1	3B	562-587	AX-158538436
GPC_pct	Q_GPC_3B_1	3B	562-587	AX-95629008
GPC_pct	Q_GPC_3B_1	3B	562-587	wsnp_Ex_c3096_5709369
GPC_pct	Q_GPC_4A_1	4A	597	AX-158524643
GPC_pct	Q_GPC_4A_1	4A	597	TA005380-0966
GPC_pct	Q_GPC_4B_1	4B	27	BS00010925_51
GPC_pct	Q_GPC_5A_1	5A	111	wsnp_Ex_c31570_40343841
GPC_pct	Q_GPC_5A_2	5A	505	RAC875_c28819_281

Table A9 continued: Final set of QTL identified using GA/SVR-pipeline for agronomic traits

Phenotype (agronmic)	QTL	Chr	Span	Peak Marker(s)
GPC_pct	Q_GPC_5A_3	5A	585-587	RAC875_rep_c116420_103
GPC_pct	Q_GPC_5A_3	5A	585-587	AX-158551053
GPC_pct	Q_GPC_5A_3	5A	585-587	wsnp_Ex_rep_c66689_65010988
GPC_pct	Q_GPC_5A_3	5A	585-587	BS00022071_51
GPC_pct	Q_GPC_5A_4	5A	708	AX-158550750
GPC_pct	Q_GPC_5A_4	5A	708	wsnp_Ex_c2171_4072995
GPC_pct	Q_GPC_5B_1	5B	589	AX-158525626
GPC_pct	Q_GPC_6A_1	6A	523	wsnp_JD_rep_c48797_33040150
GPC_pct	Q_GPC_6B_1	6B	11	AX-94465053
GPC_pct	Q_GPC_7A_1	7A	8	TA001746-1415
GPC_pct	Q_GPC_7A_2	7A	730-734	BS00020236_51
GPC_pct	Q_GPC_7A_2	7A	730-734	RFL_Contig602_627
GPC_pct	Q_GPC_7B_1	7B	519-541	wsnp_BE443010B_Ta_2_1
GPC_pct	Q_GPC_7B_1	7B	519-541	AX-158560004
GPC_pct	Q_GPC_7B_1	7B	519-541	AX-94395385
GPC_pct	Q_GPC_7B_1	7B	519-541	AX-158592758
GPC_pct	Q_GPC_7B_2	7B	584	RAC875_c60770_82
GPC_pct	Q_GPC_7B_3	7B	743	Tdurum_contig30909_76
GPC_pct	Q_GPC_7D_1	7D	5	TA013055-0991
GPC_pct	Q_GPC_7D_2	7D	488	AX-94678472
GY_g_m2	Q_GY_1A_1	1A	27-33	RAC875_c8245_272
GY_g_m2	Q_GY_1A_1	1A	27-33	CAP11_c3218_126
GY_g_m2	Q_GY_1A_2	1A	474	AX-95110122
GY_g_m2	Q_GY_1A_3	1A	501-520	wsnp_Ra_c3270_6136601
GY_g_m2	Q_GY_1A_3	1A	501-520	IAAV2694
GY_g_m2	Q_GY_1B_1	1B	4-41	BS00022504_51
GY_g_m2	Q_GY_1B_1	1B	4-41	Tdurum_contig78972_316
GY_g_m2	Q_GY_1B_1	1B	4-41	Kukri_c47342_73
GY_g_m2	Q_GY_1B_1	1B	4-41	GENE-0427_442
GY_g_m2	Q_GY_1B_2	1B	629	Tdurum_contig57927_171
GY_g_m2	Q_GY_1B_3	1B	680	Tdurum_contig13879_352
GY_g_m2	Q_GY_1D_1	1D	13-36	Ex_c6145_1877
GY_g_m2	Q_GY_1D_1	1D	13-36	RAC875_c7752_145
GY_g_m2	Q_GY_1D_1	1D	13-36	BS00025736_51
GY_g_m2	Q_GY_1D_1	1D	13-36	Kukri_c9693_1890
GY_g_m2	Q_GY_1D_1	1D	13-36	wsnp_CAP12_c633_339740
GY_g_m2	Q_GY_1D_2	1D	274	BobWhite_c8428_346
GY_g_m2	Q_GY_2A_1	2A	18-21	AX-94992901
GY_g_m2	Q_GY_2A_1	2A	18-21	wsnp_Ex_c6924_11936998
GY_g_m2	Q_GY_2A_2	2A	707-710	AX-111993689
GY_g_m2	Q_GY_2A_2	2A	707-710	AX-158572604
GY_g_m2	Q_GY_2A_2	2A	707-710	Ku_c35823_743
GY_g_m2	Q_GY_2B_1	2B	68	AX-158562556
GY_g_m2	Q_GY_2B_2	2B	139	wsnp_Ku_c11665_18999583
GY_g_m2	Q_GY_2B_3	2B	675-690	AX-94720460

Table A9 continued: Final set of QTL identified using GA/SVR-pipeline for agronomic traits

Phenotype (agronmic)	QTL	Chr	Span	Peak Marker(s)
GY_g_m2	Q_GY_2B_3	2B	675-690	CAP11_c2194_115
GY_g_m2	Q_GY_2B_3	2B	675-690	wsnp_Ra_c10658_17500498
GY_g_m2	Q_GY_2D_1	2D	27	AX-94732155
GY_g_m2	Q_GY_2D_2	2D	567	AX-95120131
GY_g_m2	Q_GY_2D_3	2D	650	IAAV6032
GY_g_m2	Q_GY_3A_1	3A	14	AX-158523996
GY_g_m2	Q_GY_3A_2	3A	511-534	AX-95205191
GY_g_m2	Q_GY_3A_2	3A	511-534	wsnp_Ex_c15269_23491104
GY_g_m2	Q_GY_3A_3	3A	572-589	Excalibur_c33545_134
GY_g_m2	Q_GY_3A_3	3A	572-589	IAAV3838
GY_g_m2	Q_GY_3A_4	3A	706	AX-94843318
GY_g_m2	Q_GY_3A_5	3A	729-734	IAAV3851
GY_g_m2	Q_GY_3A_5	3A	729-734	AX-110447070
GY_g_m2	Q_GY_3A_5	3A	729-734	RAC875_c61934_186
GY_g_m2	Q_GY_3B_1	3B	172	tplb0062h15_59
GY_g_m2	Q_GY_3B_2	3B	215	AX-111014699
GY_g_m2	Q_GY_3B_3	3B	414-416	TA001218-0519
GY_g_m2	Q_GY_3B_3	3B	414-416	AX-94800373
GY_g_m2	Q_GY_3B_3	3B	414-416	AX-110409073
GY_g_m2	Q_GY_3B_4	3B	455-480	BS00095061_51
GY_g_m2	Q_GY_3B_4	3B	455-480	RAC875_c44365_203
GY_g_m2	Q_GY_3B_4	3B	455-480	Excalibur_c29625_222
GY_g_m2	Q_GY_3B_5	3B	514	AX-158541642
GY_g_m2	Q_GY_3B_6	3B	556-562	AX-95151132
GY_g_m2	Q_GY_3B_6	3B	556-562	IACX3871
GY_g_m2	Q_GY_3B_6	3B	556-562	AX-158541608
GY_g_m2	Q_GY_3B_7	3B	594-595	AX-95155468
GY_g_m2	Q_GY_3B_7	3B	594-595	AX-158579145
GY_g_m2	Q_GY_3B_8	3B	690-697	AX-158562999
GY_g_m2	Q_GY_3B_8	3B	690-697	Excalibur_c47250_726
GY_g_m2	Q_GY_3B_8	3B	690-697	wsnp_CAP11_c2309_1201554
GY_g_m2	Q_GY_3B_8	3B	690-697	AX-110483820
GY_g_m2	Q_GY_3B_9	3B	750-782	BS00077967_51
GY_g_m2	Q_GY_3B_9	3B	750-782	BS00063624_51
GY_g_m2	Q_GY_3B_9	3B	750-782	AX-158541480
GY_g_m2	Q_GY_3B_9	3B	750-782	AX-108865765
GY_g_m2	Q_GY_3D_1	3D	332	AX-95210805
GY_g_m2	Q_GY_3D_2	3D	416	AX-94808747
GY_g_m2	Q_GY_4A_1	4A	39	wsnp_Ex_c5690_9994305
GY_g_m2	Q_GY_4A_2	4A	103-105	GENE-2768_150
GY_g_m2	Q_GY_4A_2	4A	103-105	TA001684-0426
GY_g_m2	Q_GY_4A_3	4A	424	AX-94639791
GY_g_m2	Q_GY_4A_4	4A	662	AX-95257547
GY_g_m2	Q_GY_4B_1	4B	429	Excalibur_rep_c106935_390
GY_g_m2	Q_GY_4B_2	4B	663-666	AX-94689886

Table A9 continued: Final set of QTL identified using GA/SVR-pipeline for agronomic traits

Phenotype (agronmic)	QTL	Chr	Span	Peak Marker(s)
GY_g_m2	Q_GY_4B_2	4B	663-666	AX-94575968
GY_g_m2	Q_GY_4B_2	4B	663-666	RAC875_c48025_483
GY_g_m2	Q_GY_4D_1	4D	444	AX-94632374
GY_g_m2	Q_GY_5A_1	5A	343	RAC875_rep_c106044_137
GY_g_m2	Q_GY_5A_2	5A	427	AX-158551075
GY_g_m2	Q_GY_5A_3	5A	482	Kukri_rep_c77459_316
GY_g_m2	Q_GY_5A_4	5A	570-586	wsnp_Ex_c22984_32207214
GY_g_m2	Q_GY_5A_4	5A	570-586	wsnp_Ex_rep_c66689_65010988
GY_g_m2	Q_GY_5A_5	5A	687-708	Ku_c19516_384
GY_g_m2	Q_GY_5A_5	5A	687-708	AX-158564918
GY_g_m2	Q_GY_5A_5	5A	687-708	AX-95097524
GY_g_m2	Q_GY_5A_5	5A	687-708	BobWhite_c8266_227
GY_g_m2	Q_GY_5A_5	5A	687-708	Excalibur_c2171_2728
GY_g_m2	Q_GY_5A_5	5A	687-708	wsnp_Ex_c2171_4072774
GY_g_m2	Q_GY_5B_1	5B	36	AX-158526286
GY_g_m2	Q_GY_5B_2	5B	571-577	AX-158599552
GY_g_m2	Q_GY_5B_2	5B	571-577	Ku_c55173_549
GY_g_m2	Q_GY_5B_2	5B	571-577	Tdurum_contig32812_325
GY_g_m2	Q_GY_5B_2	5B	571-577	AX-94914862
GY_g_m2	Q_GY_5B_3	5B	687	AX-94503590
GY_g_m2	Q_GY_6A_1	6A	18-22	CAP8_c1881_215
GY_g_m2	Q_GY_6A_1	6A	18-22	Ex_c13223_1847
GY_g_m2	Q_GY_6A_1	6A	18-22	AX-94990595
GY_g_m2	Q_GY_6A_1	6A	18-22	Tdurum_contig75595_586
GY_g_m2	Q_GY_6A_2	6A	49	AX-109290505
GY_g_m2	Q_GY_6A_3	6A	499	Excalibur_rep_c69275_346
GY_g_m2	Q_GY_6A_4	6A	564	Kukri_rep_c104521_601
GY_g_m2	Q_GY_6A_5	6A	603-613	AX-158526938
GY_g_m2	Q_GY_6A_5	6A	603-613	AX-109869840
GY_g_m2	Q_GY_6A_5	6A	603-613	AX-158552191
GY_g_m2	Q_GY_6B_1	6B	538-556	AX-110914919
GY_g_m2	Q_GY_6B_1	6B	538-556	AX-111013457
GY_g_m2	Q_GY_6B_1	6B	538-556	wsnp_Ku_c1876_3666308
GY_g_m2	Q_GY_6B_2	6B	634	RAC875_c7965_80
GY_g_m2	Q_GY_6B_3	6B	710	AX-94549612
GY_g_m2	Q_GY_6D_1	6D	461-463	AX-158530763
GY_g_m2	Q_GY_6D_1	6D	461-463	Ex_c7086_187
GY_g_m2	Q_GY_6D_1	6D	461-463	RAC875_c3156_630
GY_g_m2	Q_GY_6D_1	6D	461-463	wsnp_Ex_c4942_8793029
GY_g_m2	Q_GY_7A_1	7A	4-27	Tdurum_contig52015_1320
GY_g_m2	Q_GY_7A_1	7A	4-27	RAC875_c23140_909
GY_g_m2	Q_GY_7A_1	7A	4-27	AX-158626374
GY_g_m2	Q_GY_7A_2	7A	65-66	BS00098026_51
GY_g_m2	Q_GY_7A_2	7A	65-66	AX-109439139
GY_g_m2	Q_GY_7A_3	7A	106-128	AX-94815778

Table A9 continued: Final set of QTL identified using GA/SVR-pipeline for agronomic traits

Phenotype (agronmic)	QTL	Chr	Span	Peak Marker(s)
GY_g_m2	Q_GY_7A_3	7A	106-128	AX-95090243
GY_g_m2	Q_GY_7A_3	7A	106-128	BS00021769_51
GY_g_m2	Q_GY_7A_3	7A	106-128	AX-158539493
GY_g_m2	Q_GY_7A_3	7A	106-128	Ex_c44379_2197
GY_g_m2	Q_GY_7A_3	7A	106-128	AX-94534717
GY_g_m2	Q_GY_7A_3	7A	106-128	AX-158567167
GY_g_m2	Q_GY_7A_3	7A	106-128	BS00022435_51
GY_g_m2	Q_GY_7A_4	7A	225	Ku_c17257_926
GY_g_m2	Q_GY_7A_5	7A	611-625	BS00092630_51
GY_g_m2	Q_GY_7A_5	7A	611-625	Tdurum_contig42140_871
GY_g_m2	Q_GY_7A_6	7A	733-734	Tdurum_contig28828_664
GY_g_m2	Q_GY_7A_6	7A	733-734	RFL_Contig602_627
GY_g_m2	Q_GY_7B_1	7B	38	IACX3991
GY_g_m2	Q_GY_7B_2	7B	83	GENE-2472_462
GY_g_m2	Q_GY_7B_3	7B	124-191	AX-158544168
GY_g_m2	Q_GY_7B_3	7B	124-191	GENE-4867_119
GY_g_m2	Q_GY_7B_3	7B	124-191	Ra_c11468_305
GY_g_m2	Q_GY_7B_3	7B	124-191	Ra_c7974_1192
GY_g_m2	Q_GY_7B_3	7B	124-191	Ra_c7974_559
GY_g_m2	Q_GY_7B_3	7B	124-191	BS00031611_51
GY_g_m2	Q_GY_7B_3	7B	124-191	Tdurum_contig51313_408
GY_g_m2	Q_GY_7B_3	7B	124-191	AX-158554342
GY_g_m2	Q_GY_7B_3	7B	124-191	AX-94652419
GY_g_m2	Q_GY_7B_3	7B	124-191	AX-158593566
GY_g_m2	Q_GY_7B_3	7B	124-191	RAC875_c52266_76
GY_g_m2	Q_GY_7B_3	7B	124-191	BS00072941_51
GY_g_m2	Q_GY_7B_3	7B	124-191	AX-109509402
GY_g_m2	Q_GY_7B_3	7B	124-191	Tdurum_contig75931_1967
GY_g_m2	Q_GY_7B_4	7B	254	AX-94428852
GY_g_m2	Q_GY_7B_5	7B	327-331	Kukri_c15760_212
GY_g_m2	Q_GY_7B_5	7B	327-331	TA004043-0135
GY_g_m2	Q_GY_7B_5	7B	327-331	BS00062785_51
GY_g_m2	Q_GY_7B_6	7B	463	AX-158554043
GY_g_m2	Q_GY_7B_7	7B	488-506	Excalibur_c16687_476
GY_g_m2	Q_GY_7B_7	7B	488-506	Kukri_c48870_115
GY_g_m2	Q_GY_7B_7	7B	488-506	BS00053287_51
GY_g_m2	Q_GY_7B_7	7B	488-506	AX-158592412
GY_g_m2	Q_GY_7B_7	7B	488-506	RAC875_c7474_1661
GY_g_m2	Q_GY_7B_8	7B	539-584	wsnp_Ex_c47153_52447553
GY_g_m2	Q_GY_7B_8	7B	539-584	AX-158560004
GY_g_m2	Q_GY_7B_8	7B	539-584	AX-94395385
GY_g_m2	Q_GY_7B_8	7B	539-584	Tdurum_contig56342_134
GY_g_m2	Q_GY_7B_8	7B	539-584	AX-158592790
GY_g_m2	Q_GY_7B_8	7B	539-584	Excalibur_c41452_997
GY_g_m2	Q_GY_7B_8	7B	539-584	AX-111868806

Table A9 continued: Final set of QTL identified using GA/SVR-pipeline for agronomic traits

Phenotype (agronmic)	QTL	Chr	Span	Peak Marker(s)
GY_g_m2	Q_GY_7B_8	7B	539-584	BobWhite_c3269_141
GY_g_m2	Q_GY_7B_8	7B	539-584	wsnp_BE498323B_Ta_2_1
GY_g_m2	Q_GY_7B_8	7B	539-584	AX-95217675
GY_g_m2	Q_GY_7B_8	7B	539-584	BS00108573_51
GY_g_m2	Q_GY_7B_8	7B	539-584	AX-158592756
GY_g_m2	Q_GY_7B_8	7B	539-584	Kukri_c20611_293
GY_g_m2	Q_GY_7B_8	7B	539-584	wsnp_Ku_rep_c68953_68153061
GY_g_m2	Q_GY_7B_8	7B	539-584	Kukri_c7495_824
GY_g_m2	Q_GY_7B_8	7B	539-584	RAC875_c60770_82
GY_g_m2	Q_GY_7B_9	7B	606	BobWhite_c3541_152
GY_g_m2	Q_GY_7B_9	7B	606	RAC875_c7123_1703
GY_g_m2	Q_GY_7B_10	7B	634-649	AX-110369629
GY_g_m2	Q_GY_7B_10	7B	634-649	AX-94992026
GY_g_m2	Q_GY_7B_10	7B	634-649	AX-158592717
GY_g_m2	Q_GY_7B_10	7B	634-649	AX-158592724
GY_g_m2	Q_GY_7B_10	7B	634-649	AX-158601244
GY_g_m2	Q_GY_7B_11	7B	713	AX-94694846
GY_g_m2	Q_GY_7B_12	7B	742	RFL_Contig2647_624
GY_g_m2	Q_GY_7D_1	7D	5	TA013055-0991
GY_g_m2	Q_GY_7D_2	7D	576	AX-158554692
PH_cm	Q_PH_3A_1	3A	557	AX-94770277
PH_cm	Q_PH_3A_2	3A	599	TA001092-0715
PH_cm	Q_PH_3B_1	3B	562	AX-158598372
PH_cm	Q_PH_4A_1	4A	578	RAC875_c19303_228
PH_cm	Q_PH_4B_1	4B	31-59	AX-94685504
PH_cm	Q_PH_4B_1	4B	31-59	AX-111081978
PH_cm	Q_PH_4B_1	4B	31-59	AX-158537142
PH_cm	Q_PH_4B_1	4B	31-59	IAAV971
PH_cm	Q_PH_4B_1	4B	31-59	BS00040305_51
PH_cm	Q_PH_4B_1	4B	31-59	Excalibur_c56787_95
PH_cm	Q_PH_4B_2	4B	86	AX-158618580
PH_cm	Q_PH_4D_1	4D	19-26	TG0011a
PH_cm	Q_PH_4D_1	4D	19-26	TG0011b
PH_cm	Q_PH_4D_1	4D	19-26	BobWhite_s64797_152
PH_cm	Q_PH_6A_1	6A	214	RAC875_c15872_141

7.11 Manhattan Plots for Spectral Time Series

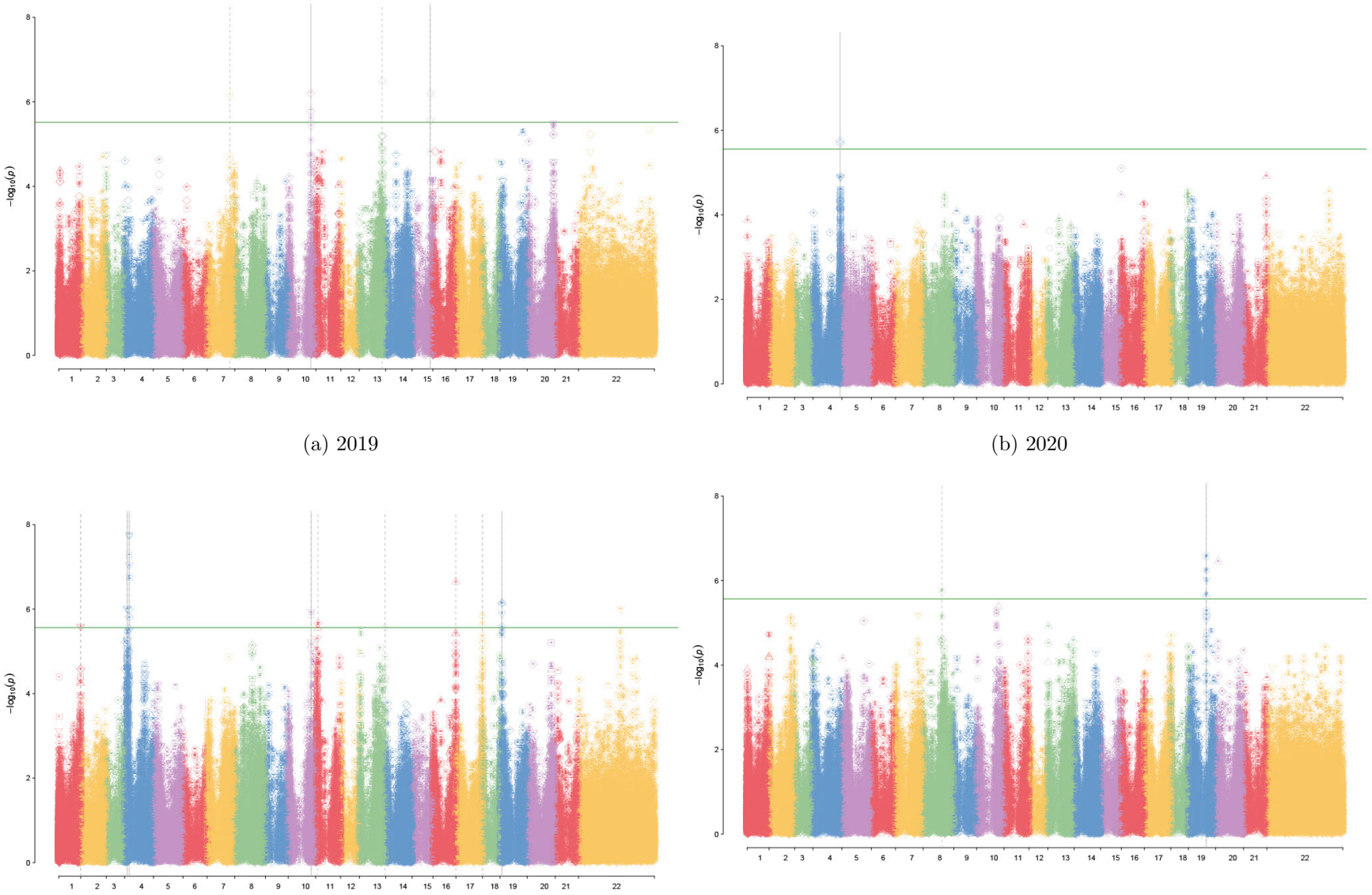

(a) 2019

(b) 2020

(c) 2021

(d) 2022

Figure A4: Manhattan plots flight trials in the years 2019-2022

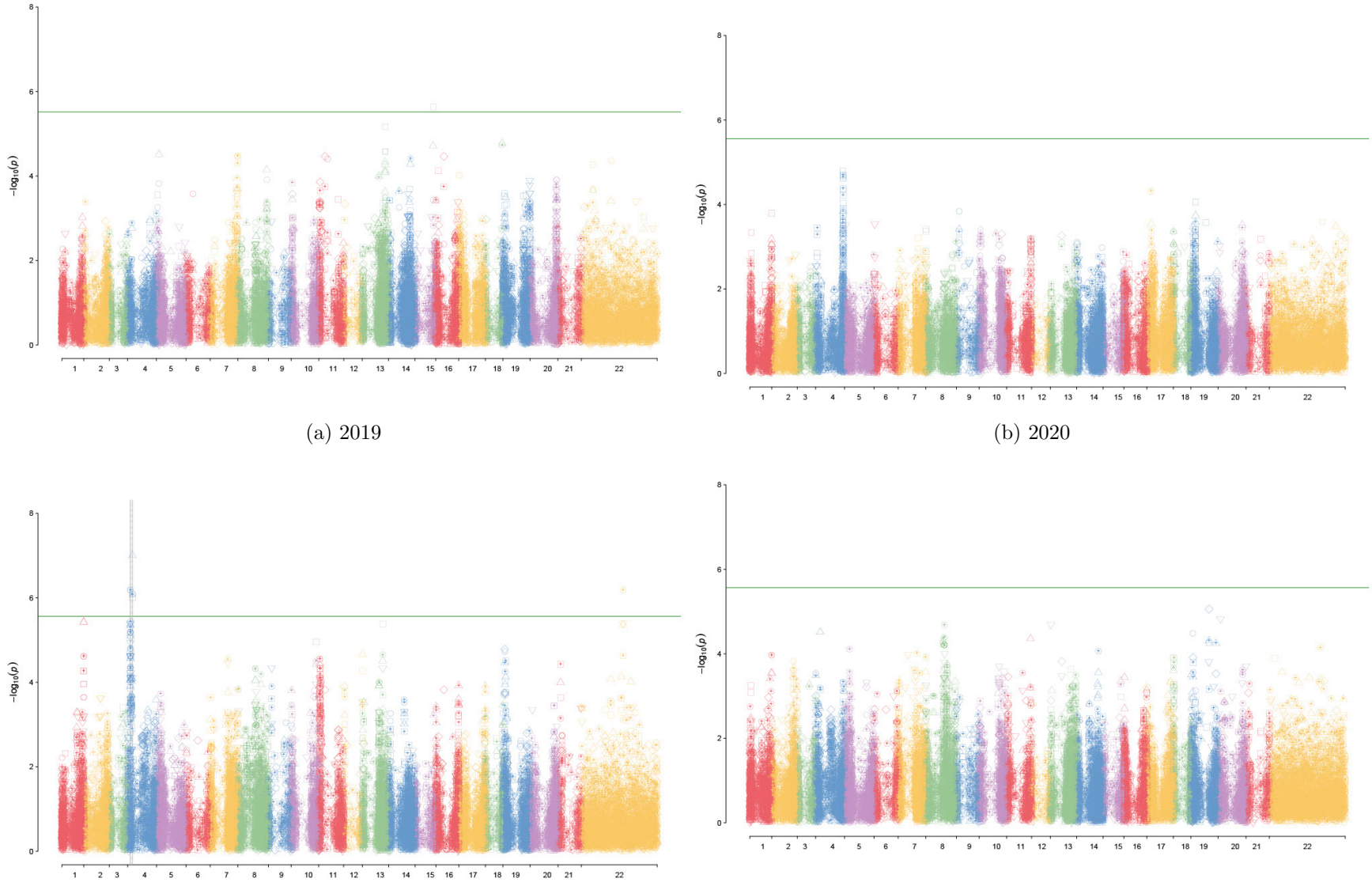

(a) 2019

(b) 2020

(c) 2021

(d) 2022

Figure A5: Manhattan plots trial means in the years 2019-2022

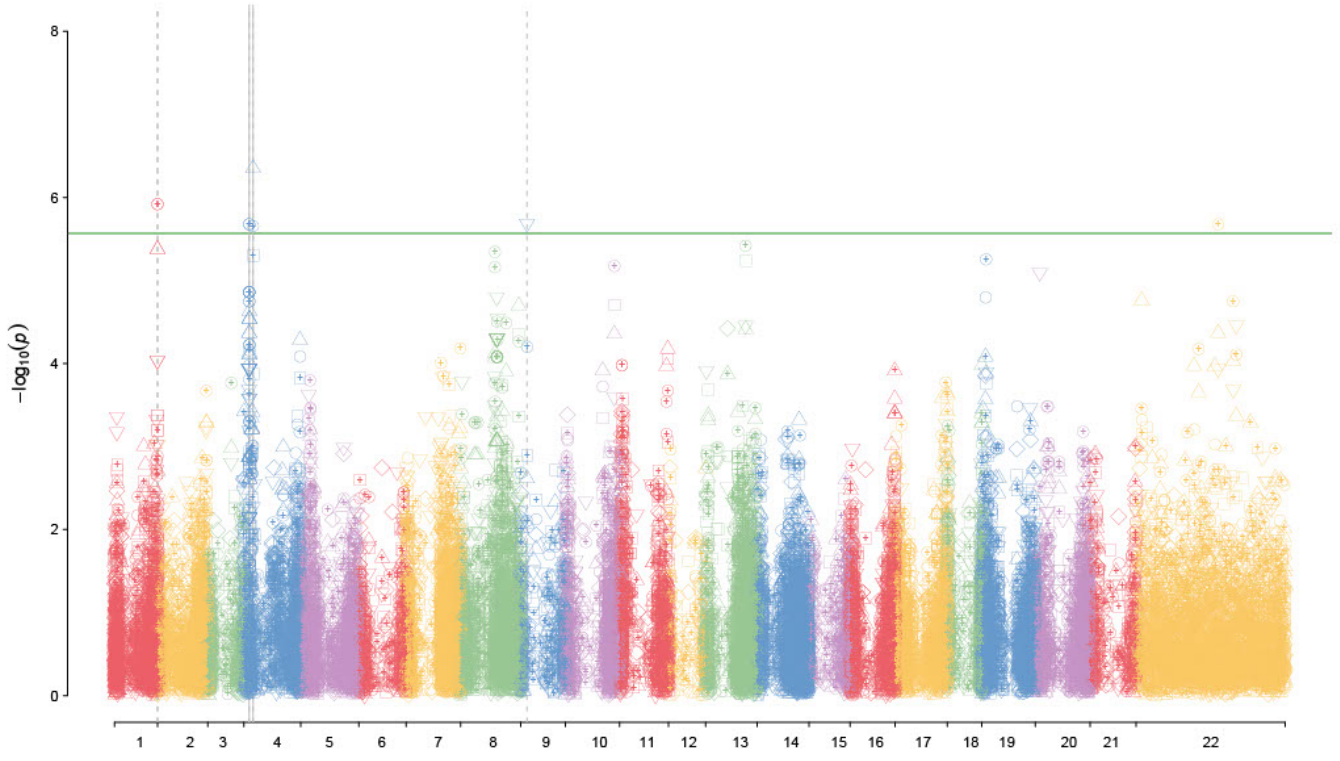

Figure A6: Manhattan plot for global means trial

7.12 Manhattan Plots for AUC-values of VIs

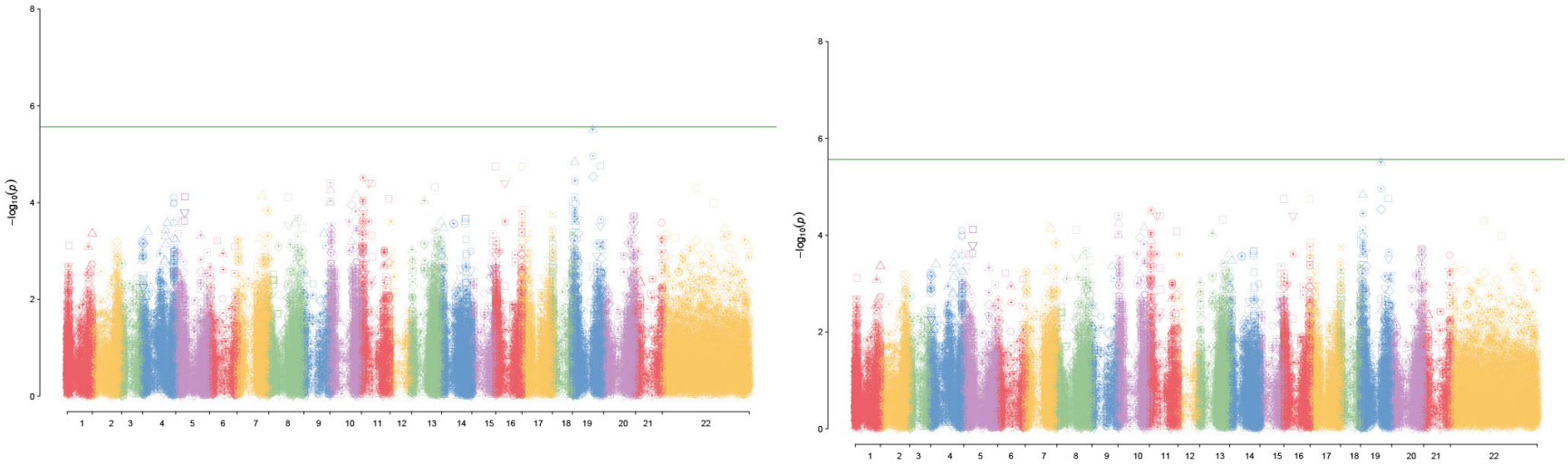

(a) Seaonsal Trials

(b) Global Means

Figure A7: Manhattan plots seasonal trials and global means for AUC-values of VIs

7.13 Manhattan Plots for Agronomic Traits

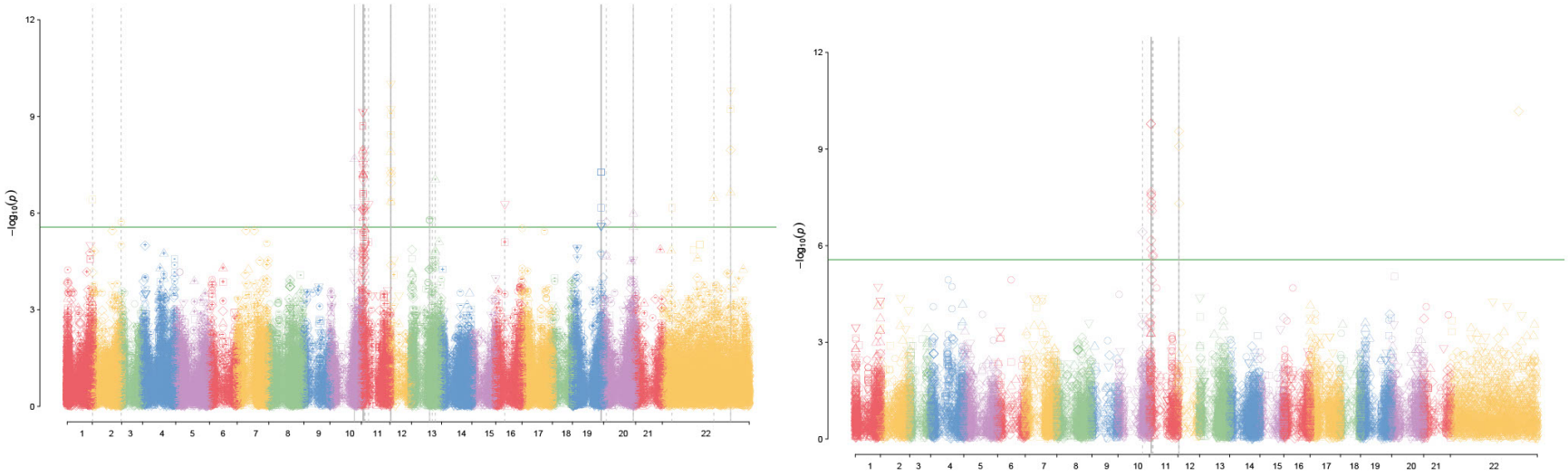

(a) Seaonsal Trials

(b) Global Means

Figure A8: Manhattan plots seasonal trials and global means for agronomic traits

7.14 Grouping of SNPs of VIs Using Spearman's Correlation

Table A10: Results for grouping SNPs for seasonal trials of AUC-values

Year	Phenotype	p-thresholds	Group Size
2019	gndvi_median	1×10^{-9}	1
2019	gndvi_median	1×10^{-8}	4
2019	gndvi_median	1×10^{-7}	12
2019	gndvi_median	1×10^{-6}	37
2019	gndvi_median	1×10^{-5}	123
2019	ndvi_median	1×10^{-6}	10
2019	ndvi_median	1×10^{-5}	73
2019	sr_median	1×10^{-8}	1
2019	sr_median	1×10^{-7}	5
2019	sr_median	1×10^{-6}	29
2019	sr_median	1×10^{-5}	106
2020	gndvi_median	1×10^{-6}	2
2020	gndvi_median	1×10^{-5}	15
2020	ndvi_median	1×10^{-8}	1
2020	ndvi_median	1×10^{-7}	3
2020	ndvi_median	1×10^{-6}	15
2020	ndvi_median	1×10^{-5}	78
2020	sr_median	1×10^{-6}	1
2020	sr_median	1×10^{-5}	20
2021	gndvi_median	1×10^{-8}	1
2021	gndvi_median	1×10^{-7}	3
2021	gndvi_median	1×10^{-6}	4
2021	gndvi_median	1×10^{-5}	26
2021	ndvi_median	1×10^{-8}	1
2021	ndvi_median	1×10^{-7}	2
2021	ndvi_median	1×10^{-6}	6
2021	ndvi_median	1×10^{-5}	23
2021	sr_median	1×10^{-9}	7
2021	sr_median	1×10^{-8}	7
2021	sr_median	1×10^{-7}	20
2021	sr_median	1×10^{-6}	71
2021	sr_median	1×10^{-5}	169
2022	gndvi_median	1×10^{-9}	33
2022	gndvi_median	1×10^{-8}	78
2022	gndvi_median	1×10^{-7}	198
2022	gndvi_median	1×10^{-6}	438
2022	gndvi_median	1×10^{-5}	774
2022	ndvi_median	1×10^{-9}	14
2022	ndvi_median	1×10^{-8}	33
2022	ndvi_median	1×10^{-7}	68
2022	ndvi_median	1×10^{-6}	234
2022	ndvi_median	1×10^{-5}	556

Table A10: Results for grouping SNPs for seasonal trials of AUC-values

Year	Phenotype	p-thresholds	Group Size
2022	sr_median	1×10^{-9}	8
2022	sr_median	1×10^{-8}	23
2022	sr_median	1×10^{-7}	49
2022	sr_median	1×10^{-6}	133
2022	sr_median	1×10^{-5}	338

Table A11: Results for grouping SNPs for global means of AUC-values

p-thresholds	GNDVI	NDVI	SR
1×10^{-9}	14	4	14
1×10^{-8}	34	17	32
1×10^{-7}	89	42	68
1×10^{-6}	230	169	132
1×10^{-5}	559	380	355

Table A12: Results for grouping SNPs for seasonal trials of agronomic traits

Year	Phenotype	p-thresholds	Group Size
2019	DH_dss	1×10^{-5}	11
2019	DM_dss	1×10^{-6}	10
2019	DM_dss	1×10^{-5}	53
2019	GPC_pct	1×10^{-6}	5
2019	GPC_pct	1×10^{-5}	26
2019	GY_g_m2	1×10^{-8}	1
2019	GY_g_m2	1×10^{-7}	4
2019	GY_g_m2	1×10^{-6}	43
2019	GY_g_m2	1×10^{-5}	167
2019	PH_cm	1×10^{-9}	10
2019	PH_cm	1×10^{-8}	20
2019	PH_cm	1×10^{-7}	29
2019	PH_cm	1×10^{-6}	53
2019	PH_cm	1×10^{-5}	117
2020	DH_dss	1×10^{-6}	1
2020	DH_dss	1×10^{-5}	23
2020	DM_dss	1×10^{-9}	10
2020	DM_dss	1×10^{-8}	25
2020	DM_dss	1×10^{-7}	71
2020	DM_dss	1×10^{-6}	182
2020	DM_dss	1×10^{-5}	464
2020	GPC_pct	1×10^{-9}	644
2020	GPC_pct	1×10^{-8}	946
2020	GPC_pct	1×10^{-7}	1378
2020	GPC_pct	1×10^{-6}	2034
2020	GPC_pct	1×10^{-5}	2922

Table A12 continued: Results for grouping SNPs for seasonal trials of agronomic traits

Year	Phenotype	p-thresholds	Group Size
2020	GY_g_m2	1×10^{-9}	1172
2020	GY_g_m2	1×10^{-8}	1681
2020	GY_g_m2	1×10^{-7}	2387
2020	GY_g_m2	1×10^{-6}	3226
2020	GY_g_m2	1×10^{-5}	4321
2020	PH_cm	1×10^{-9}	2
2020	PH_cm	1×10^{-8}	4
2020	PH_cm	1×10^{-7}	9
2020	PH_cm	1×10^{-6}	19
2020	PH_cm	1×10^{-5}	29
2021	DH_dss	1×10^{-7}	1
2021	DH_dss	1×10^{-6}	16
2021	DH_dss	1×10^{-5}	55
2021	DM_dss	1×10^{-9}	72
2021	DM_dss	1×10^{-8}	145
2021	DM_dss	1×10^{-7}	302
2021	DM_dss	1×10^{-6}	588
2021	DM_dss	1×10^{-5}	1158
2021	GPC_pct	1×10^{-9}	291
2021	GPC_pct	1×10^{-8}	544
2021	GPC_pct	1×10^{-7}	907
2021	GPC_pct	1×10^{-6}	1459
2021	GPC_pct	1×10^{-5}	2184
2021	GY_g_m2	1×10^{-9}	1056
2021	GY_g_m2	1×10^{-8}	1484
2021	GY_g_m2	1×10^{-7}	1977
2021	GY_g_m2	1×10^{-6}	2701
2021	GY_g_m2	1×10^{-5}	3656
2021	PH_cm	1×10^{-9}	22
2021	PH_cm	1×10^{-8}	33
2021	PH_cm	1×10^{-7}	44
2021	PH_cm	1×10^{-6}	83
2021	PH_cm	1×10^{-5}	247
2022	DH_dss	1×10^{-9}	1
2022	DH_dss	1×10^{-8}	4
2022	DH_dss	1×10^{-7}	9
2022	DH_dss	1×10^{-6}	57
2022	DH_dss	1×10^{-5}	180
2022	DM_dss	1×10^{-9}	142
2022	DM_dss	1×10^{-8}	338
2022	DM_dss	1×10^{-7}	614
2022	DM_dss	1×10^{-6}	1076
2022	DM_dss	1×10^{-5}	1755
2022	GPC_pct	1×10^{-9}	1
2022	GPC_pct	1×10^{-8}	4

Table A12 continued: Results for grouping SNPs for seasonal trials of agronomic traits

Year	Phenotype	p-thresholds	Group Size
2022	GPC_pct	1×10^{-7}	11
2022	GPC_pct	1×10^{-6}	33
2022	GPC_pct	1×10^{-5}	144
2022	GY_g_m2	1×10^{-9}	1470
2022	GY_g_m2	1×10^{-8}	2062
2022	GY_g_m2	1×10^{-7}	2701
2022	GY_g_m2	1×10^{-6}	3655
2022	GY_g_m2	1×10^{-5}	4973
2022	PH_cm	1×10^{-9}	9
2022	PH_cm	1×10^{-8}	14
2022	PH_cm	1×10^{-7}	20
2022	PH_cm	1×10^{-6}	34
2022	PH_cm	1×10^{-5}	65

Table A13: Results for grouping SNPs for global means of agronomic traits

p-thresholds	DH	DM	GY	PH	GPC
1×10^{-9}	0	162	1786	17	483
1×10^{-8}	0	316	2334	21	784
1×10^{-7}	1	595	3084	26	1171
1×10^{-6}	7	1068	4111	39	1765
1×10^{-5}	56	1810	5363	88	2684

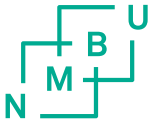

Norges miljø- og biovitenskapelige universitet
Noregs miljø- og biovitskapelege universitet
Norwegian University of Life Sciences

Postboks 5003
NO-1432 Ås
Norway